

**THERMODYNAMICS OF
COMPLEXATION OF ACTINIDES AND LANTHANIDES
WITH LIGANDS RELEVANT TO ENVIRONMENTAL AND
SEPARATION SCIENCE**

by

**Neetika Rawat
Radiochemistry Division,
Bhabha Atomic Research Centre,
Mumbai 400085, India**

A thesis submitted to the
Board of studies in Chemical Sciences
in partial fulfillment of the requirements
for the degree of

Doctor of Philosophy

of

Homi Bhabha National Institute



March, 2011

HOMI BHABHA NATIONAL INSTITUTE

Recommendations of the Viva Voce Board

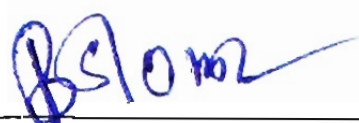
As members of the Viva Voce Board, we certify that we have read the dissertation prepared by **Smt. Neetika Rawat** entitled “**Thermodynamics of complexation of actinides and lanthanides with ligands relevant for environment and separation science**” and recommend that it may be accepted as fulfilling the dissertation requirement for the Degree of Doctor of Philosophy.

Date: 10.06.2011



Chairman – **Prof. K. L. Ramakumar**

10.06.2011



Guide / Convener – **Prof. B. S. Tomar**

10.06.2011



Member 1 - **Prof. A. K. Singh** (External Examiner)

10.06.2011



Member 2 – **Prof. A. V. R. Reddy**

10.06.2011



Member 3 – **Prof. P. K. Mohapatra**

Final approval and acceptance of this dissertation is contingent upon the candidate's submission of the final copies of the dissertation to HBNI.

I hereby certify that I have read this dissertation prepared under my direction and recommend that it may be accepted as fulfilling the dissertation requirement.

Date: 10.06.2011

Place: B. A. R. C, Trombay

STATEMENT BY AUTHOR

This dissertation has been submitted in partial fulfillment of requirements for an advanced degree at Homi Bhabha National Institute (HBNI) and is deposited in the Library to be made available to borrowers under rules of the HBNI.

Brief quotations from this dissertation are allowable without special permission, provided that accurate acknowledgement of source is made. Requests for permission for extended quotation from or reproduction of this manuscript in whole or in part may be granted by the Competent Authority of HBNI when in his or her judgment the proposed use of the material is in the interests of scholarship. In all other instances, however, permission must be obtained from the author.

Neetika Rawat
Neetika Rawat

DECLARATION

I, hereby declare that the investigation presented in the thesis has been carried out by me. The work is original and has not been submitted earlier as a whole or in part for a degree / diploma at this or any other Institution / University.

Neetika Rawat

Neetika Rawat

ACKNOWLEDGMENTS

I wish to express my sincere gratitude to my guide Prof. B. S. Tomar for the continuous support for my Ph.D study and research, for his patience, motivation, enthusiasm, and immense knowledge. His guidance helped me in all the time of research and writing of this thesis.

I would also like to thank members of the doctoral committee: Prof. V. K. Manchanda (Chairman), Prof. A. V. R. Reddy (Member) and Prof. P. K. Mohapatra (Member), for their encouragement and insightful comments.

I am thankful to Dr. A. Bhattacharyya for his valuable suggestions and support in theoretical calculations. My sincere thanks are also due to my colleagues, Mr. Sumit Kumar and Ms. Aishwarya Kar for many stimulating discussions and their invaluable co-operation during the course of this work. I express my sincere gratitude to Dr. M. S. Murali, Dr. P. N Pathak, Mr. D. R. Prabhu, Dr. S. A Ansari, Mr. R. B. Gujar, Mr. A. S. Kanekar, Mr. D. R. Raut, Mr. Pankaj Kandwal, Ms. Sharayu Kasar and Ms. Neelam Soni for their cooperation and help during this work.

My special thanks are due to my husband, Neerav Rawat for his constant love, encouragement and support. Last, but not the least, I would like to thank my parents for their affection and encouragement to complete this work.

Neetika Rawat

TABLE OF CONTENTS

Synopsis	1
List of Figures	18
List of Tables	22
Chapter 1 Introduction	24
1.1. Introduction to actinides.....	24
1.2. Actinides in the environment	26
1.2.1. Nuclear weapon testing	26
1.2.2. Nuclear power generation	26
1.3. Chemistry of actinides	32
1.3.1. Electronic Configuration	32
1.3.2. Oxidation state	34
1.3.3. Coordination number and ionic radii	34
1.3.4. Chemistry of actinides in aqueous solution	35
1.3.5. Complex formation	40
1.4. Environmental chemistry of actinides	42
1.4.1. Precipitation.....	42
1.4.2. Adsorption	43
1.4.3. Colloid formation	43
1.4.4. Complexation.....	43
1.4.5. Humic substances	44
1.5. Thermodynamics of complexation of actinides.....	45
1.5.1. Actinide complexation by inorganic ligands	46
1.5.2. Actinides complexation by organic ligands	47
1.6. Motivation for the present work.....	50
1.6.1. Complexation of actinides with ligands of environmental importance	50
1.6.2. Complexation of actinides and lanthanides with ligands relevant to separation science and technology.....	52
1.7. Scope of the thesis	53

Chapter 2	Experimental Techniques	55
2.1.	Introduction.....	55
2.2.	Stability constants	55
	2.2.1 <i>Specific Ion Interaction Theory (SIT)</i>	56
	2.2.2 <i>Pitzer model</i>	57
2.3.	Determination of stability constant	59
	2.3.1 <i>Potentiometric titration</i>	59
	2.3.2 <i>UV- vis absorption spectroscopy</i>	68
	2.3.3 <i>Time Resolved Fluorescence Spectroscopy (TRFS)</i>	70
2.4.	Calorimetry	74
	2.4.1 <i>Types of calorimeters</i>	75
	2.4.2 <i>Instrumentation</i>	77
	2.4.3 <i>Methodology</i>	80
	2.4.4 <i>Calibration of calorimeter</i>	83
	2.4.5 <i>Determination of ΔG_C, ΔH_C and ΔS_C</i>	87
Chapter 3	Thermodynamics of Complexation of Actinides with Simple Carboxylates: Effect of Ligand Structure and Metal Ion Oxidation State	91
3.1.	Introduction.....	91
3.2.	Experimental.....	94
3.3.	Theoretical calculations	97
3.4.	Results and discussion	98
	3.4.1 <i>Protonation of ligands</i>	98
	3.4.2 <i>Effect of functional group: Thermodynamics of Eu(III) complexation by carboxylates</i>	101
	3.4.3 <i>Effect of unsaturation in dicarboxylates: Thermodynamics of complexation of Eu(III) and U(VI) by maleate and fumarate</i>	108
	3.4.4 <i>Effect of ring size: Thermodynamics of complexation of Th(IV) by dicarboxylates</i>	121
3.5.	Conclusion	129
Chapter 4	Thermodynamics of Complexation of Actinides at Elevated Temperatures	131
4.1	Introduction.....	131

4.1.1	<i>Born equation</i>	132
4.1.2	<i>Extended Born equation</i>	133
4.2	Experimental	135
4.2.1.	<i>Reagents</i>	135
4.2.2.	<i>Experimental setup</i>	136
4.2.3.	<i>Potentiometric titrations</i>	136
4.2.4.	<i>Calorimetric titrations</i>	137
4.3.	Results and Discussion.....	137
4.3.1.	<i>Protonation of succinate</i>	137
4.3.2.	<i>Complexation of U(VI) by succinate at elevated temperatures..</i>	140
4.4.	Conclusions.....	150
Chapter 5	Thermodynamics of Complexation of Lanthanides with (2,6- bis (5,6- diethyl-1,2,4-triazin-3-yl) Pyridines (Ethyl-BTP)	151
5.1	Introduction.....	151
5.1.1	<i>Solvent extraction studies</i>	152
5.1.2	<i>Complexation studies with alkyl - BTP</i>	155
5.2	Experimental	157
5.2.1	<i>Synthesis of ethyl-BTP (IV)</i>	157
5.2.2	<i>Reagents</i>	158
5.2.3	<i>Spectrophotometry</i>	158
5.2.4	<i>Theoretical calculations</i>	158
5.2.5	<i>Time resolved fluorescence spectroscopy (TRFS)</i>	159
5.2.6	<i>Microcalorimetry</i>	159
5.3	Results and Discussion.....	160
5.3.1	<i>Spectrophotometry</i>	160
5.3.2	<i>Theoretical Calculations</i>	161
5.3.3	<i>Time resolved fluorescence spectroscopy (TRFS)</i>	168
5.3.4	<i>Calorimetry</i>	173
Summary	176
References	180

List of Publications

Journal

1. Thermodynamics of complexation of Sr(II) and Ba(II) by 18 crown 6 in water–ethanol binary mixture using titration calorimetry, **Neetika Rawat**, R.S. Sharma, B.S. Tomar, V.K. Manchanda, *Thermochim. Acta*, 501, 13 (2010).
2. Thermodynamic study of complexation of Eu(III) with carboxylates by potentiometry and calorimetry, **N. Rawat**, R. S. Sharma, B. S. Tomar, V. K. Manchanda, *Thermochimica Acta* 501, 13 (2010).
3. Thermodynamics of U(VI) and Eu(III) complexation by unsaturated carboxylates, **Neetika Rawat**, A. Bhattacharyya, B. S. Tomar, T. K. Ghanty, V. K. Manchanda, *Thermochim. Acta* (2011) (in press).
4. Thermodynamic study of Th(IV) complexes with dicarboxylates by potentiometry and calorimetry. **Neetika Rawat**, R. S. Sharma, Abdul Nishad, B.S.Tomar, V. K. Manchanda, *Radiochim Acta* (2011) (in press).
5. Thermodynamics of U(VI) complexation by succinate at variable temperatures, **Neetika Rawat**, B. S. Tomar and V. K. Manchanda, *J. Chem. Thermodynamics* (2011) (in press).
6. Thermodynamics of complexation of lanthanides with 2,6-bis(5,6-diethyl-1,2,4-triazin-3-yl) pyridines, **Neetika Rawat**, A. Bhattacharyya, T. Gady, S. K. Ghosh, B. S. Tomar and V. K. Manchanda, *Radiochimica Acta* (communicated).

Symposia

1. Effect of Solvent on Thermodynamics of Sr(II) with 18 Crown 6 and Dicyclohexano 18 Crown 6, **Neetika Rawat**, R.B.Gujar, M.S.Murali, B.S.Tomar and V.K.Manchanda, In proceedings of DAE-BRNS Symposium on Nuclear and Radiochemistry (NUCAR – 2009), held at SVKM's Mithibai College, Mumbai, India, during Jan 7-10, 2009, p 329.
2. Thermodynamic of Th(IV) complexation with dicarboxyate ligands: A potentiometric and calorimetric study, **N. Rawat**, A.Nishad, R. S. Sharma, B. S. Tomar and V. K. Manchanda, Asia-Pacific Symposium on Radiochemistry – 09, held at NAPA valley California, U.S. during Nov 29-Dec 4, 2009.
3. Thermodynamics of Uranyl succinate at Elevated Temperature, **N. Rawat**, B. S. Tomar and V. K. Manchanda, In proceedings of DAE-BRNS Symposium on Nuclear and Radiochemistry (NUCAR – 2011), held at GITAM University, Vishakhapatnam, India, during Feb-22-25, 2011, p 307.
4. Thermodynamics of complexation of Eu(III) with 2,6-bis(5,6-diethyl-1,2,4-triazin-3-yl)pyridines, **N. Rawat**, A. Bhattacharyya, S. V. Godbole, T. Gadly, S. K Ghosh and B. S. Tomar, In proceedings of DAE-BRNS Symposium on Nuclear and Radiochemistry (NUCAR – 2011), held at GITAM University, Vishakhapatnam, India, during Feb-22-25, 2011, p 473

Synopsis

Actinide (Ac-Lr) and lanthanide (La-Lu) elements occupy unique position in the periodic table owing to the filling of f orbitals. The chemistry of early actinide elements is much like that of transition elements due to the small difference in the energy of 5f and 6d orbitals which results in the variable valency among these elements. Beyond Americium ($Z > 95$) the 5f orbitals get sufficiently stabilized and these actinide elements have chemical properties similar to lanthanides (prevalent +3 oxidation state) [1, 2]. The chemistry of actinide elements have been of great interest to radiochemists ever since the discovery of transuranium elements as well as nuclear fission process, which led to the harnessing of nuclear energy for peaceful purposes (e.g. production of electricity). All the transuranic elements (actinide) were discovered in a short span of nearly 15 years through bombardment of uranium and heavier elements with neutron or charged particles and followed by the finest chemical separations (ion exchange separation of trivalent actinides (An(III)) (Cm – Lr) in the history of chemical sciences [3].

While the subject of actinide chemistry has been a frontier area of research in chemistry, the generation of long-lived actinide isotopes during burning of the nuclear fuel in reactors has opened new challenges to radiochemists with regard to their impact on biosphere and human health. The spent nuclear fuel is reprocessed to separate the uranium and plutonium, the latter to be used in the next generation reactors e.g. fast reactors. The high level waste, generated during the reprocessing, contains minor actinides (Np, Am and Cm) and long lived fission products which need to be contained in suitable matrix and stored in such a manner that they do not come in to public domain even after thousands of years [4]. Presently the high level waste (HLW) is being vitrified in borosilicate glass matrix which after an interim

storage for few decades is proposed to be buried in a deep geological repository [5]. However, there is a finite probability of the release of the long lived radionuclides from deep geological repository over a long period of time.

Apart from their possible release from vitrified waste form, actinides have also entered the environment due to regular low level discharges from operating nuclear power plants, mining and milling of uranium, re-entry of nuclear powered satellites to the earth and fallout from nuclear tests carried out during the last century.

Once released from their source to the geosphere, actinides may undergo different types of reactions depending upon the conditions of aquatic environment e.g., metal ion concentrations, pH, E_h , presence of complexing anions, colloids, rocks and sediments in the vicinity of water bodies [6]. Complexation of actinides by organic anions is one of the important pathways of their speciation which influences their migration. The organic anions present in the ground water include simple carboxylates, such as acetate, oxalate, citrate etc., as well as complex molecules like humic and fulvic acid which are known to have strong affinity for actinides [7].

Thermodynamic studies of actinide complexation by organic complexing anions helps in understanding the speciation of actinides in aquatic environment. The thermodynamic parameters for complexation (ΔG_C , ΔH_C and ΔS_C) of actinides by different complexing anions are required as input in the data base for geochemical codes meant for speciation studies [8]. In addition, these data provide insight into the mechanism of the complexation reactions. While the enthalpy of the complexation reveals the role of bond formation and desolvation of metal ion and the ligand, the entropy term reflects the contribution of change in order / disorder

around the reacting species [9]. The temperature of water in the vicinity of the deep geological repository for nuclear waste could be much higher than ambient temperature, and therefore, the data on enthalpy of complexation (ΔH_C) are required to determine the stability constants at higher temperature, using Van't Hoff equation. For the higher temperature range, where the Van't Hoff equation cannot be used, direct measurement of ΔH_C would be needed. Though a large number of reports on stability constant data are available [10], the complete thermodynamic parameters are scarcely available. Hence there is need to determine the thermodynamic parameters for complexation of actinides by complexing anions at elevated temperatures.

Lanthanide elements are invariably associated with actinides not only from the point of view of their natural occurrence, but also their formation in nuclear fission of actinides. In fact, lanthanides constitute nearly 17 % of the fission products and hence are present in abundance in the HLW. Further, the lanthanides are also used as analogues of trivalent actinides in speciation and migration studies. Separation of lanthanides from trivalent actinides is an important step in the partitioning and transmutation of minor actinides present in HLW [11]. During the partitioning of minor actinides, Am(III) and Cm(III) are invariably separated along with lanthanides (La – Gd) present in HLW. The concentration of lanthanides (~ 1000 mg/L) in HLW is much more than that of minor actinides (~ 10 mg/L) and hence their presence affects the efficiency of transmutation owing to their high neutron absorption cross section. It is, therefore, essential to separate lanthanides from trivalent actinides (An(III)). For this purpose soft 'N' and 'S' donor ligands are being extensively studied worldwide [12]. 'S' donor ligands e.g. thiophosphinic acids with synergistic extraction have shown very high separation factors for An(III)

over Ln(III) [13, 14]. However they can be used only at lower acidity of the aqueous solution. 'N' donor ligands have been found to work at higher acidity and are more radiation resistant owing to their aromatic structure. In this context alkyl derivatives of BTP appear to be quite promising [15, 16].

In the present thesis thermodynamic studies of complexation of actinides and lanthanides with various ligands have been carried out using potentiometry, spectrophotometry and microcalorimetry. In some cases time resolved fluorescence spectroscopy (TRFS) has also been used to reveal the stoichiometry of complexes. Theoretical calculation of charge density in the free ligand as well as the metal ligand complex has been carried out in some cases to study the charge polarization effects. The thesis has been divided into six chapters. A brief description of different chapters is given below.

CHAPTER – 1: INTRODUCTION

This is the introductory chapter of the thesis that elaborates the importance of thermodynamics of complexation of actinides and lanthanides. The chemistry of the lanthanide and actinide elements, which is important in the solution phase, viz. electronic configurations, redox behaviour, hydrolysis and complexation reactions have been described. Various steps in nuclear fuel cycle which lead to the generation of nuclear waste have been described. The composition of HLW has been described, followed by the different waste management strategies (partitioning and transmutation, Ln(III)/An(III) separation, vitrification of HLW) being considered worldwide. A brief description of deep geological repository for nuclear wastes is followed by the possible interactions of actinides with natural systems in case of their release from the repository. The importance of complexing anions in

influencing the speciation of actinides in aquatic environment has been discussed. The chapter ends with the motivation for the work carried out as a part of this thesis.

CHAPTER – 2: EXPERIMENTAL TECHNIQUES

This chapter describes the various experimental techniques used in the present work. The stability constants were determined by potentiometric and, in some cases, spectrophotometric titrations / fluorescence emission spectroscopy. The instrumentation for these experimental techniques, such as, potentiometric autotitrator, UV-visible spectrophotometer, time resolved fluorescence spectrophotometer is described in detail. The calorimetric titration experiments for enthalpy determinations were carried out by heat flow type titration calorimeter. The complete description of calorimeter and its calibration procedures are given in this chapter. In case of 1:1 adduct formation reactions, ΔG_C , ΔH_C and ΔS_C can be determined directly by titration calorimetry. The reaction between Ba(II) and 18 Crown 6 was used for chemical calibration of the calorimetric system. Thermodynamic parameters for Ba(II)-18 Crown 6 and Sr(II)-18 Crown 6 were determined in water ethanol binary mixtures of different compositions [17]. The standardization of metal ion concentration was carried out by UV visible spectrophotometry and complexometry.

The methodology for determination of stability constant from potentiometric and spectrophotometric titrations using Hyperquad 2008 and Hyperquad 2006 software respectively have been described in this chapter. Likewise the details of the procedure for determination of enthalpy data from calorimetric titrations have been given in this chapter. The general methodology for determination of stability constant and stoichiometry of the metal ligand complexes from TRFS spectra and fluorescence decay life time, respectively, have been explained.

CHAPTER – 3: THERMODYNAMICS OF COMPLEXATION OF ACTINIDES WITH SIMPLE CARBOXYLATES: EFFECT OF LIGAND STRUCTURE AND METAL ION OXIDATION STATE

The migration of actinides in aquatic environment depends on their interaction with organic and inorganic ligands. Most of the organic ligands, present in the natural water, constitute carboxylate as the most important functional group, though hydroxyl and other groups are also known to determine the complexing ability of the naturally occurring complexing anions. Carboxylate anions are also used as model systems to investigate the binding of actinides to complex molecules, such as, humic and fulvic acid, which are known to greatly influence the migration of actinides in the aquatic environment [18]. In order to understand the mechanism of complexation of actinides, it is therefore, important to carry out the thermodynamic studies of their complexation reactions with carboxylates of varying alkyl chain length, rigidity, extent of unsaturation and functional groups.

With this in view, complexation of actinides of different oxidation states namely, Th(IV), U(VI) and Eu(III) (chemical analogue of An(III)) with different carboxylate anions have been studied by potentiometry and calorimetry at constant temperature (298 K) and fixed ionic strength (1.0 M NaClO₄). Th(IV) is used to study the behavior of tetravalent actinides viz., Pu(IV), while U(VI) have been used to study the complexation of hexavalent actinides such as Np(VI) and Pu(VI). Owing to the high specific activity of Am(III) and Cm(III), calorimetric studies of these actinides are carried out using Eu(III). Further it can also be used as a fluorescent probe to provide additional information about the coordination environment around the metal ion. The carboxylate anions studied in the present work included mono-carboxylate (acetate), aliphatic di-carboxylate of varying chain

length ($\text{OOC}-(\text{CH}_2)_n-\text{COO}^-$) with $n = 1-4$, aromatic di-carboxylate (phthalate), hydroxy carboxylate (2-hydroxy 2-methyl propanonate) and unsaturated di-carboxylates, namely, fumarate and maleate (figure 1).

The protonation constant(s) ($\log K_P$) of the carboxylate anions were determined by the potentiometric titration of the acidic solution of the ligand with standard NaOH solution. These data were in turn used as input to determine the stability constants ($\log \beta$) of the metal-carboxylates using the potentiometric titration of metal ion solution (20 ml) by buffered ligand solution. For this purpose the potentiometric data analysis program Hyperquad 2008 was used. In the case of Eu(III) complexation studies with maleate and fumarate, TRFS was also used to deduce the coordination mode of the ligands. Calorimetric titrations of the metal ion solutions (2.7 ml) with buffered ligand solutions were carried out using the isothermal titration calorimeter (TAM III, Sweden). The stability constants obtained from potentiometric titration experiments were used to analyze the calorimetric titration data to obtain the ΔH_C [19, 20, 21].

Theoretical calculations of charge distribution in the free ligand as well as the metal ligand complex were carried out in the case of unsaturated carboxylate complexes of Eu(III), to reveal the charge polarization during complexation process.

Complexation of Eu(III) with carboxylates with different functionality, namely mono-carboxylate (acetate), aliphatic di-carboxylate (succinate), aromatic di-carboxylate (phthalate) and hydroxyl carboxylate (2-hydroxy 2-methyl propanoate) revealed that the reactions are mainly endothermic due to high dehydration energy required for complexation except for hydroxyl carboxylate where participation of hydroxyl group increases metal ligand interaction thus making the reaction slightly exothermic. The participation of hydroxyl group has

also been supported by higher stability of the complex with hydroxy carboxylate than with mono-carboxylate of same basicity. The reactions were driven mainly by entropy as evident from large positive entropy term. Complexation of Eu(III) by di-carboxylates is more endothermic due to higher dehydration of metal ion as well as the ligand. The aliphatic di-carboxylates (succinate) have similar thermodynamic parameters as aromatic di-carboxylates (phthalate) of same ring size. The higher basicity of succinate in Eu(III)-succinate is compensated by higher rigidity of the ligand in Eu(III)-phthalate.

The studies on unsaturated carboxylates are interesting and different from saturated carboxylates due to their rigid structure and higher tendency of charge polarization. The complexation of Eu(III) and U(VI) with fumarate and maleate showed higher stability constant of these complexes than expected for mono-carboxylates of same basicity, which was revealed in the plot of $\log \beta_1$ vs $\log K_P$. The higher stability of fumarate complexes than mono-carboxylates has been attributed to charge polarization. Ab initio calculation for the structure optimization and Mulliken charge of maleate and fumarate complexes with trivalent metal ion (Eu^{3+}) corroborate the charge polarization in fumarate complexes. The higher stability constants of maleate complexes have been explained on the basis of chelate effect which is not possible in fumarate complexes due to its trans nature. The high stability constants of U(VI) compared to Eu(III) are due to higher entropy values. The difference in ΔH_C of fumarate and maleate complexes is more prominent in U(VI) complexes due to restricted space available for coordination around $[\text{O}=\text{U}=\text{O}]^{2+}$. The stability constant of Eu(III)-complexes determined by TRFS are in good agreement with those obtained by potentiometry. The fluorescence lifetime

data indicate greater degree of metal ion dehydration in Eu(III)-maleate compared to Eu(III)-fumarate which corroborate the ΔS_C values.

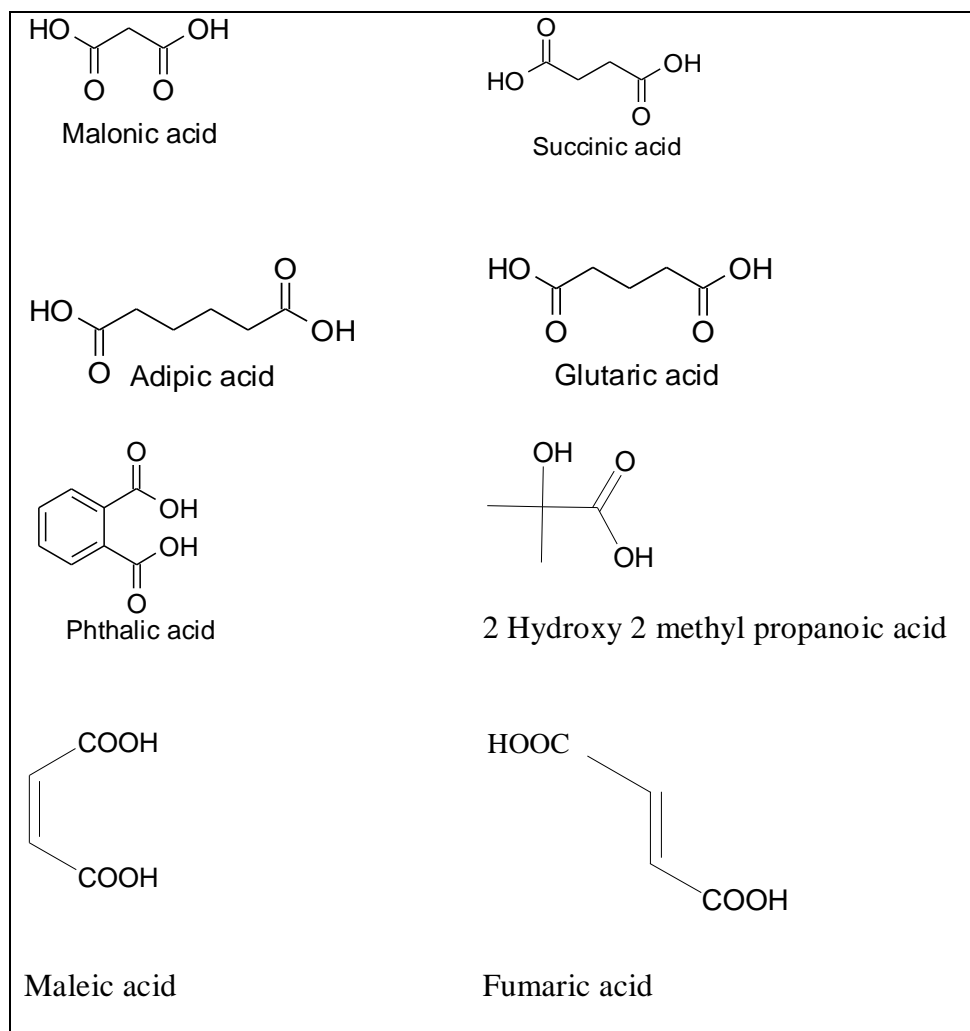
The studies on complexation of di-carboxylates with increasing chain length (malonate, succinate, glutarate and adipate) with Th(IV) revealed the dominant role of ring size over ligand basicity in thermodynamic parameters. The stability of ring size decreases with increasing chain length which reflects in its ΔH_C values. The variation in stability constant is determined by variation in ΔH_C values while ΔS_C (which is a measure of extent of dehydration) remains nearly constant. The ΔG_C , ΔH_C , ΔS_C for the same family of ligand have been compared with the results reported in the literature for other actinides to reveal the effect of metal ion oxidation state. Comparison of ΔG_C , ΔH_C , ΔS_C of various oxidation states of actinides reveals the maximum variation in case of VI oxidation state due to restricted space available for coordination around the $O=U=O^{2+}$ ion.

CHAPTER – 4: THERMODYNAMICS OF COMPLEXATION OF ACTINIDES AT ELEVATED TEMPERATURES

The thermodynamics parameters of actinide complexation are required for predicting their migration in aquatic environment. The temperature near the waste repository could be as high as 90°C. Thus, determination of exact thermodynamic parameters at elevated temperature is essential for performance assessment of the repository. The $\log \beta$ value at higher temperatures can be calculated using Van't Hoff equation. However, the use of Van't Hoff equation may lead to large errors in stability constants as ΔH_C may not be constant at higher temperatures. In addition, the structure and dielectric constant of water also changes at elevated temperatures. Thus, the studies at elevated temperatures are also important for understanding the effect of solvent structure on actinide complexation [22].

The present chapter describes the work carried out on thermodynamics of complexation of U(VI) by succinate at elevated temperatures. The $\log \beta$ for U(VI)-succinate was determined in the temperature range 25-65°C in steps of 10°C using potentiometric titrations wherein the acidic metal ion solution was titrated with buffered succinate solution. The ΔH_C for complexation were determined by calorimetric titration carried out under conditions similar to potentiometric titrations. The protonation constants and enthalpy of protonation at different temperatures are required as input for determination of $\log \beta$ and ΔH_C respectively and were determined by potentiometric and calorimetric titrations respectively [23].

Figure 1. Structure of the carboxylic acid studied for thermodynamic parameters of complexation



The stability constant of U(VI) succinate increased from 4.1 to 4.69 on changing the temperature from 25 to 65°C. As the interactions are mainly electrostatic in nature, the variation in $\log \beta$ with temperature is in good agreement with that predicted on the basis of Born equation. The increase in $\log \beta$ is due to increase in ΔS_C as ΔH_C was found to increase with temperature. The variation in $\log \beta$ with temperature is attributed to the change in the dielectric constant of water and randomness of the bulk water. The linear variation of ΔH_C with temperature suggests the constant heat capacity in the temperature range 25-65°C. The data have been compared with those for uranyl malonate and oxalate complexes to understand the effect of ligand size and hydrophobicity on the temperature dependence of thermodynamic quantities.

CHAPTER – 5: THERMODYNAMICS OF COMPLEXATION OF LANTHANIDES WITH (2,6- BIS (5,6- DIETHYL-1,2,4- TRIAZIN-3-YL) PYRIDINES (ETHYL-BTP)

Lanthanide actinide separation is an important step in actinide partitioning. Recent reports on terdentate 'N' donor ligands, particularly (BTP), have shown good extraction efficiency and selectivity for

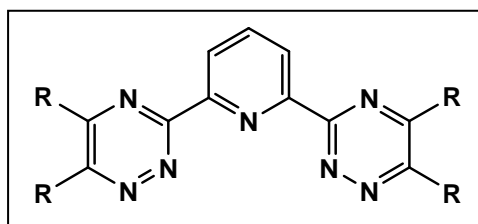


Figure 2. Structure of R-BTP

trivalent actinides (An(III)) in acidic medium, which is the proposed feed for Ln(III)/An(III) separation. The kinetics of extraction and Am(III)/Eu(III) selectivity were found to be dependent on the alkyl (R) substitution on pyridyl or triazinyl ring of BTP molecule (figure 2). Therefore, it is important to understand the mechanism of complexation process and effect of alkyl substituent on complexation properties of Ln(III) and An(III) by BTP based extractants.

In the present work, the stability constants ($\log \beta$) were determined for complexes of ethyl-BTP with Ln(III), namely, La(III), Nd(III), Eu(III), Tb(III), Ho(III), Tm(III) and Lu(III) in methanol medium by spectrophotometric titrations. Variation in π - π^* absorption bands of ligand on addition of metal ions were followed and the spectra were analysed for $\log \beta$ using Hyperquad 2006. Thermodynamic parameters (ΔG_C , ΔH_C and ΔS_C) for Eu(III) and Tb(III) complexation were determined by calorimetry. In the case of Eu(III)-ethyl-BTP, TRFS was used to obtain the fluorescence lifetimes of different species in order to corroborate the stoichiometry of complexes obtained by spectrophotometric titration [24].

The stoichiometry of the complexes was found to vary along the Ln(III) series. Early Ln(III) (except La(III)), namely, Nd(III) and Eu(III) form 1:2 as well 1:3 complexes with ethyl-BTP while in the case of latter Ln(III), namely, (Tb(III), Ho(III), Tm(III) and Lu(III)), only 1:2 complex has been observed. This has been explained on the basis of decrease in the coordination number from 9 to 8 near Ho(III) owing to decrease in ionic radius. In the case of La(III), 1:1 complex was formed. The stoichiometry of the complexes in case of Eu(III)-ethyl-BTP were corroborated by fluorescence lifetimes obtained by TRFS. Comparison of $\log \beta$ for Ln(III) - ethyl-BTP complexes with other alkyl derivatives showed increase in the stability with increasing length of the alkyl group due to hydrophobic interactions. The thermodynamic parameters (ΔG_C , ΔH_C , ΔS_C) for complexation of Eu(III) and Tb(III) with ethyl-BTP revealed strong metal ion – ligand interaction with the reactions driven mainly by enthalpy.

CHAPTER 6: SUMMARY

In the last chapter of the thesis the observations of the experiments carried out on complexation of actinides and lanthanides by different carboxylates and N donor ligands have been summarized. The central theme of the present thesis was the determination of thermodynamic parameters of lanthanides and actinides complexation by microcalorimetry in conjunction with various techniques used for stability constant determination viz., potentiometry, spectrophotometry and fluorescence spectroscopy. The studies carried out as a part of this thesis can be summarized as follows.

1. An isothermal titration calorimeter was installed and calibrated electrically and chemically using complexation of Ba^{2+} and 18 Crown 6.
2. Complexation of Eu(III) by mono-carboxylates, di-carboxylates (aliphatic and aromatic) and hydroxyl carboxylates by potentiometry and calorimetry revealed that the reactions are mainly driven by entropy with the enthalpy being small and positive, except for hydroxy carboxylate where ΔH_C was slightly negative.
3. Complexation of Th(IV) by di-carboxylates of varying alkyl chain length showed that the $\log \beta$ decreases with the chain length with the maximum stability associated with 6 member chelate ring. In the case of Th(IV), ΔS_C , which is measure of extent of dehydration of metal ion, remains constant, while ΔH_C increases with increase in chain length. Though, the reactions are driven by ΔS_C for all the Th(VI)-di-carboxylate complexes, the decrease in ΔG_C with increase in chain length is due to increase in ΔH_C . Comparison of the thermodynamic data for Th(IV) di-carboxylates with that for U(VI) and

Ln(III) revealed the important role of the coordination space available for the ligand around the metal ion.

4. In the case of complexation of U(VI) and Eu(III) by unsaturated dicarboxylates, viz., maleate and fumarate, higher stability constants were observed for maleate than that for fumarate, due to the chelate effect in the former. Fumarate complexes were found to have higher $\log \beta$ than monocarboxylates of same basicity, indicating the occurrence of charge polarization during complexation of the metal ion by fumarate, which was also corroborated by theoretical calculations.
5. The stability constant of U(VI)-succinate was found to increase with temperature (25 - 65⁰C) which was well explained by Born equation indicating the complexation being governed by electrostatic factors. The ΔH_C increased linearly with temperature, but the reaction became more feasible owing to higher increase in ΔS_C . The ΔC_P for U(VI)-succinate was found to be higher than oxalate and malonate suggesting role of hydrophobicity of the ligand in determining the heat capacity.
6. Thermodynamic studies on the complexation of Ln(III) with ethyl-BTP revealed the role of ionic potential and changing coordination number of metal ion along the Ln(III) series. The stability constant of Eu(III)-alkyl-BTP complexes was found to increase with the increase in alkyl chain length of substituent group to the triazinyl ring. The complexation was found to be driven mainly by the ΔH_C .

The thermodynamic parameters determined in this thesis are not only helpful in improving basic understanding of lanthanide and actinide complexation with hard

and soft donor ligands, but also help in closing the gap in available data base which are required for predicting actinide migration in aquatic environment.

REFERENCES

1. G. T. Seaborg and J. J. Katz, *The Actinide elements*, Ed I, McGraw – Hill book company, Inc (1954) 733.
2. S. Ahrland, J.O. Liljenzin and J. Rydberg, *Solution Chemistry*, In “Comprehensive Inorganic Chemistry”, J.C. Bailar Jr., H.J. Emeleus, R. Nyhlom and A.F.T. Dickenson (Eds.), Pergamon Press, Oxford Vol. 5 (1973) 465.
3. A. Ghiorso, B. Harvey, G. Choppin, S. Thompson, G. Seaborg, *Physical Review* 98 (1955) 1518.
4. K.D. Crowley, *Nuclear waste disposal: The technical challenges*, *Physics Today*, 50 (1997) 32.
5. *Moving forward with geological disposal of Radioactive waste- A collective statement by the NEA Radioactive Waste Management Committee*, OECD/NEA No. 6433 (2008).
6. R. J. Silva and H. Nitsche, *Radiochim Acta*, 70/71 (1995) 377.
7. H. Geckeis, Th. Rabung, T. N. Manh, J. I. Kim and H. P. Beck, *Environ. Sci. Technol.*, 36 (2002) 2946.
8. A. E. Martell, R. M. Smith, R. J. Motekaitis, *NIST Critically Selected Stability Constants of Metal Complexes*. Version 7, Texas A&M University, College Station, TX (2003).
9. G. R. Choppin, *J. of Less Common Metal*, 112 (1985) 193.
10. M. J. Keith Roach, *Science of the Total Environment* 396 (2008) 1.

11. Actinide and Fission Product Partitioning and Transmutation—Status and Assessment report, OECD/NEA, 1999; L.H. Baestle, Burning of Actinides: A complementary waste management option? IAEA Bulletin, 34 (1992) 32.
12. C. Madic, M. J. Hudson, J. Liljenzin, R. Nannicini, A. Facchini, Z. Kolarik, R. Odoj, New partitioning techniques for minor actinides, European Report, EUR 19149 (2000).
13. Y. Zhu, J. Chen, and R. Jiao, Solv. Extr. Ion Exch. 14 (1996) 61.
14. A. Bhattacharyya, P. K. Mohapatra and V. K. Manchanda, Solv. Ext. Ion Exch. 26 (2006) 1.
15. Z. Kolarik, U. Müllich and F. Gassner, Solv. Extr. Ion. Exch., 17 (1999) 88.
16. Z. Kolarik, U. Müllich and F. Gassner, Solv. Extr. Ion. Exch., 17(1999) 1155.
17. Neetika Rawat, R.B.Gujar, M.S.Murali, B.S. Tomar and V. K. Manchanda, Thermochim. Acta, 499 (2009) 21.
18. S. N. Kalmykov, A. P. Novikov, A. B. Khasanova, N. S. Scherbina and Yu. A. Sapozhnikov, in: Irina V. Perminova, Kirk Hatfield and Norbert Hertkorn, Use of Humic Substances to Remediate Polluted Environments: From Theory to Practice, NATO Science Series, 2005, Volume 52, Part 2, pp 175-184.
19. Neetika Rawat, R.S. Sharma, B.S. Tomar, V.K. Manchanda, Thermochim. Acta, 501 (2010) 13.
20. Neetika Rawat, A. Bhattacharyya, B. S. Tomar, V. K. Manchanda, Thermochim. Acta (in press).

21. Neetika Rawat, R. S. Sharma, Abdul Nishad, B.S.Tomar, V. K. Manchanda, *Radiochim Acta* (in press).
22. T. G. Srinivasan, P. L. Zanonato, P. Di Bernardo, A. Bismondo and L. Rao, *J of Alloys and Compounds*, 408-412 (2008) 1252.
23. Neetika Rawat, B. S. Tomar and V. K. Manchanda, *J. Chem. Thermodynamics* (in press).
24. Neetika Rawat, A. Bhattacharyya, T. Gadly, S. K. Ghosh, B. S. Tomar and V. K. Manchanda, *Radiochimica Acta* (communicated).

List of Figures

Fig. 1.1:	Relative profile of activity of HLW with and without actinide partitioning.....	29
Fig. 1.2:	Ionic radii of lanthanides and actinides	35
Fig. 1.3:	Proposed structure of humic acid	45
Fig. 1.4:	Plot of $\log K_1$ vs $\log K_P$ for U(VI)-monocarboxylates complexation	49
Fig. 2.1:	Picture of Metrohm autotitrator 905	62
Fig. 2.2:	Typical plot of emf vs pH obtained during electrode calibration	64
Fig. 2.3:	Grans plot for titration of standard HClO ₄ with standard NaOH	65
Fig. 2.4:	Titration of 20 ml of acidified succinic acid (total ligand = 4.0 mM, total proton = 0.011 M) by standard NaOH (0.0766)	67
Fig. 2.5:	Grans potentiometric plot for acidity determination in Th(IV) solution	67
Fig. 2.6:	Potentiometric titration data of complexation of Th(IV) with buffered malonate (Reaction vessel: 3.63 mM in 0.0165 M HClO ₄ , Titrant = total malonate = 0.383 M, total proton = 0.388 M)	68
Fig. 2.7:	Schematic diagram of double beam spectrophotometer	69
Fig. 2.8:	Photograph of the PC controlled spectrophotometer (JASCO V 530)....	69
Fig. 2.9:	The schematic diagram of TRFS setup.....	70
Fig. 2.10:	Fluorescence emission spectrum of Eu(III) in aqueous medium	73
Fig. 2.11:	Fluorescence decay of Eu(III) in aqueous medium	74
Fig. 2.12:	Temperature time curves after a short heat pulse for adiabatic type calorimeter. a) Ideal adiabatic calorimeter b) Semi adiabatic calorimeter	76
Fig. 2.13:	Titration Calorimeter	79
Fig. 2.14:	Calorimetric peak for a fast chemical reaction	82

Fig. 2.15: Calorimetric data (Power Vs Time) for titration of 18Crown 6 solution by Sr^{2+} solution in pure water. Cup solution: 2.7ml of 20mM 18Crown 6 in pure water, Titrant: 0.5M $\text{Sr}(\text{NO}_3)_2$ in pure water.	85
Fig. 2.16: Calorimetric titration curve for Ba^{2+} -18Crown 6 complexation	86
Fig. 2.17: Calorimetric data for protonation of succinate (0.004 M) with 0.0512 M HClO_4	89
Fig. 3.1: Structure of the carboxylate anions studied for thermodynamic parameters of complexation	94
Fig. 3.2 (a): Calorimetric titration of fumarate solution ($C_L = 6.6 \times 10^{-3}$ M, $[\text{OH}^-] = 1 \times 10^{-4}$ M) with 0.098 M HClO_4 (b) Calorimetric titration of maleate solution ($C_L = 4.0 \times 10^{-3}$ M, $[\text{OH}^-] = 1.1 \times 10^{-4}$ M) with 0.098 M.....	99
Fig. 3.3: Potentiometric titration data of Eu(III) with α -HIB.....	102
Fig. 3.4: Calorimetric titration data of Eu(III)-phthalate complexation: Titration vessel: 2.7ml of Eu(III) (7.78mM) + HClO_4 (0.012M), Titrant: Total ligand ($C_L = 0.217$ M) + Total proton ($C_H = 0.046$ M).....	104
Fig. 3.5: Integrated calorimetric titration data of of Eu(III) solution (2.7ml of 7.78mM Eu(III) in 0.012 M HClO_4) by buffered (left y axis) acetate, succinate, phthalate and (right y axis) α -HIB (concentrations are given in table 1b)	105
Fig. 3.6: Plot of $\log \beta$ Vs $\log K_p$ for Eu(III) carboxylates.....	106
Fig. 3.7: Mode of binding in AC (mode 1) and A-HIBA (mode 2)	107
Fig. 3.8: Potentiometric titration of Eu(III) solution ($C_M = 4.95$ mM in 0.007 M HClO_4) with fumarate solution ($C_L = 0.5$ M and $C_H = 0.186$ M).....	110
Fig. 3.9: Potentiometric titration of U(VI) solution ($C_M = 5$ mM in 0.022 M HClO_4) with maleate solution ($C_L = 0.5$ M and $C_H = 0.071$ M)	110
Fig. 3.10: Plot of $\log K_I$ Vs $\log K_p$ for (a) Eu(III) carboxylates (b) U(VI)-carboxylate. Data in parenthesis: plotted vs ($\log K_{P1} + \log K_{P2}$).....	114
Fig. 3.11: NPA atomic charges of free fumarate (a) and maleate (b) and their 1:1 complex with Eu^{3+} (c and d) and UO_2^{2+} (e and f).....	115
Fig. 3.12: (a) Normalized fluorescence emission spectra of Eu(III) as a function of increasing maleate concentration (b) Decay of fluorescence emission at two different concentrations of ligand (0.016 M and 0.035 M) (Cup	

solution: 2.7 ml Eu(III) (5 mM in 0.016 M HClO ₄), Titrant : Maleate solution (C _L = 0.500 M and C _{OH} = 0.009M).....	117
Fig. 3.13: Variation of AR and fluorescence lifetime with volume of titrant	119
Fig. 3.14: Potentiometric data for Th(IV)-malonate complexation along with speciation diagram (conditions are given in table 3.1)	122
Fig. 3.15: (a) Raw calorimetric data and (b) plot of Q _i ^r vs volume of titrant for Th(IV)-malonate . (Injection volume = 10 μl) (conditions are given in table 3.1)	123
Fig. 3.16: Plot of h _{vi} vs n _{avg} for Th(IV)-dicarboxylate at I = 1.0 M at 25 ⁰ C. Symbols (○,□,Δ,◇) : experimental data; lines: fitted data. Th(IV)-malonate (right y axis)	124
Fig. 3.17: Thermodynamic parameters of Np(V), Sm(III), U(VI), Th(IV) (1:1) complexation with dicarboxylates	125
Fig. 4.1: Potentiometry titration of 20 ml of acidified succinic acid (total ligand = 4.0 mM, total proton = 0.011 M) by standard NaOH (0.0766)	138
Fig. 4.2: Calorimetric data for protonation of succinate (4.0 mM) with 0.051 M HClO ₄ at T = 25 ⁰ C	139
Fig. 4.3: Potentiometric data for titration of U(VI) (5.0 mM in 27.5 mM) with buffered succinate (total succinate = 0.500 M and total proton 0.516 M) at 25 ⁰ C along with the speciation diagram at (a) T=25 ⁰ C and (b) T = 65 ⁰ C.....	142
Fig. 4.4: Calorimetric data of titration of U(VI) (5.0 mM in 0.028 M HClO ₄) with buffered succinate solution (total ligand concentration = 0.500 M and total proton concentration = 0.516 M) at different temperatures	144
Fig. 4.5: Plot of h _{vi} vs n _{avg} for titration of U(VI) with succinate at different temperatures.....	146
Fig. 4.6: Thermodynamic parameters (ΔG _C , ΔH _C , TΔS _C and ΔS _C) for U(VI)-succinate at varying temperatures.	148
Fig. 4.7 Enthalpy entropy compensation in U(VI)-succinate complexation	148
Fig. 5.1: Separation factors for An(III) and Ln(III) using different extractants ..	154
Fig. 5.2: Spectral variation of Ethyl-BTP (1.0x10 ⁻⁴ M) on titration with Eu(III) solution (3.8x10 ⁻⁴) in methanol at I = 0.01 M (TPAN).....	160

Fig. 5.3:	Variation of absorbance for the titration of ethyl-BTP by Ln(III)	162
Fig. 5.4:	Structure of R-BTP	163
Fig. 5.5:	Variation in stability constant with number of carbon atoms (n_c).Symbol: (\square)-water methanol ML_2 , (\circ) methanol ML_2 (Δ) methanol ML_3	165
Fig. 5.6:	Varaition of $\log \beta_{12}$ of Ln(III) complexation with ethyl-BTP at I =0.01 TPAN with Z	167
Fig. 5.7:	Fluorescence emission spectra of Eu(III) (dashed line) and Eu(III)-ethyl- BTP at L/M = 8.3 (solid line)at I = 0.01 M	169
Fig. 5.8:	Schematic representation of Eu(III) sensitization process	169
Fig. 5.9:	Fluorescence emission intensity vs time for Eu(III)-Ethyl-BTP at ligand to metal ratio 8.3 and Eu(III) in methanol and ionic strength, I = 0.01 M	171
Fig. 5.10:	Plot of $1/\tau$ vs. number of BTP molecules (N_{BTP}).....	172
Fig. 5.11:	Calorimetric data for titration of Ethyl-BTP with Eu(III) at I = 0.01 TPAN.....	174

List of Tables

Table 1.1: Nuclear data of long lived isotopes of transuranium elements	25
Table 1.2: Typical calculated composition of high level waste for thermal and fast reactor spent fuel	30
Table 1.3: Electronic configuration of lanthanide and actinide elements	33
Table 1.4: Oxidation states of actinide elements	34
Table 1.5: Stability constants of actinide carboxylate complexes in perchlorate media at 25°C	48
Table 2.1: Specifications of the TAM III calorimeter	78
Table 2.2: Stability constant, enthalpy and entropy of complexation of Sr ²⁺ -18C6 and Ba ²⁺ -18C6 in water ethanol binary mixture	86
Table 3.1a: Experimental conditions for potentiometric titration of metal ions with carboxylates. I = 1.0 M, T= 25°C , Initial volume =20.00 ml.....	96
Table 3.1b: Experimental conditions for calorimetric titration of metal ions with carboxylates. I = 1.0 M, T= 25°C , Initial volume =2.70 ml.....	97
Table 3.2: Thermodynamic data for protonation of carboxylates, at I = 1.0 M and 25 ⁰ C	100
Table 3.3: Theoretically calculated free energies of protonation of unsaturated dicarboxylates	101
Table 3.4: Thermodynamic data for Eu(III) complexation by carboxylates at 25° C and I = 1.0 M	103
Table 3.5: Thermodynamic data for complexation of Eu(III) and U(VI) with maleate and fumarate at I = 1.0 M and 25° C.....	111
Table 3.6: Results of TRFS measurements on Eu(III)-maleate and Eu(III)-fumarate at I= 0.01 M NaClO ₄	116

Table 3.7: Thermodynamic quantities of complexation of Th(IV) with dicarboxylates at 25 ⁰ C, <i>I</i> = 1.0 M (NaClO ₄) (Conditions are given in table 3.1)	124
Table 4.1: Protonation constant for succinate at different temperatures (<i>T</i>) and <i>I</i> = 1.0 M.....	139
Table 4.2: Thermodynamic data for protonation of succinate at different temperatures (<i>T</i>) and <i>I</i> = 1.0 M	140
Table 4.3: Thermodynamic parameters for complexation of U(VI) with succinate (UO ₂ ²⁺ + L ²⁻ = UO ₂ L) at different temperatures (<i>T</i>) and <i>I</i> = 1.0 M	141
Table 4.4: Calculated temperature dependence log <i>K</i> ₁ for U(VI)-succinate (UO ₂ ²⁺ + L ²⁻ = UO ₂ L).....	143
Table 4.5: Effect of temperature on stability constant acetate complexes.....	143
Table 4.6: Δ <i>C_p</i> for uranyl complexes with carboxylates.	143
Table 4.7: Calorimetric data Q _i ^f (J) for U(VI)-succinate complexation reaction ...	144
Table 4.8: Thermodynamic parameters (Δ <i>G_C</i> , Δ <i>H_C</i> and Δ <i>S_C</i>) for complexation of U(VI)-succinate at different temperatures.....	147
Table 5.1: Various ‘N’ and ‘S’ donor extractants evaluated for the separation of trivalent actinides and lanthanides	153
Table 5.2: Theoretical calculation for charge density distribution in alkyl substituted BTPs.	163
Table 5.3: Stability constants for complexation of Ln(III) with Ethyl-BTP in methanol medium.....	164
Table 5.4: Fluorescence lifetimes (τ ₁ and τ ₂) at different ligand to metal ratio.....	171
Table 5.5: Thermodynamic data for complexation of Eu(III) and Tb(III) with ethyl-BTP in methanol medium (<i>I</i> = 0.01 M TPAN).....	174

CHAPTER 1

Introduction

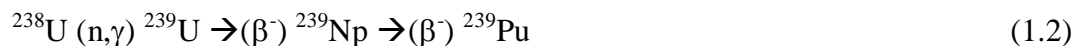
1.1. Introduction to actinides

The discovery of radioactivity by Henry Becquerel in 1896, brought uranium, thorium and other naturally occurring elements to the forefront of research in physics and chemistry in the early twentieth century. However, this research got an impetus after the discovery of neutron by James Chadwick in 1932, when Enrico Fermi initiated the experiments with neutron induced reactions on a range of target elements with increasing atomic number and ultimately thought of producing element 93 by bombardment of uranium ($Z=92$) with neutron followed by beta decay, viz.,



The series of experiments performed by Fermi led to the formation of a large number of radioisotopes and the scene of the study shifted to the laboratories of the renowned radiochemists led by Irene Curie and Frederick Joliot in Paris and Otto Hahn and Lise Meitner, in Berlin. The latter group of Hahn and Strassmann finally unraveled the puzzle of the so many radioisotopes through their discovery of nuclear fission in 1939. Soon, in 1940, element 93 (neptunium) was discovered at University of California, Berkeley, by McMillan and Abelson, and subsequently in 1940-41, the element 94 (plutonium) was discovered by Glenn T. Seaborg et al. The Berkeley group led by Seaborg contributed significantly towards the discovery of higher transuranic elements in the subsequent years, in multiple neutron capture or charged particle induced reactions on lower Z target elements. Based on their chemical properties, Seaborg proposed the actinide concept in 1944 [1], and placed the 15 elements, Actinium (89) to Lawrencium (103) below the lanthanides in the periodic table [2].

The fissile nature of some of the isotopes of Pu (^{239}Pu and ^{241}Pu) led to the production of tones of this element by neutron activation of ^{238}U through the following route.



The process of neutron capture followed by β^- decay results in the formation of higher Z elements, viz.,



and so on [3].

Thus, the burning of uranium in the reactor for generating electricity results in the formation of large quantities of transuranium elements, Np, Pu, Am, Cm, etc., with many of their isotopes having long half-life and decaying by alpha decay. Table 1.1 gives the nuclear data of the long lived isotopes of transuranium elements. Out of these transuranium elements Np, Am and Cm are known as minor actinides (MA) in the spent fuel.

Table 1.1: Nuclear data of long lived isotopes of transuranium elements

Radioisotope	Half-life (years)	Decay mode
^{237}Np	2.14×10^6	α
^{238}Pu	87.74	α
^{239}Pu	2.411×10^4	α
^{240}Pu	6.55×10^3	α
^{241}Pu	14.4	β^-
^{242}Pu	3.763×10^5	α
^{241}Am	432.6	α
^{243}Am	7.37×10^3	α
^{244}Cm	18.11	α
^{245}Cm	8.5×10^3	α

The chemistry of actinide elements is of great importance from the point of view of their migration in the environment, their separation from spent fuel and nuclear waste management.

1.2. Actinides in the environment

The presence of actinides in the environment is a matter of concern owing to their long half life and alpha activity. Actinides have been injected into the environment through different means. Some of these are discussed below.

1.2.1. Nuclear weapon testing

Tones of plutonium have been used in the atmospheric as well as underground nuclear tests conducted by the nuclear weapon countries, during the second half of the 20th century. It is estimated that nearly 10^{20} Bq of plutonium has been dumped in ocean waters [4], most of which has been deposited in the ocean beads, thanks to the highly insoluble nature of the hydroxide of plutonium (K_{sp} of $\text{Pu}(\text{OH})_4 = 10^{-58}$). However, the presence of complexing anions in water results in solublizing plutonium thereby increasing the risk to the living world.

1.2.2. Nuclear power generation

1.2.2.1 Uranium mining and milling

The uranium ore, after crushing, grinding, filtration and chemical treatment is converted into ammonium diuranate (ADU) near the site of the uranium mine. The ADU (yellow cake) is converted to oxide and used for fuel fabrication, while the tailings of the milling process are dumped in specially designed reservoirs, called mill tailing ponds, and contain the large quantities of naturally occurring radionuclides of U, Th and their daughter products Ra, Po, Bi and Pb. There is a finite possibility of leaching of these radionuclides from the tailing ponds to the ground water and thereby to the public domain [5, 6].

1.2.2.2 Fuel reprocessing

The spent nuclear fuel is cooled for a suitable length of time to allow for the decay of short lived fission products. Subsequently it is de-cladded, dissolved in suitable solvent and reprocessed to recover the plutonium and un-burnt uranium which can be used in next generation reactors. The most common process for fuel reprocessing is the Plutonium Uranium Reduction Extraction (PUREX) process [7] wherein U(VI) and Pu(IV) are solvent extracted into 30% tributyl phosphate (TBP) in an inert hydrocarbon diluent, such as, n-dodecane or n-paraffin, leaving the MAs and fission products in the raffinate, which is converted into high level liquid waste (HLW) after concentration and conditioning.

1.2.2.3 Nuclear waste management

The reprocessing of spent nuclear fuel generates different types of waste streams, which are called as, low level waste (LLW), intermediate level waste (ILW) and high level waste (HLW) depending upon the level of radioactivity [8]. LLW is also generated during the normal operation of nuclear power plants and is treated with suitable reagents to precipitate the bulk of the radionuclides [9]. The solid residue is stored in a near surface repository, while the supernatant is discharged after dilution and monitoring. The ILW contains the fission products, such as, ^{137}Cs , ^{90}Sr , etc., at mCi/L level and is given suitable treatment to remove these radionuclides, which are then immobilized in a solid matrix, viz., cement and stored in a near surface repository. For instance, an indigenously developed Resorcinol Formaldehyde Polycondensate Resin (RFPR) is used in repeated loading-elution-regeneration cycles for efficient removal of ^{137}Cs from ILW. A chelating iminodiacetic acid resin is used for the selective removal of ^{90}Sr [10].

1.2.2.4 High level waste (HLW)

During the reprocessing of spent nuclear fuel by PUREX process the aqueous raffinate after first stage of extraction of uranium and plutonium is called High Active Aqueous Raffinate (HAAR). The aqueous solution left after reducing the volume of HAAR by evaporating is termed as HLW, which, though comprises of only 3% of total radioactive waste volume, but contains > 95% of total radioactivity. HLW contains unextracted uranium and plutonium, fission products (Sr, Zr, Mo, Tc, Ru, Pd, Cs, Ba and lanthanides), structural materials, activation products and MA [11]. Typical composition of HLW is given in table 1.2 [12].

The long lived radionuclides of interest from the point of long term surveillance, include, ^{99}Tc , ^{129}I , ^{135}Cs , ^{237}Np , ^{241}Am , ^{243}Am , ^{245}Cm etc., apart from the left over plutonium. MAs viz., Np, Am and Cm are considered most toxic due to their alpha emitting properties and long half life.

1.2.2.5 Deep geological disposal

HLW contains more than 95% of the fission products and MAs produced during the burning of the fuel in the reactor. This waste is presently being vitrified in the borosilicate glass matrix. During the vitrification process, the HLW is mixed with inactive glass-forming additives inside a multi-zone furnace for evaporation. The matrix is calcined, followed by melting at elevated temperature (950-1000°C) and soaking, and finally casting the melt [13]. Waste oxides thus immobilized in the frozen glass matrix are stored inside stainless steel canisters and sealed by remote welding. The waste forms are being stored in an interim storage facility, and after a few decades, are proposed to be buried in a deep geological repository [13]. In the repository, the waste forms are placed in cavities made in the hard rock (e.g., granite) hundreds of meters underground. The vacant space between the host rock and the waste form is filled with the buffer

materials (e.g., clays). Backfill material (clay) is used to close the repository. These engineered barriers are expected to prevent the release of the radionuclides from the repository to the far field areas over hundreds of thousands of years, that is, the time period till the radioactivity has come to the natural level.

However, owing to the decay heat, the radionuclides may diffuse out of the glass matrix. Further, the engineered barriers may be breached due to earth quakes, volcanic eruptions, resulting in the ground water to come in contact with the waste form. Corrosion of the canisters may also lead to the water coming in contact with the glass, and consequently leaching of the radionuclides from the glass matrix to the ground water.

Apart from these, actinides can also enter the biosphere due to reentry of satellites containing ^{238}Pu , use of ^{241}Am in smoke detectors, (Am,Be) neutron sources etc.

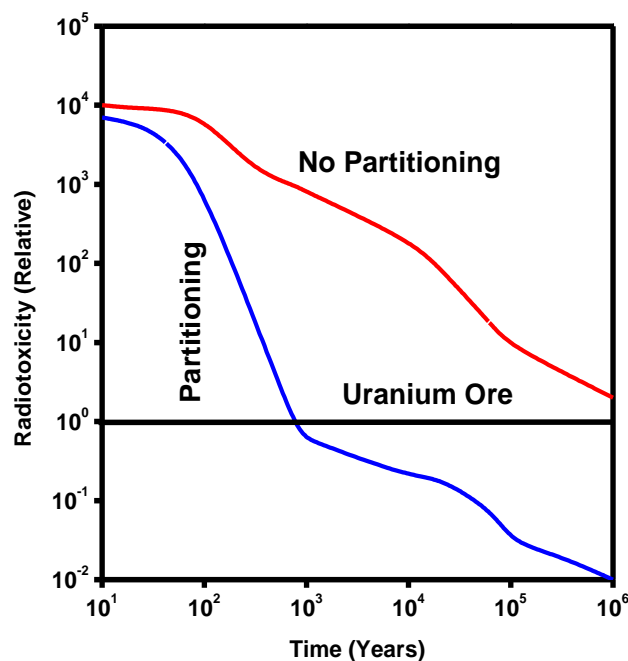


Fig. 1.1: Relative profile of activity of HLW with and without actinide partitioning

Table 1.2: Typical calculated composition of high level waste for thermal and fast reactor spent fuel .

Reactor	Thermal	Fast
Burn up (MWD/t)	6700	150000
Cooling Time (y)	5	1
Volume (L/t)	800	13000
U	6182	500
Np	30	3.4
Pu	23.6	30
Am	52	13.6
Cm	0.09	0.05
Se	14.33	2.81
Sr	210.2	28.6
Y	115	16.5
Zr	906.8	176.3
Nb	--	0.13
Mo	857.6	218.3
Tc	213	57.6
Ru	543.1	212.6
Rh	149.9	68.5
Pd	328.2	167.9
Ag	22.4	19
Cd	19.28	9
In	1.02	0.8
Sn	18	8.96
Sb	4.86	3.35
Te	122.3	31.2
Cs	623.2	275
Ba	379	95
La	309.6	81.8
Ce	613.3	150.6
Pr	285.7	80.25
Nd	1024.8	232.2
Pm	19.2	11.1
Sm	215.6	66.6
Eu	26.45	10.1
Gd	22.9	6.23
Tb	0.62	0.58

1.2.2.6 Partitioning and transmutation (P&T)

Due to long half life of minor actinides (MAs), these radionuclides are responsible for radioactivity of HLW after 10^3 y. Thus, the presence of MAs in HLW to be buried in geological repository, requires its long term surveillance. Figure 1.1 shows the variation in radiotoxicity of HLW with and without actinide partitioning [14]. Thus it can be seen that separation of MAs from the HLW will bring down its alpha radioactivity to such a low level that its long term surveillance might not be needed thereby minimizing the cost as well as the risk associated with its long term impact on the living world. Minor actinide partitioning is, therefore, one of the important steps in the management of HLW. P&T is an alternative strategy to get rid of actinides from HLW. It involves separation of actinides from HLW and transmuting them to short lived radionuclides by nuclear fission, in the accelerator driven sub-critical (ADS) reactor system. In ADS, a high energy (~1000 MeV) proton accelerator is used to bombard the liquid metal target (Pb,Bi) to produce spallation neutrons (each proton generating tens of neutrons) which are subsequently used to induce fission in the MA target as fuel. The energy released in the fission of these MAs can be used to run the ADS system, thus resulting in a self sustaining burner of MAs [15].

1.2.2.7 Actinide partitioning

Several extractants have been proposed and evaluated for the separation of actinides (U, Pu, Np, Am, Cm) from the HLW by different groups worldwide. Notable among these are the diamides viz., N,N'-dimethyl-N,N'-dibutyl tetradecyl malonamide (DMDBTDMA), N,N'-dimethyl-N,N'-dioctyl-2-(2-hexylethoxy) malonamide (DMDOHEMA), tetraoctyl diglycolamide (TODGA), tetra (2 ethyl hexyl) diglycolamide (TEHDGA), and derivatives of phosphoric and phosphinic acids viz., octyl(phenyl)-N,N-diisobutyl carbamoyl methyl phosphine oxide (CMPO), Di 2-ethyl

hexyl phosphoric acid (HDEHP) etc. Significant progress has been made in this direction and pilot plant scale operations are underway worldwide [16].

1.2.2.8 Lanthanide Actinide separation

The minor actinides separated from HLW are accompanied by lanthanides due to the similar chemical properties of trivalent actinides (An(III)) and lanthanides (Ln(III)). Therefore, during the partitioning of actinides with various ligands like CMPO, TEHDGA, TODGA etc, lanthanides are also extracted along with actinides. Due to high neutron absorption cross-section of lanthanide ($^{155, 157}\text{Gd}$, $^{147, 149}\text{Sm}$ etc), the presence of lanthanides may reduce the transmutation efficiency. Further, lanthanides might also interfere in the glass formation process with the HLW, as they do not form solid solution with the raw materials of glass and segregate in separate phase with the tendency to grow under thermal treatments. Thus, lanthanide-actinide separation is a key step in actinide partitioning. Several soft (S,N) donor ligands are being investigated to separate Ln(III) from An(III). The S donor ligands, e.g., Cyanex 301 have good separation factor for An(III) over Ln(III) but can not be used at higher acidity of the aqueous feed solution [17]. Nitrogen donor ligands show promise to be used at higher acidity of the feed solution, however, the kinetics of the extraction process appears to be slow [18].

1.3. Chemistry of actinides

1.3.1. Electronic Configuration

The actinide hypothesis was advanced by Seaborg, according to which successive electrons are added to the inner 5f shell beginning with thorium and ending with lawrencium. In the lanthanide series, fourteen 4f electrons are added beginning formally with cerium (Z=58) and ending with lutetium (Z=71). This hypothesis proposed before the discovery of heavier actinides, greatly facilitated the search for new

elements. The first member of the lanthanides series (La) does not have any 4f electron, and has electronic configuration, $6s^2 5d^1$. In the case of lanthanides, the 4f orbital becomes appreciably lower in energy compared to 5d orbital immediately after La. Consequently the electrons fill the 4f orbitals in a regular manner among the lanthanides (except in the case of half filled 4f shell). However, in the case of actinides the difference between energies of 5f and 6d orbitals is very small for the first four elements, Th, Pa, U and Np. Consequently, electron may occupy either 5f or 6d or both. Only in the latter actinides, the 5f orbital gets appreciably lower in energy than 6d and hence from Pu onwards 5f shell is filled regularly [19] as shown in table 1.3.

Table 1.3: Electronic configuration of lanthanide and actinide elements

Lanthanides			Actinides		
Element	Atomic number	Electronic configuration	Element	Atomic number	Electronic configuration
La	57	$5d^1 6s^2$	Ac	89	$6d^1 7s^2$
Ce	58	$4f^1 5d^1 6s^2$	Th	90	$6d^2 7s^2$
Pr	59	$4f^3 6s^2$	Pa	91	$5f^2 6d^1 7s^2$
Nd	60	$4f^4 6s^2$	U	92	$5f^3 6d^1 7s^2$
Pm	61	$4f^5 6s^2$	Np	93	$5f^4 6d^1 7s^2$
Sm	62	$4f^6 6s^2$	Pu	94	$5f^6 7s^2$
Eu	63	$4f^7 6s^2$	Am	95	$5f^7 7s^2$
Gd	64	$4f^7 5d^1 6s^2$	Cm	96	$5f^7 6d^1 7s^2$
Tb	65	$4f^9 6s^2$	Bk	97	$5f^9 7s^2$
Dy	66	$4f^{10} 6s^2$	Cf	98	$5f^{10} 7s^2$
Ho	67	$4f^{11} 6s^2$	Es	99	$5f^{11} 7s^2$
Er	68	$4f^{12} 6s^2$	Fm	100	$5f^{12} 7s^2$
Tm	69	$4f^{13} 6s^2$	Md	101	$5f^{13} 7s^2$
Yb	70	$4f^{14} 6s^2$	No	102	$5f^{14} 7s^2$
Lu	71	$4f^{14} 5d^1 6s^2$	Lr	103	$5f^{14} 6d^1 7s^2$

1.3.2. Oxidation state

Lanthanides exist predominantly in +3 oxidation state as 4f orbitals are too low in energy to participate in bonding. Other than +3, +2 (Eu and Yb) and +4 (Ce and Tb) oxidation states are also present corresponding to vacant, half filled or filled 4f orbitals. Due to the low and comparable binding energies of 5f, 6d, 7s and 7p electrons in early actinides, these elements show variable oxidation states. For instance, plutonium can exist in all the oxidation states simultaneously. As the 5f orbital is less stabilized in early actinides, all of these electrons have low ionization energy leading to f^0 as the most stable configuration (upto uranium). With increase in Z, f orbital gets more stabilized compared to 6d and 7s orbitals. Later actinides (after Americium) behave like lanthanides due to stabilization of 5f orbitals and exhibit +3 as the most stable oxidation state [20]. Table 1.4 gives all the oxidation states of actinides.

Table 1.4: Oxidation states of actinide elements

89	90	91	92	93	94	95	96	97	98	99	100	101	102	103
Ac	Th	Pa	U	Np	Pu	Am	Cm	Bk	Cf	Es	Fm	Md	No	Lr
						(2)		(2)				2	2	
<u>3</u>	(3)	(3)	3	3	3	<u>3</u>								
	<u>4</u>	4	4	4	<u>4</u>	4	4	4						
		<u>5</u>	5	<u>5</u>	5	5								
			<u>6</u>	6	6	6								
				7	7									

Underlined: most stable oxidation state, in parenthesis: exists only in solid state

1.3.3. Coordination number and ionic radii

In case of lanthanides and actinides, the electrons are added to the f orbital with increase in atomic number, which have poor shielding properties due to their diffused character. The effective nuclear charge for the electron cloud increases resulting in the contraction of the atom with increasing Z. This phenomenon of decrease in atomic/ionic size with atomic number among the lanthanides is called lanthanide contraction. Similar

actinide contraction occurs among the actinide atomic/ionic radii [20]. The variation in ionic radii of lanthanides and actinides in +3 and +4 oxidation states is given in figure 1.2.

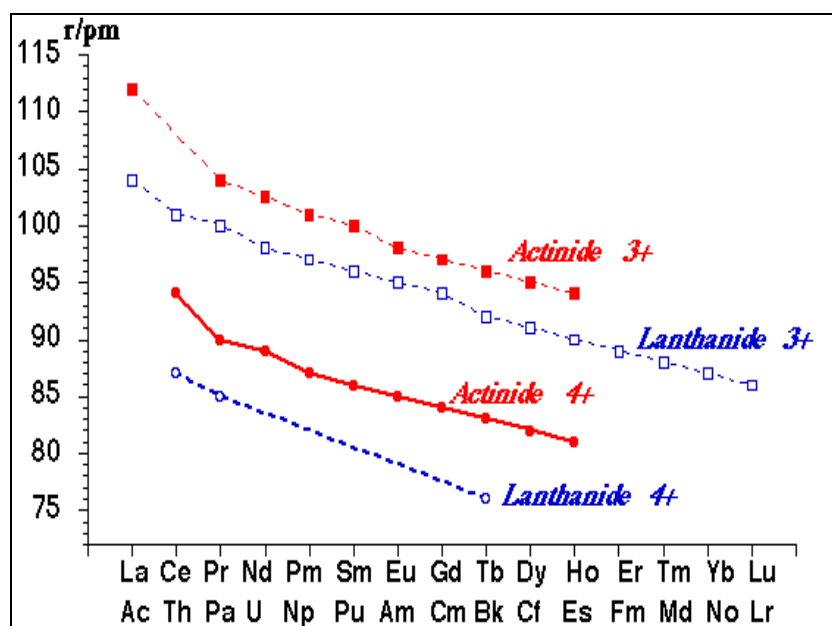


Fig. 1.2: Ionic radii of lanthanides and actinides

Coordination number of trivalent lanthanides (Ln(III)) varies from 6 to 9 depending upon the atomic number of Ln and nature of complexing ligand. For instance, the coordination number of Ln(III) in $\text{HLnEDTA} \cdot 4\text{H}_2\text{O}$ is ten where as that in $\text{KTbEDTA} \cdot 8\text{H}_2\text{O}$ and $\text{KLaEDTA} \cdot 8\text{H}_2\text{O}$ is eight and nine respectively [21]. The variation in physical properties like molal volume, heat capacities and relative viscosities reveal the change in coordination number across the Ln^{3+} series. This has been supported by variation in thermodynamic parameters across the series [22].

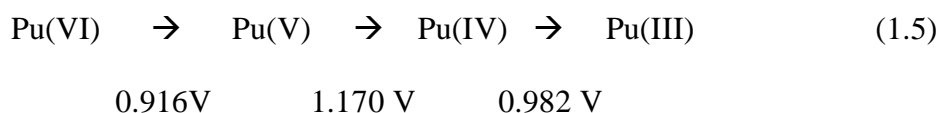
1.3.4. Chemistry of actinides in aqueous solution

Lanthanides and actinides are type A hard acids (like alkali and alkaline earth metals ions) and have strong preference for ‘O’ donor ligands. Chemistry of actinides is similar to that of lanthanides, especially in case of trans-plutonium elements which exist

predominantly in 3+ oxidation state in solution. Lanthanides and actinides do not show strong ligand field effects due to shielding of f orbital by outer orbital (d, s, p) electrons which is more so in lanthanides. However this becomes advantageous as other phenomena can be easily studied in absence of ligand field effects. For example, the cation size varies across the series and thereby the ionic potential, thus the role of cation size and electrostatic interaction can be studied. In absence of ligand, the difference in the complexation behavior of lanthanides and actinides can clearly be attributed to the properties of 4f and 5f orbitals. The lanthanide and actinide ions interact and form solvent structure around them and hence the solvent effects can be best studied [23].

1.3.4.1 Oxidation states in solution

In aqueous solution, actinides are known to exist in a variety of oxidation states (2+ to 7+). The most common oxidation state being trivalent (Am, Cm, etc.), tetravalent (Th, U, Np, Pu), pentavalent (Np, Pu) and hexavalent (U, Np, Pu). However, the stability of a particular oxidation state varies across the actinide series. Some of the actinides show co-existence of several oxidation states in solution, viz., Pu(III), Pu(IV), Pu(V) and Pu(VI), which is due to the small differences in their redox potentials, as shown below (in 1 M HClO₄).



In view of this, the chemistry of different oxidation states of plutonium is often studied using other actinides, e.g., Th(IV), U(VI), which are quite stable in aqueous solution.

Trivalent oxidation state is the most stable form of trans-plutonium actinide ions, (Am onwards) in aqueous solution. Pu(III) is readily produced by reduction, but is slowly oxidized to Pu(IV) by radiolytic products of alpha decay. Tetravalent oxidation

state is the only stable state of thorium in solution, while U(IV), Np(IV) are stable in the absence of oxygen. In the case of plutonium, (IV) state is stable in acidic solution even in presence of oxygen. But it is difficult to maintain high concentration of Pu(IV) owing to its tendency to undergo dis-proportionation reaction. Pentavalent oxidation state is the most stable state of neptunium and protactinium in aqueous solution, though NpO_2^+ disproportionates to Np(VI) and Np(IV) at high neptunium concentration and acidities ($>2 \text{ M HNO}_3$). Pentavalent uranium and plutonium are highly prone to disproportionation, though become stable at low metal ion concentration and high pH. In fact plutonium is known to exist as PuO_2^+ in natural waters. Hexavalent oxidation state is known for actinides from uranium to americium. Uranium exists as UO_2^{2+} in aqueous solutions and is very stable.

1.3.4.2 Hydration of actinide cations

The chemistry of actinide cations in aqueous solution is governed to a large extent by their hydration. The hydration number (h) of the actinide ions, (the number of water molecules that feel the effect of cation), obtained by electrophoretic and diffusion methods, has been found to be more than the coordination number (CN), indicating the coordination of the cation by water molecule beyond the inner coordination sphere [24]. For instance, the value of 'h' and CN for Am^{3+} are 13.6 and 9.0 respectively. The CN undergoes a decrease from 9 to 8 between Am^{3+} and Cf^{3+} (Nd^{3+} and Tb^{3+} , in the case of lanthanides), while 'h' shows correspondingly opposite behaviour from ~ 12.6 to ~ 14 . The increase in the 'h' reflects the increasing ionic potential of the actinide ions of the same oxidation state with increasing atomic number owing to decreasing ionic radius.

While extensive studies have been carried out on the hydration number (h) and coordinated water molecules for the trivalent actinides/lanthanides, similar data for tetravalent actinide ions are limited. The number of water molecules coordinated to

Th⁴⁺ in perchlorate medium was found to be 8-10, while the ‘h’ from conductivity measurements was found to be 20-22 [25]. The hydration of pentavalent and hexavalent actinides is relatively less compared to that of trivalent and tetravalent actinides, owing to their di-oxo cation structure. Optical absorption spectra of NpO₂⁺ are consistent with 5 water molecules in its primary coordination sphere while Raman spectra of uranyl solutions are best explained with the assumption of six water molecules in the equatorial plane of O=U=O axis [26]. Time resolved laser fluorescence spectroscopy (TRLFS) of Cm(III) and Eu(III) has been extensively used during the last two decades to study the primary coordination number of trivalent actinides/lanthanides. An empirical relationship was proposed by Kimura and Choppin [27] for calculating the number of water molecules in the primary coordination sphere (N_{H₂O}) from the fluorescence decay constant (k),

$$N_{H_2O} = 0.65k - 0.88 \quad (1.6)$$

for Cm(III) and similar expression was proposed for Eu(III). The technique has been found very convenient to study the dependence of the N_{H₂O} with pH of the solution as well as the denticity of the coordinating ligand. The determination of hydration number from fluorescence lifetimes makes it possible to characterize Cm(III) species in aqueous solution with high sensitivity, providing valuable insight into the primary structure of the complexes in solution [28].

1.3.4.3 Hydrolysis of actinide cations

Actinide ions having oxidation state +3, +4 and +6 undergo hydrolysis in weakly acidic to alkaline solutions. The hydrolysis reaction can be represented as,



The hydrolysis constant, β_{pq}^* is given by,

$$\beta_{pq}^* = [An_p(OH)_q^{pz-q}][H^+]^q / [An^{z+}]^p \quad (1.8)$$

The driving force for hydrolysis is the polarization of the water molecules by the positive charge of the metal ions resulting in release of proton. This is related to complexation by hydroxide ion,



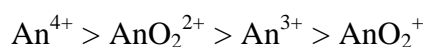
The stability constant for the hydroxide complex,

$$\beta_{pq} = [\text{An}_p(\text{OH})_q^{pz-q}] / [\text{An}^{z+}]^p [\text{OH}^-]^q \quad (1.10)$$

is related to ionic product of water (K_w) by,

$$\beta_{pq} = \beta_{pq}^* / K_w^q \quad (1.11)$$

The strength of hydrolysis among the actinides follows the order,



Complexation by hydroxide competes significantly with that by other anions at higher $\text{pH} > 8$. The stability constants for hydroxide complex formation of Cm(III) have been determined by TRIFS by Fanghanel and Kim [29]. The values are,

$$\log \beta_{11} = 6.67 \pm 0.18 \text{ and } \log \beta_{12} = 12.6 \pm 0.28.$$

Compared to the trivalent actinides, tetravalent actinides are much more susceptible to hydrolysis. In fact, An^{4+} hydrolyse even in acidic solutions with $\text{pH} \leq 2$. Among the tetravalent actinides Th^{4+} is the least hydrolyzed owing to its higher ionic radius and hence is often used as a model for Np(IV) and Pu(IV), which are considerably hydrolyzed even at $\text{pH} \sim 1.0$. The $\log \beta_{1n}$ values for $\text{Th}(\text{OH})_n^{(4-n)+}$ are 11.8, 22.0, 31.0 and 38.5 for $n = 1-4$ respectively, the last value being almost 10 orders of magnitude lower than that for Pu(IV) [30]. In the case of Pu(IV), preparation and maintenance of a solution with only Pu(IV) is a challenge in any experiment on Pu(IV). Consequently the data on hydrolysis constant available in the literature are not consistent. At total Pu(IV) concentrations smaller than 1 mM, plutonium has been found in colloidal form even at $\text{pH} = 0$ to 1.

Pentavalent actinides are least susceptible to hydrolysis, owing to their low ionic potential. Further, the hydrolysis of U(V) and Pu(V) is difficult to study owing to their strong tendency to disproportionate. Only NpO_2^+ is relatively stable and has been used to study the chemistry of pentavalent actinides. It has been found that NpO_2^+ does not hydrolyze even up to pH=8. Hydrolysis of hexavalent actinides decreases in the order $\text{UO}_2^{2+} > \text{NpO}_2^{2+}, \text{PuO}_2^{2+}$, though based on the actinide contraction, the order would have been reversed. U(VI) forms mononuclear hydrolyzed species $\text{UO}_2(\text{OH})_q^{2-q}$ at lower ($<10^{-6}$ M) concentrations, while at higher concentrations, polynuclear species $(\text{UO}_2)_p(\text{OH})_q^{(2p-q)+}$ are formed depending upon the pH and metal ion concentration. The predominant species are dimeric, $(\text{UO}_2)_2(\text{OH})_2^{2+}$, and trimeric $(\text{UO}_2)_3(\text{OH})_5^+$ complexes. The hydrolysis constants for U(VI) are given in [31].

1.3.5. Complex formation

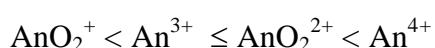
Actinide ions in common oxidation states (+2 to +6) behave as hard Lewis acids. Consequently, they form predominantly ionic compounds having kinetically labile, non-directional bonds. These cations prefer to bind with the hard donor (O, F) part of the ligand. The thermodynamics of actinide complexation is mainly governed by electrostatic attraction between the actinide ion and the ligand, as well as the steric constraints. The electrostatic factor is proportional to the product of the effective charges of the metal ion and ligand divided by the distance between the two. The steric constraint arises due to the property of the actinide cation viz., ionic size and presence or absence of actinyl oxygen atoms, and that of the ligand, viz., number of ligands as well as the number and spatial relationship of donor atoms, size of chelate ring and rigidity.

The steric constraints become dominant in the case of actinyl ions, wherein the ligand can approach the metal ion only in the equatorial plane. This is particularly

important in the case of ligands having rigid structure. An example of this was found in the case of tetrahydrofuran-2,3,4,5-tetra acetic acid for which the stability constant of uranyl complex was found to be two orders of magnitude lower than that for trivalent lanthanides, where there is no steric constraint [32].

The ionic character of the actinide–ligand bonds is evident from the linear variation of stability constant ($\log K$) of actinide amino poly carboxylate complexes as a function of inverse of cation radii [33, 34]. The predominantly ionic bonding in actinide complexes is also evident from the magnitude of entropy and enthalpy of complexation reactions. The large entropy of actinide complex formation is due to the displacement of the water molecules from the inner sphere of actinide ion by the ligand. Part of the entropy is compensated by the endothermic (positive and unfavourable) enthalpy required for dehydration of the reacting ions. In some cases the enthalpy could be moderately exothermic (negative and favorable) owing to the donor atoms and chelate ring size.

The strength of the bonds in actinide complexes follows the order,



provided no steric effects exist.

This order shows that the effective charge (Z_{eff}) felt by the ligand while binding to the actinyl cation is more than the formal charge of the cation, indicating that the oxygen atoms of the actinyl cation retain partial negative charge. The effective charge has been estimated to be +2.2 and +3.2 for NpO_2^+ and UO_2^{2+} respectively [35].

Complexes of actinides show greater degree of covalency compared to that of lanthanides, particularly in the case of ligands with soft donor atoms, viz., S, Cl, etc. This is evident from the large differences in the enthalpy of complexation of trivalent actinides and lanthanides both in aqueous and non-aqueous solutions [36].

Actinide cations can form inner sphere and outer sphere complexes. In aqueous solution, actinide cations are hydrated strongly forming $M(H_2O)_q^{z+}$ type of species. Interaction of the ligand (L^{x-}) with the hydrated metal ion may result in the formation of an outer sphere complex ($M(H_2O)_q^{z+}L^{x-}$) or inner sphere complex ($(M(H_2O)_{q-1}L)^{z-x}$). The formation of outer sphere complex is rapid, while that of inner sphere complex is slow and is the rate determining step [37]. Thermodynamic quantities provide information about the inner sphere and outer sphere complex formation. In the case of outer sphere complex formation, the inner coordination of the metal ion is not affected and cation ligand interaction resulting in exothermic enthalpy with negative entropy. On the other hand, in the case of inner sphere complexation the primary coordination sphere is disturbed significantly resulting in large positive entropy changes which far exceed the endothermic enthalpy changes.

1.4. Environmental chemistry of actinides

Actinides can be released into aquatic environment through milling and mining, release from geological repository, testing of nuclear weapon etc. The determination of chemical speciation is necessary in order to predict actinide migration into the aquatic environment, evaluation of strategies for cleanup operation of contaminated site and safety assessment of georepository. The environment is a complex system containing large number of molecules which can interact with actinides, different types of mineral surfaces and colloids. The actinide behavior in aquatic environment is resultant of various processes like precipitation, adsorption, complexation and colloid formation [38].

1.4.1. Precipitation

Introduction of actinides in water at large concentrations may result in their precipitation as hydroxides, particularly when the metal concentration exceeds the

solubility. Tetravalent actinides e.g Pu(IV) are highly prone to precipitation under natural water condition owing to the very low K_{sp} of $\text{Pu}(\text{OH})_4$ (10^{-58}). Precipitation reduces the concentration of actinide in solution and thus retards the migration process.

1.4.2. Adsorption

Actinides may get adsorbed onto the surfaces of the sediments or rocks in the vicinity of water bodies, thereby retarding their migration. The interaction is mainly by ion exchange and/or complex formation with surface sites. The sediments and rocks contain mostly mineral oxides of Si, Al, Fe etc which determine their sorption characteristics.

1.4.3. Colloid formation

Actinide ions can be associated with two types of colloids, namely, intrinsic and pseudo colloids. Formation of intrinsic colloids occurs through the hydrolysis of actinide ions followed by polymerization of the hydrolysed species. The size of intrinsic colloids has been determined by dynamic light scattering and laser induced breakdown detection technique. Pseudo-colloids are formed as a result of adsorption of actinide particles on to the foreign colloidal particles which are present in aquatic environment as a result of weathering of rocks. The colloid formation is known to significantly enhance the migration process.

1.4.4. Complexation

There are a large number of complexing anions present in the aquatic environment which have strong tendency to bind with actinides. The complexing anion are inorganic (F^- , Cl^- , CO_3^{2-} , SO_4^{2-} and PO_4^{3-}) and organic (acetate, oxalate, humate and fulvate etc.). The complexation process increases the solubility of metal ions in the aquatic environment thereby enhancing their migration.

1.4.5. Humic substances

Humic substances are naturally occurring organic substances that are formed randomly from decay of plant tissues and their properties depend on the ecosystem in which they are formed [39]. These substances play an important role in pH balance and in migration of various organic and inorganic pollutants in the environment. Humic substances are classified as fulvic acid (FA), humic acid (HA), and humins, depending upon their solubility in water. FA is soluble at all pH values, HA is soluble at pH above 3, while humins are insoluble at all pH values. The higher solubility of FA compared to HA is due to its more aliphatic structure and lower molecular weight (300 to 2000 amu). The typical molecular weight for HA of aquatic origin is 1000 to 50000 amu, while HA derived from soil has molecular weight in the range 50000 to 100000 amu. The concentration of HA varies from 0.1mg/l in deep groundwater to 50 mg/l in swamp waters. The concentration of HA in world's oceans is 0.5–1.2 ppm.

HA is considered as polyelectrolyte macromolecule containing hydrophobic part due to its organic back bone and hydrophilic part due to functional groups like carboxylic and phenolic. Figure 1.3 gives the proposed structure of HA. Due to the presence of carboxylic and phenolic groups, HA forms complexes with metal ion and the stability constant of these complexes vary with pH and degree of dissociation. The typical values of $\log K$ for Am(III), Pu(IV), Np(V) and U(VI) at pH 7 are nearly 12, 16, 5 and 8 respectively [38,40]. These stability constants are nearly 100 time higher than that of carbonate. Thus, despite of its low concentration, HA complexation with actinides is important in affecting their migration behavior [41, 42].

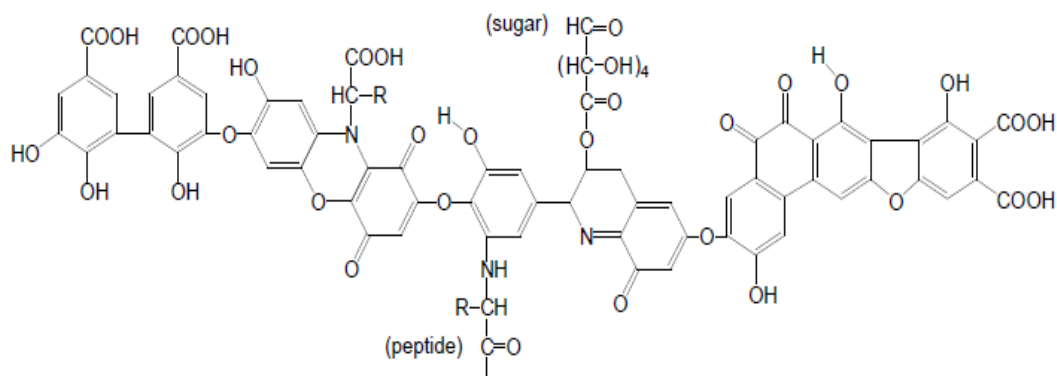


Fig. 1.3: Proposed structure of humic acid

As the humic acid is a complex molecule, its binding with metal ions is still not clearly understood. There are two proposed models, namely, (i) site specific binding model [43] and (ii) poly-condensate model [44]. In site binding model the metal ion binds specifically at different binding sites whereas in poly-condensate model, HA behaves as a large anion interacting with metal ion. As humic acid contains a large number of binding sites having different affinities for metal ions, the complexation studies provide an average picture of binding mechanism. To understand the binding mechanism of actinides to various binding sites of humic acid, simple model compounds containing carboxylic and phenolic groups are used.

1.5. Thermodynamics of complexation of actinides

Thermodynamic studies of actinides complexation reaction are useful in predicting their speciation in any medium. The thermodynamic parameters (ΔG_C , ΔH_C and ΔS_C) for the complexation reactions with naturally occurring ligands help in generating the speciation diagram under different conditions of temperature, pH, ionic strength, metal ion concentration and concentration of complexing anion. The thermodynamic data help

in predicting the dominant species when several complexing anions and metal ions coexist in the solution. In addition, they provide insight into the balance of forces governing the complexation process. It helps in finding out enthalpy and entropy contributions in ΔG_C . The enthalpy contributions are from bond formation and breaking during the reaction whereas entropic contribution is due to order/disorder of the solution as a whole. For a complexation process in aqueous solution, where metal ions are hydrated by water molecules, ΔH_C is the resultant of dissociation of bond between the metal ion and water molecules and bond formation between metal ion and ligand.

$$\Delta H_C = \Delta H_{\text{metal-ligand}} - \Delta H_{\text{metal-water}} \quad (1.12)$$

ΔS_C of complexation process is determined mainly by dehydration process, which increases the randomness of the system by releasing highly oriented water molecules in the bulk water, and conformation change of ligand during complexation. In the case of highly hydrated system, the dehydration term dominates ΔS_C . In the case of outer sphere complex formation, the inner coordination sphere water molecules of metal ion remains intact and complexation process does not proceed through release of water molecules, consequently the ΔH_C as well as ΔS_C are negative. In the case of inner sphere complex formation, water molecules are released from the inner coordination sphere. Hence along with ΔS_C , ΔH_C also increases as the energy is required for breaking the bond. Thus inner sphere complexes are characterized by positive ΔH_C and $T\Delta S_C$. Higher value of $T\Delta S_C$ compared to ΔH_C makes the overall process feasible.

1.5.1. Actinide complexation by inorganic ligands

As the Ln(III) and An(III) complexation is mainly through electrostatic interaction, the order of stability of the complex increases with the basicity of the ligand. Actinides form weak complexes with halides, except fluoride complexes. The strength of mono-halogeno complexes decreases in the order $\text{Cl}^- > \text{Br}^- > \text{I}^-$ and the

complexes are outer sphere in nature [45]. The general order of stability for actinides of same oxidation state is, $F^- > CH_3COO^- > SCN^- > NO_3^- > Cl^- > Br^- > I^-$. The stability of actinide complexes with inorganic oxo-anions varies in the order, $ClO_4^- < NO_3^- < SO_4^{2-} \ll CO_3^{2-} < PO_4^{3-}$, which is expected from the increasing charge and basicity of the ligands [33]. Normally the stability constants of sulfate, carbonate and phosphate complexes with actinides increase in the order, $AnO_2^+ < An^{3+} < AnO_2^{2+} < An^{4+}$. Carbonate anion plays a dominant role in determining the speciation of actinides in natural water owing to its high concentration and high stability constants of actinide carbonate complexes. The high uranium concentration in sea water is due to the tris carbonato uranyl complex $UO_2(CO_3)_3^{4-}$ [46]. The stability constant of actinyl (VI) tris carbonato complexes decreases by four orders of magnitude from UO_2^{2+} to PuO_2^{2+} owing to the decrease in the effective charge on the actinide.

1.5.2. Actinides complexation by organic ligands

Actinide cations interact strongly with hard donor ligands, e.g., carboxylate anions, which are the most commonly studied complexes of actinides. In the case of soft donor ligands, the actinide hydrolysis competes strongly resulting in the precipitation of actinide hydroxides rather than the complex formation in aqueous solutions. Consequently, complexation of actinides by the soft donor ligands is best studied in non-aqueous solutions. Complexes of actinides by simple carboxylates are stronger than that with sulphate, but weaker than hydroxide and carbonate complexes. Table 1.5 gives the stability constants of some of the actinide carboxylate complexes in perchlorate media [23].

The thermodynamics of actinide complexes with monocarboxylates of low basicity resembles those of simple inorganic ligands, that is, the reactions are driven by entropy, with weakly positive or negative enthalpy. In the case of monocarboxylates with low

pK_a , (e.g., dichloroacetate (1.1) and trichloroacetate (-0.5)), outer sphere complexes are formed.

Table 1.5: Stability constants of actinide carboxylate complexes in perchlorate media at 25°C .

Ligand	Actinide	Ionic strength (M)	Log β_{11}	Log β_{12}	Log β_{13}
CH ₃ COO ⁻	Am ³⁺	0.5	1.99	3.28	
	Cm ³⁺	0.5	2.06	3.09	
	Th ⁴⁺	1	3.86	6.97	8.94
	NpO ₂ ⁺	2	0.87		
HOCH ₂ COO ⁻	UO ₂ ²⁺	1	2.42	4.41	6.40
	Am ³⁺	0.5	2.82	4.86	6.3
	Cm ³⁺	0.5	2.85	4.75	
	Th ⁴⁺	1	4.11	7.45	10.1
(COO) ₂ ²⁻	NpO ₂ ⁺	2	1.43	1.90	
	UO ₂ ²⁺	1	2.35	3.97	5.17
	Am ³⁺	1	4.63	8.35	11.15
	Th ⁴⁺	1	8.23	16.77	22.77
(CH ₂ COO) ₂ ²⁻	NpO ₂ ⁺	1	3.71	6.12	
	UO ₂ ²⁺	1	5.99	10.64	11.0
	Th ⁴⁺	1	7.47	12.79	16.3
	NpO ₂ ⁺	1	2.63	4.28	
(CH ₂ COO) ₂ ²⁻	UO ₂ ²⁺	1	5.42	9.48	5.17
	Th ⁴⁺	1	6.44		
	NpO ₂ ⁺	1	1.51	2.14	
O(CH ₂ COO) ₂ ²⁻	UO ₂ ²⁺	1	3.85		
	Th ⁴⁺	1	8.15	14.8	18.2
	NpO ₂ ⁺	1	3.79		
	UO ₂ ²⁺	1	5.11		

As the actinide complexation by hard donor ligands is primarily governed by electrostatic forces, the stability of the complexes is expected to be well correlated with the basicity of the ligand. Considering the ligand basicity as the affinity of the ligand for protons (Bronsted basicity) or that for Lewis acids, the pK_a as well as the complex (M_pL_q) stability constant are directly proportional to the Gibbs energy of reaction,

$$\Delta G_{\text{protonation}} = -2.303 RT pK_a \quad (1.13)$$

$$\Delta G_{\text{complexation}} = -2.303 RT \log \beta_{pq} \quad (1.14)$$

Thus one expects a linear correlation between the stability constant and the ligand basicity (pK_a) called as linear free energy relationship (LFER). Figure 1.4 gives the plot of $\log K$ as a function of pK_a for some of the carboxylate complexes of actinides. Excellent linear correlation has been observed for a range of metal ligand complexes [23]. However, deviations from linearity arise in the case of multifunctional ligands, such as, polycarboxylates, aminopolycarboxylates, hydroxycarboxylates, etc.

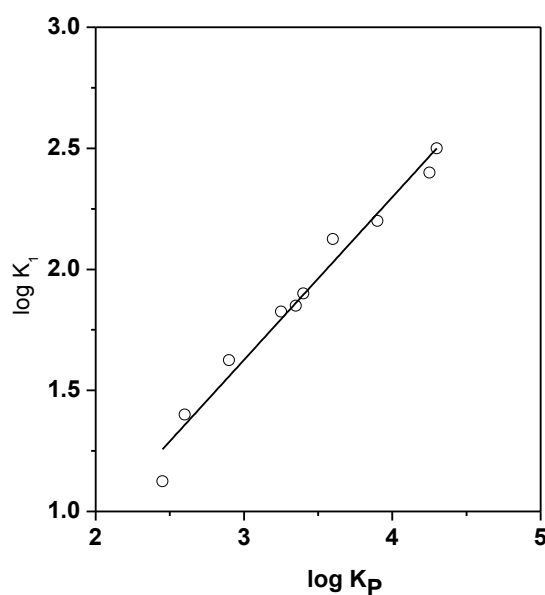


Fig. 1.4: Plot of $\log K_1$ vs $\log K_p$ for U(VI)-monocarboxylates complexation

The linear correlation between the $\log K$ of the complex and the pK_a of the ligand suggests the strongly ionic character of the metal ligand bonds. The electrostatic interaction energy between a metal cation (M^{z+}) and the ligand anion can therefore be given as,

$$\Delta G_{\text{complexation}} (M^{z+}) \propto Z^2/Dr \quad (1.15)$$

Where r is the radial distance between the two charged species and D is the dielectric constant of the solvent. This originates from the Born equation for solvation of a metal ion in solution [47]. Born equation has been modified to estimate and compare the stability constants for actinide ligand complexes [48]. Thus, for cations of same charge, the modified Born equation predicts a linear correlation between the $\log K_f$ and $1/r_{\text{cation}}$. Such a correlation has been observed for actinide and lanthanide complexes with different carboxylate complexes [23].

1.6. Motivation for the present work

Fundamental understanding of the complexation of actinides in solution is of great importance in predicting their migration in the aquatic environment. It also helps in the selection of efficient extractants for the separation of actinides from waste solutions as well as spent fuel. The motivation for the work carried out as a part of this thesis was two fold. (i) Thermodynamics of complexation of actinides and lanthanides with complexing anions of environmental importance. This study is important to understand the speciation and thereby the fate of actinides in the aquatic environment. (ii) Thermodynamics of complexation of actinides and lanthanides with ligands relevant to separation science and technology. This study is important in understanding the underlying phenomena responsible for the selectivity of trivalent actinides over lanthanides.

1.6.1. Complexation of actinides with ligands of environmental importance

Nuclear fuels (Th, U, Pu) have been accepted as a clean source of energy. Mining of Uranium from the earth's crust has resulted in the generation of concentrated regions of uranium in the mill tailing ponds. There is a finite probability of migration of uranium and its daughter products (Th, Ra, Po, etc.) with the rainwater to the underground water table and hence into the biosphere. Like wise when the spent fuel is

reprocessed to recover unspent uranium and plutonium to be recycled, large activity due to minor actinides (Np, Am, Cm) and long lived fission products, (^{137}Cs , ^{90}Sr , $^{99}\text{Tc}^g$, ^{129}I , etc.) are left in the HLW. At present this HLW is being immobilized in a suitable borosilicate glass matrix and stored in an interim storage facility. However, eventually the waste form will have to be buried in a deep geological repository. Though the series of engineered barriers are in place (viz., glass matrix, canister, backfill material and the host rock), over a long period of hundreds of years it is possible that these engineered barriers might get breached and the actinides may come in contact with the underground water. The interaction of the complexing anions (inorganic and organic) present in the underground water will enhance their migration in the aquatic environment. It is, therefore, important to understand the complexation of actinides with the complexing anions present in the underground water. Among the organic complexants, humic and fulvic acid have high affinity for actinides. Further, smaller organic acids, such as, carboxylic acids, can also form strong complexes with actinides and thereby influence their migration.

Though the stability constants of actinides with the common carboxylic acids have been determined, the thermodynamic data of complexation are scarcely available in the literature. These data are required to obtain the stability constants at higher temperatures using Van't Hoff equation, though up to a limited temperature range. For still higher temperatures, prevalent in the vicinity of the nuclear waste repository in the distant future, thermodynamic data need to be measured at elevated temperatures as the enthalpy of complex formation is not constant over such a wide temperature range.

With this in view, thermodynamics of complexation of actinides (U(VI), Th(IV), Eu(III)- as chemical analogue of Am(III) and Cm(III)), with different carboxylates have been determined at room temperature by potentiometry and microcalorimetry. In some

cases, time resolved fluorescence spectroscopy (TRFS) has also been used to determine the log K as well as the stoichiometry of the complexes. Thermodynamics at elevated temperatures have also been studied in the case of a dicarboxylate anion.

1.6.2. Complexation of actinides and lanthanides with ligands relevant to separation science and technology

Another thrust area wherein intense research activity is focused worldwide is the separation of trivalent actinides (An(III)) from lanthanides (Ln(III)), which get separated along with the former during the actinide partitioning stage in the back end of nuclear fuel cycle. The lanthanides, owing to their high neutron absorption cross section and higher concentration than minor actinides (Am, Cm) will reduce the transmutation efficiency. It is, therefore, essential to separate lanthanides from trivalent actinides. For this purpose, use is made of the soft (N, S donor) ligands which have shown higher selectivity for An(III) over Ln(III). The mechanism of this selectivity is not clearly understood, that is, if the selectivity is due to structure or stability of the complex. Recent investigations by extended X-ray absorption fine structure (EXAFS) spectroscopy do indicate the same metal donor atom bond distances in both An(III) as well as Ln(III) complexes, indicating the stability being the main factor for the selectivity. The thermodynamic studies will provide the better understanding of the mechanism of these complexation reactions.

With this in view, thermodynamics of the complexation of Ln(III) with 'N' donor ligands, namely, derivatives of bis-triazinyl pyridine (BTP) have been studied by spectro-photometric and micro-calorimetric titrations. In some cases, TRFS has also been used to study the stoichiometry of the complex.

1.7. Scope of the thesis

The complexation of actinides in solution is not only important in understanding the behaviour of various ligands used in reprocessing of nuclear fuel and management of nuclear waste but also in understanding behavior of actinide ions in environment. The migration of actinides in aquatic environment depends on the various organic and inorganic ligands present in the surrounding media. Humic acid plays an important role in the migration of actinides in aquatic environment. As it is a complex molecule, simple model compounds are used to understand its complexation behaviour. As the carboxylate and phenolate groups are predominant functional groups responsible for metal binding, simple carboxylates are used for complexation studies. In addition simple carboxylates are also present in aquatic environment. The thermodynamic parameters are fundamental properties of particular reaction and provide information about the various interactions involved in reaction.

In the present work, thermodynamic parameters complexation of actinide/lanthanide ions with simple carboxylate ligand of varying functional groups and ligand structure have been determined. These studies provide insight in to the role of various factors like chelation, ring size, basicity, charge polarization and participation of hydroxyl groups in complexation processes. The comparison of these parameters for various oxidation states of actinides also reveals the effect of ionic potential and coordination space on complexation reaction. The TRFS of Eu(III) has been used to obtain information about coordination environment around metal ion which helps in corroborating the thermodynamic parameters.

The thermodynamic parameters for complexation of U(VI) by succinate have been determined at elevated temperatures wherein, the structure as well as dielectric properties of water change. The thermodynamic studies at elevated temperatures also

help in improving basic understanding of coordination chemistry of actinides. The variation in thermodynamic parameters with temperature has been explained on the basis of Born equation.

Thermodynamic studies have been carried out on the complexation of Ln(III) by ethyl-BTP in methanol medium. The results have been compared with the corresponding data for other alkyl derivatives of BTP to reveal the effect of alkyl substituent to the triazinyl ring. These studies will help in understanding the phenomena responsible for selectivity of An(III) over Ln(III).

CHAPTER 2

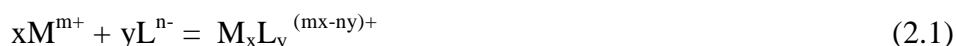
Experimental Techniques

2.1. Introduction

The study of thermodynamics of complexation reactions, entails the measurement of the stoichiometry of the complexes, its thermodynamic stability constants, enthalpy and entropy of complexation. In the present chapter, the details of the experimental technique used for determination of stability constant (potentiometry, spectrophotometry, fluorimetry) and enthalpy (isothermal titration calorimetry) have been described. The methodologies for analysis of data and calibration of the instruments have also been described. The details of the instruments used in the present work are also given in this chapter.

2.2. Stability constants

For a complexation reaction between a metal ion (M^{m+}) and ligand (L^{n-}),



The thermodynamic equilibrium constant (β^0) for the reaction (2.1) can be given by,

$$\beta^0 = \frac{a_{M_xL_y}}{a_M^x a_L^y} \quad (2.2)$$

where ' a_X ' represents the activity of the species 'X'. The activity is related to the concentration (C_X), through the equation,

$$a_X = C_X \gamma_X \quad (2.3)$$

where γ_X is the activity coefficient of the species 'X'. Thus,

$$\beta^0 = \frac{C_{M_xL_y}}{C_M^x C_{L_y}^y} \cdot \frac{\gamma_{M_xL_y}}{\gamma_M^x \gamma_L^y} \quad (2.4)$$

or

$$\beta^0 = \beta \frac{\gamma_{M_x L_y}}{\gamma_M^x \gamma_L^y} \quad (2.5)$$

where β_c is the apparent formation constant of the complex ($M_x L_y$) and is conventionally known as the cumulative stability constant.

$$\beta = \frac{C_{M_x L_y}}{C_M^x C_L^y} \quad (2.6)$$

The measured β is corrected for the activity coefficients of the reacting species to obtain the β^0 . This can be achieved by three means.

- i) Carrying out the experiments at the infinite dilution so that the activity coefficients are equal to unity and hence $\beta^0 = \beta$ (equation 2.4). Measurements at such low concentrations are possible in a few cases, viz., electrical conductivity. However, in most cases, it is not practical to work at such low concentrations.
- ii) Calculation of activity coefficient theoretically: Debye Huckel theory is used for calculation of activity coefficient at low ionic strength. However, the equation can be applied to simple ions. For large size ligands, the calculations are not accurate enough to provide a reasonable estimate of the activity coefficient.
- iii) Measurement of β at various ionic strengths and extrapolation of the β data to zero ionic strength. This is the most widely used method. Extrapolation of $\beta(I)$ to $\beta(0)$ is done by following different prescription namely specific ion interaction theory, Pitzer model etc.

2.2.1 Specific Ion Interaction Theory (SIT)

The activity coefficient is related to the ionic strength (I_m) by the following SIT expression.

$$\log \gamma_i = -z_i^2 D(I_m) + \epsilon_i I_m \quad (2.7)$$

z_i is valency of ion 'i', D is Debye Huckel coefficient and is given by

$$D = 0.509 (I)^{0.5} / (1 + B (I_m)^{0.5}) \quad \text{where } B = 1.5 \quad (2.8)$$

First term corresponds to Debye Huckel term and is important at low I_m and accounts for long range electrostatic interactions. ϵ_i is SIT parameter for i th species which accounts for short range non electrostatic interactions between i th and other species in the system. The SIT parameters are assumed to be zero for interaction of ions of same charge and neutral species as these species are usually far apart and no short range interactions are possible among them [49]

Using above equations 2.5 and equation 2.6, β^0 and β can be related by,

$$\log \beta^0 = \log \beta - \Delta z^2 D + \Delta \epsilon_i I_m \quad (2.9)$$

2.2.2 Pitzer model

The SIT theory has been found to explain the experimental data on ionic strength dependence of β_C upto $I_m = 1.0$ M. Beyond this ionic strength, Pitzer model has been proposed to explain the ionic strength dependence of β . In Pitzer model explicit function is developed which relates ion interaction coefficient to I_m . The activity coefficient for single electrolyte solution is given as;

$$\ln \gamma = |z_M z_X| f^\gamma + m \frac{(2\nu_M \nu_X)}{\nu} B_{MX}^\gamma + m^2 \left(\frac{2(\nu_M \nu_X)^{3/2}}{\nu} \right) C_{MX}^\gamma \quad (2.10)$$

where ν_M and ν_X are the number of M and X ions in formula unit and Z_M and Z_X are their charges. m is the molality of the solution and $\nu = \nu_M + \nu_X$. In aqueous solutions other parameters of equation 2.10 are given as;

$$f^\gamma = -0.392 \left(\frac{\sqrt{I_m}}{1 + 1.2\sqrt{I_m}} + 1.667 \ln(1 + 1.2\sqrt{I_m}) \right) \quad (2.11)$$

$$B_{MX}^\gamma = 2V_{MX}^{(0)} + \frac{V_{MX}^{(1)}}{2I_m} \left(1 - (1 + 2\sqrt{I_m} - 2I_m) e^{-2\sqrt{I_m}} \right) \quad (2.12)$$

$$C_{MX}^{\gamma} = \frac{3}{2} C_{MX}^{\phi} \quad (2.13)$$

where f^{γ} is the extended Debye Huckel term which includes osmotic effects, $V_{MX}^{(0)}$ and $V_{MX}^{(1)}$ define the second virial coefficient. C_{MX}^{ϕ} defines the third virial coefficient. Pitzer equations have been extended for electrolyte mixtures and the ion interaction terms for the same charge ions have been included. Further details of the model are given in [50]

The stability constant can be expressed either in terms of the molar concentrations (C) or molal concentrations (m), viz.,

$$\beta_m = \frac{m_{M_x L_y}}{m_M^x m_L^y} \quad (2.14)$$

β can be converted into β_m using the density of the solution e.g., in the case of 1M NaClO₄,

$$\beta = \beta_m + (x + y - 1) \times 0.02 \quad (2.15)$$

The stability constant (β) is related to Gibbs free energy (ΔG_C) by following expression

$$\Delta G_C = -RT \ln \beta \quad (2.16)$$

where R is the gas constant and T is the absolute temperature in Kelvin. Expressing free energy in terms of enthalpy and entropy of complexation,

$$\Delta G_C = \Delta H_C - T\Delta S_C \quad (2.17)$$

It can be shown that,

$$\frac{d \ln \beta}{dT} = \frac{\Delta H_C}{RT^2} \quad (2.18)$$

which is the well known Van't Hoff equation. Thus the measurement of stability constant as a function of temperature provides the data on enthalpy of the complexation, and thereby entropy of complexation (cf equation 2.17).

2.3. Determination of stability constant

There are a number of methods which can be used for determination of stability constant.

- i) Potentiometry
- ii) Spectrophotometry
- iii) Fluorimetry
- iv) Calorimetry
- v) Polarography
- vi) Solubility measurements
- vii) Electrical conductivity

In the present thesis, the stability constants are determined by potentiometry, spectrophotometry and fluorimetry. Brief description of these techniques is given below.

2.3.1 Potentiometric titration

The use of potentiometry for determination of $\log \beta$ was introduced by Arrhenius, Ostwald and Nernst [51]. The determination of activity coefficient by Bjerrum, Bronsted and Mc Guinness and theory of strong electrolyte in solution by Debye and Huckel provided exact theory for complexation constant [52]. Abegg and co-workers [53] were the first to determine the stepwise stability constants by potentiometry. I Lenden and J Bjerrum introduced the general method for determination of stepwise stability constants [54]. Bjerrum used this methodology to determine the successive complex formation constants for the amines of a large number of metal ions, and chelate stability constant for the successive ethylene diamine chelates of Fe^{+2} , Co^{+2} , Ni^{+2} , Zn^{+2} and Cd^{+2} [55].

For reactions involving formation of ML , ML_2 ... ML_n complexes with stepwise stability constants $K_1, K_2 \dots K_N$, respectively, the average number of ligands bound per metal ion (n_{avg}) is given by the following equation,

$$n_{avg} = \frac{[ML] + 2[ML_2] + \dots + N[ML_N]}{[M] + [ML] + \dots + [ML_N]} \quad (2.19)$$

which transforms to the following equation.

$$n_{avg} = \frac{K_1[L] + 2K_1K_2[L]^2 + \dots + NK_1K_2 \dots K_N[L]^N}{1 + K_1[L] + K_1K_2[L]^2 + \dots + K_1K_2 \dots K_N[L]^N} \quad (2.20)$$

This equation is called formation function of the system. n_{avg} , can be easily determined using,

$$n_{avg} = \frac{C_L - [L]}{C_M} \quad (2.21)$$

where C_L and C_M are the total concentration of ligand and metal ion respectively and $[L]$ is the equilibrium concentration of free ligand. Thus, the problem of solving the formation function for stability constants is reduced to the solving of a series of simultaneous equations. Calvin and Wilson determined the stability constant by more complicated and rigorous calculation using mass balance equations [56]. The development of computers has led to easy handling of complex systems and also approximations used during the data analysis have been eliminated. A number of softwares are available for potentiometric data analysis e.g Miniquad, BEST, Psquad, Hyperquad [57] etc.

The general methodology for determination of $\log \beta_{xy}$ from potentiometric/ spectrophotometric/ fluorimetric titration data involves following steps.

i) Definition of equilibrium

The first step in potentiometric data analysis is to define a chemical model where a set of probable species are given as input with estimated value to $\log \beta_{xy}$ for the species involved. For instance, in case of actinide carboxylates, different model given as input are (a) Only ML (b) Simultaneous formation of ML, $ML_2 \dots ML_n$ (c) ML, ML_n and M_xL_y . In all the above models mono-protonated and diprotonated ligand were also considered with protonation constant determined in separate experiment.

ii) Speciation calculations

The equilibrium concentrations of all the species involved in reaction are calculated using the defined chemical equilibria and known analytical concentrations at each titration point. The equilibrium concentration calculations involve solving following mass balance equations using Newton Raphson method.

$$C_M = [M] + \sum x\beta_{xy}[M]^x[L]^y \quad (2.22)$$

$$C_L = [L] + \sum y\beta_{xy}[M]^x[L]^y \quad (2.23)$$

where [M] is the equilibrium concentration on metal ion.

iii) Equilibrium refinement

Using equilibrium concentrations, the calculated parameter (pH/ absorbance/ fluorescence Intensity) obtained at each injection is compared with the experimental parameter. The equilibrium constants are refined until the best fit in the calculated and experimental data is obtained. Several chemically possible species (M_xL_y) ($x = 1-2$ and $y = 1-3$) are submitted as input. The specific set of metal complex species where the software program consistently converges (lowest χ^2) is finally considered.

2.3.1.1 Instrumentation for potentiometric titration

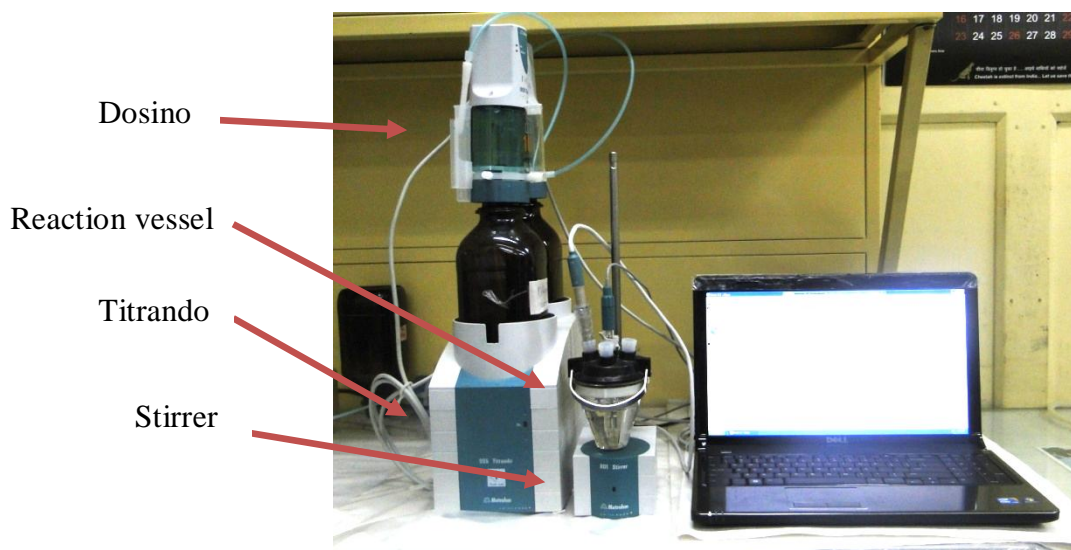


Fig. 2.1: Picture of Metrohm autotitrator 905

The potentiometric titrations were carried out using Metrohm 905 autotitrator. Figure 2.1 shows the photograph of the autotitrator. It consists of following components:

Titrand system: The Titrand is the core of the autotitrator system. Operations are carried out by a computer using software Tiamo. Titrand is connected to different devices, such as, stirrer / stand, dosino and computer, through various measuring interfaces. A measuring interface is used for pH/redox/ISE electrodes and other measuring input for temperature sensor. It also controls the dosing devices through four MSB (Metrohm Serial Bus) connectors.

Metrohm 807 Dosing unit (Dosino): Dosino is a buret unit mounted on the top of the titrant reservoir. The Dosino units of 10 and 20 ml were used. The Titrant is added to the reaction vessel through dosing tube containing antidiffusion tip which prevent outside liquid from diffusing inwards. Titrant is added by the movement of the computer controlled piston. The transparent housing of the dosino helps in visual

monitoring of the piston movement and hence the presence of air bubbles in the cylinder can be observed.

Stirrer: The reaction vessel is placed on a stirrer which provides variable stirring speed and is also controlled by computer

All the Potentiometric titrations were carried out at ionic strength (I) 1.0 M and temperature 298 K using the Metrohm autotitrator. The titrant is added only when the drift is < 0.05 mV/min. The electrolyte solution of the glass electrode (KCl) was replaced by 1 M NaCl solution to prevent precipitation of KClO_4 and hence clogging of the frit. The protonation constant of the ligands were determined by the potentiometric titration of the ligand solution by standard NaOH solution or potentiometric titration of sodium salt of the ligand with standard HClO_4 solution. The acid concentration of the metal ion stock solution was determined by titration of the solution with standard NaOH solution and following Gran's method [58]. In the case of potentiometric titration for complexation constant determination, acidic solution of metal ion was titrated with buffered ligand solution.

2.3.1.2 Electrode Calibration

Calibration of the glass electrode is the most critical part of the potentiometric titration experiments. The calibration requires determination of emf for number of solutions with known concentration of hydrogen ion under constant temperature and ionic strength (I). This is achieved conveniently by titrating the standard acid solution with standard NaOH under same conditions of temperature and I_m . A typical calibration plot of emf (mV) vs pH is given in figure 2.2.

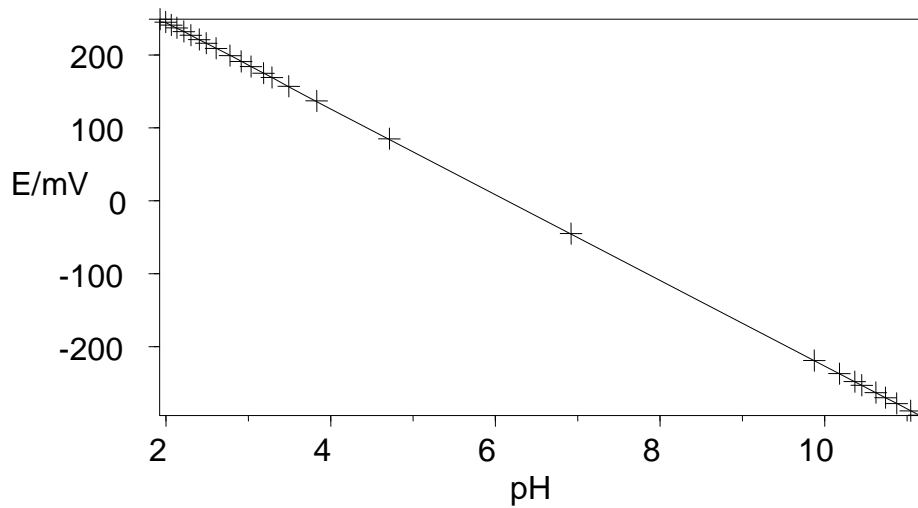


Fig. 2.2: Typical plot of emf vs pH obtained during electrode calibration

The data can be fitted into the following linear equation,

$$E = E_0 + s \ln [H^+] \quad (2.24)$$

which gives,

$$[H^+] = 10^{\frac{-(E_0 - E)}{s}} \quad (2.25)$$

Gran's plot

Gran's plot is used for electrode calibration and to check for impurities in the titrant, for example, carbonate in alkali. In figure 2.3, the electrode calibration is presented in the form of Gran's plot [59]. During the titration of v_0 ml of strong acid ($[H^+]_0$) by strong base ($[OH^-]_0$), following equations will hold at its titration point.

In acidic region

$$\frac{v_0 [H^+]_0 - v_i [OH^-]_0}{v_0 + v_i} = [H^+]_i = 10^{-pH_i} \quad (2.26)$$

At equivalence point

$$\frac{v_0[H^+]_0 - v_i[OH^-]_0}{v_0 + v_i} = 0 \quad (2.27)$$

In basic region

$$\frac{v_0[H^+]_0 - v_i[OH^-]_0}{v_0 + v_i} = [OH^-]_i = -K_W 10^{-pH_i} \quad (2.28)$$

where K_W is ionic product of water.

The $[OH^-]$ can be obtained from the slope of the plot of $(v_0 + v_i) 10^{-pH_i}$ (Gran's function, G) vs v_i . The equivalence point can be obtained from the intercept of the Gran's plot and is given by

$$v_e = v_0 [H^+]_0 / [OH^-]_0 \quad (2.29)$$

The difference in the equivalence point from acid and base side is used to estimate carbonate impurity (CO_2 content) in the base used for the titration.

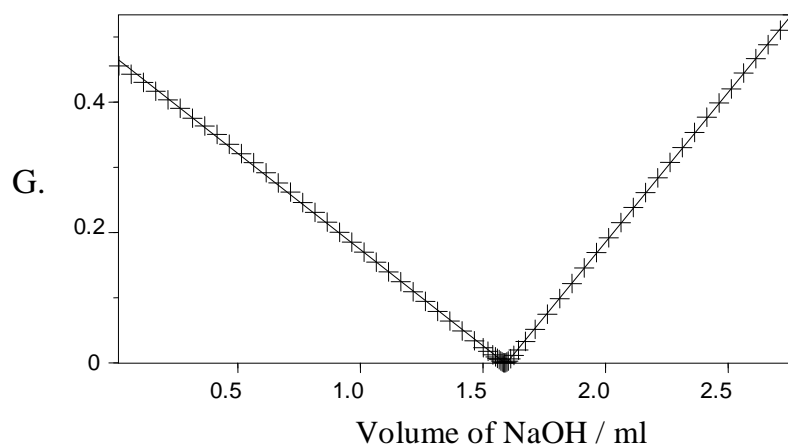


Fig. 2.3: Grans plot for titration of standard $HClO_4$ with standard $NaOH$

In low (< 2) and high (> 12) pH regions, the junction potential at glass electrode becomes important. This is caused by an unequal distribution of ions in the two solutions and the diffusion of the ions across the liquid junction gives rise to an

additional potential. The *emf* (in mV) in acidic and basic regions can be expressed as equation 2.30a and 2.30b respectively (modified Nernst equation)

$$E = E_0 + RT/F \ln [H^+] + \gamma_H[H^+] \quad (2.30a)$$

$$E = E_0 + RT/F \ln K_w - RT/F \ln [OH^-] + \gamma_{OH}[OH^-] \quad (2.30b)$$

where F is the Faraday constant. The terms $\gamma_H[H^+]$ and $\gamma_{OH}[OH^-]$ are the electrode junction potentials for the hydrogen and hydroxyl ions. The calibration gives the parameters E_0 , γ_H and γ_{OH} . Calculation of these parameters allows the calculation of hydrogen ion concentrations from the electrode potentials in the subsequent titrations.

2.3.1.3 Protonation constant of ligand

A typical reaction representing the protonation of a dicarboxylate anion is given as,



The protonation constant, which is a measure of affinity of the ligand towards H^+ , is determined either by titrating the protonated ligand solution with standard NaOH or by titrating the solution of sodium salt of ligand anion by standard acid solution. A typical plot for titration of succinic acid by NaOH at 25⁰ C and $I = 1.0$ M is given in figure 2.4. The methodology for data analysis is described 2.3.1.

2.3.1.4 Stability constant of metal ligand complex

For the determination of stability constant for carboxylate complexes, the acidic metal ion solution is titrated with buffered carboxylate solution. The free acid concentration in metal ion solution is determined by titration of the metal ion solution with standard NaOH and determining end point using Grans method (figure 2.5). The potentiometric data is analysed by Hyperquad 2008 where protonation constant of ligand anion obtained (2.3.1.3) are provided as input. A typical potentiometric titration

plot for complexation of Th(IV)-malonate along with the speciation is given in figure 2.6

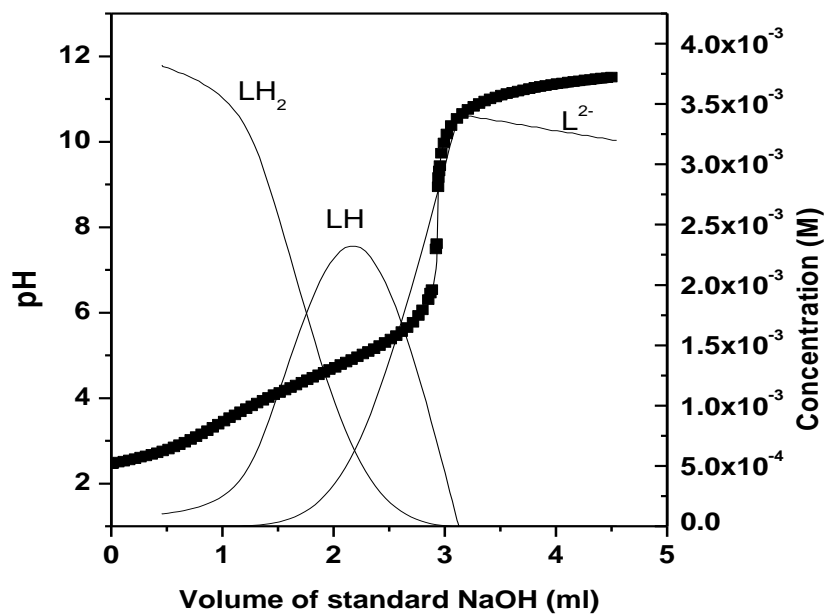


Fig. 2.4: Titration of 20 ml of acidified succinic acid (total ligand = 4.0 mM, total proton = 0.011 M) by standard NaOH (0.0766)

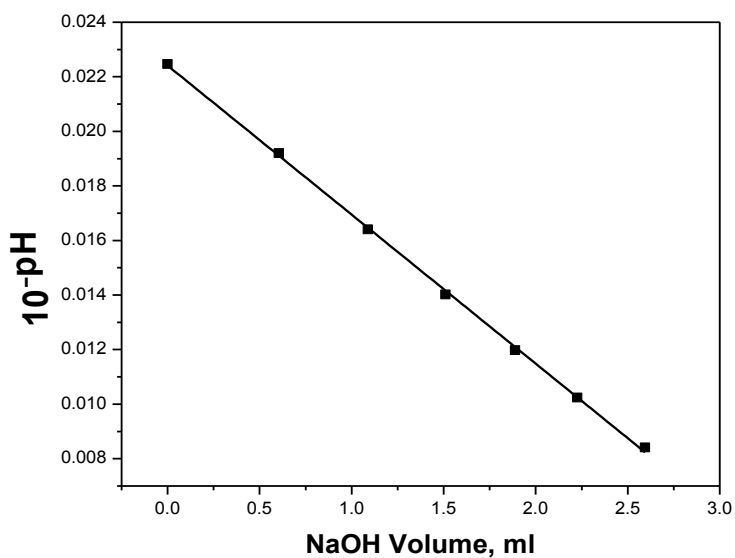


Fig. 2.5: Grans potentiometric plot for acidity determination in Th(IV) solution

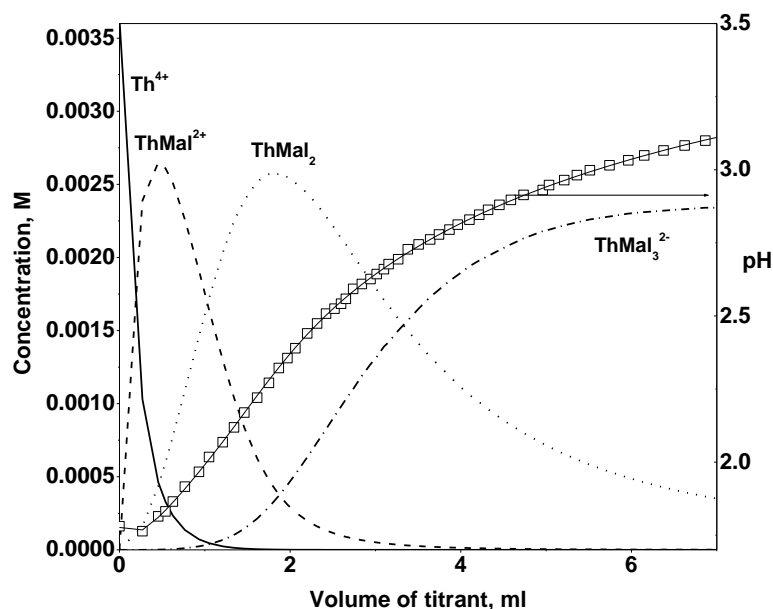


Fig. 2.6: Potentiometric titration data of complexation of Th(IV) with buffered malonate (Reaction vessel: 3.63 mM in 0.0165 M HClO₄, Titrant = total malonate = 0.383 M, total proton = 0.388 M)

2.3.2 UV- vis absorption spectroscopy

Spectroscopic methods are more direct for determining concentration of the species as the characteristic spectra for different species are observed. The spectra observed provide information about the species formed and thus help in defining equilibrium reactions. In addition, using spectroscopic methods, experiments can be carried out at low concentrations of metal ion and ligand, thereby precluding the complication of hydrolysis or polynuclear species.

2.3.2.1 Instrumentation

Measurement of UV-visible absorption spectra is carried out using the spectrophotometer. Modern spectrophotometers employ double beam arrangements, whereby the absorbance is measured through two cells, a reference cell and a sample cell. The reference cell usually contains the solvent used to prepare the solution. A

block diagram of the double beam spectrophotometer is given in figure 2.7. Figure 2.8 shows the photograph of the JASCO V 530 spectrophotometer used in the present work.

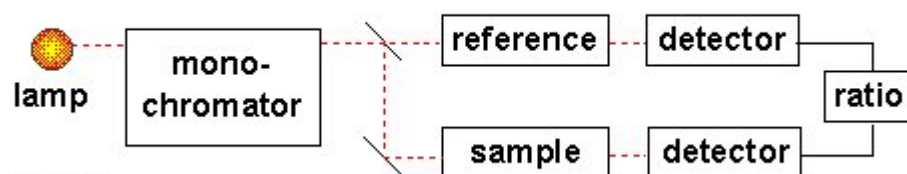


Fig. 2.7: Schematic diagram of double beam spectrophotometer

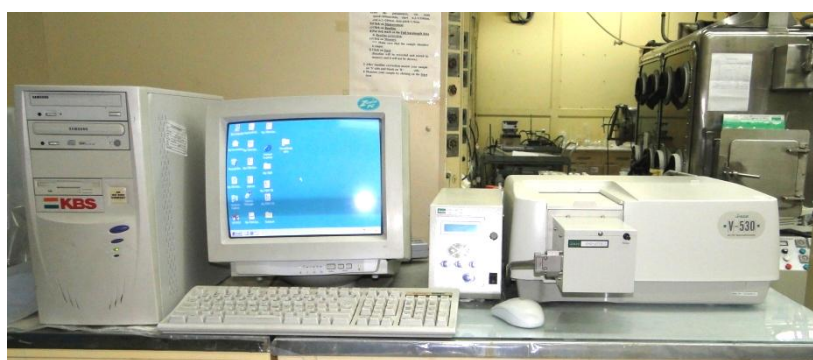


Fig. 2.8: Photograph of the PC controlled spectrophotometer (JASCO V 530)

2.3.2.2 Methodology

The solution to be titrated (titre) is kept in the sample cell and known weight (volume) of the titrant is added to the cell. The absorbance is recorded for the suitable wavelength range at each addition of the titrant. It is assumed that the reaction has reached equilibrium before the spectrum is recorded. During the spectrophotometric titration the complexation of the metal ion by the ligand results in the appearance of absorbance maxima due to the complex and disappearance of the absorbance maxima due to the reacting species. This results in isobestic points in the absorption spectrum. The absorbance, ($A^i(\lambda)$) at a particular wavelength (λ) for i th injection can be related to free concentrations of different absorbing species (C_j^i is the concentration of j th species at i th injection) using Lambert Beer's law.

$$A^i(\lambda) = l \sum \varepsilon_j(\lambda) C_j^i \quad (2.32)$$

where $\varepsilon_j(\lambda)$ is the molar extinction coefficient of j th species.

The matrix $A(N, \Lambda)$ for N titration points and Λ spectral point is solved in conjunction with the mass balance equations for the total metal ion and ligand concentration to obtain the free concentrations of the species and thereby the equilibrium constant. The program Specfit or Hyperquad 2006 are used to analyse the spectrophotometric titration data to obtain the complex stability constants. The methodology for determination of stability constant is same as that for potentiometric titrations (2.3.1).

2.3.3 Time Resolved Fluorescence Spectroscopy (TRFS)

TRFS has become one of the most widely used spectroscopic techniques for studying the complexation reactions during the last two decades. The technique has triple advantage of (i) characteristic excitation wavelength, (ii) characteristic emission wavelength and (iii) characteristic lifetime. This helps in accurate assignment of the complex stoichiometry and structure. [28]. The selective excitation of different species helps in reducing interferences from other species. The fluorescence emission spectra are characteristics of different species involved in reaction.

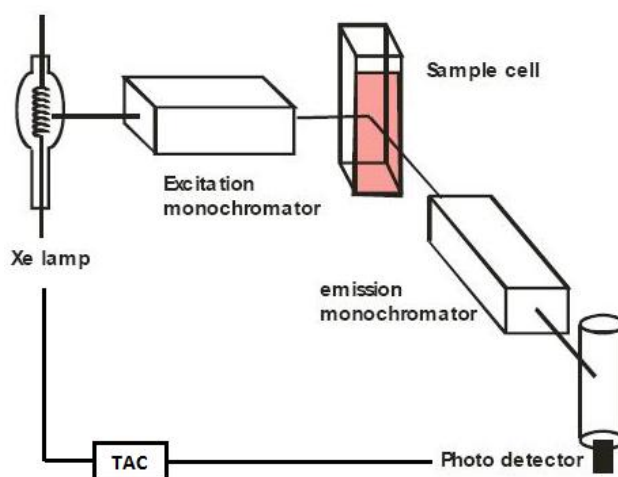


Fig. 2.9: The schematic diagram of TRFS setup.

2.3.3.1 Instrumentation

A schematic of the TRFS instrument is given in figure 2.9. In modern systems, the excitation source is a primary (e.g., NdYAG) laser which pumps another laser (e.g., dye or OPO) to generate the laser photons with wavelength close to excitation wavelength of the system under investigation. In the present work, TRFS instrument from Jovin Yuon (Sweden) is used. The excitation source is a xenon flash lamp having a frequency of 10 and 100 Hz. The monochromators placed before and after the sample are used to select the wavelength of interest. The monochromatic light from the source falls on the 1 cm thick quartz cell and the fluorescence light emitted at 90° is monitored by an array of diode detectors cooled to -26° C by Peltier cooling method. The fluorescence decay spectra are collected in a 2048 channel analyser with a time calibration of 1µs per channel.

2.3.3.2 Methodology

The fluorescence intensity of a luminescent species is proportional to its concentration as explained below.

The intensity of the emission spectrum (F) is proportional to the intensity of the excitation beam that is absorbed ($I_0 - I$) by the sample.

$$F = K'(I_0 - I) \quad (2.33)$$

The constant K' depends upon the quantum efficiency of the luminescence process. Using the Beer's law,

$$\frac{I}{I_0} = e^{-\epsilon Cl} \quad (2.34)$$

$$F = K' I_0 (1 - e^{-\epsilon Cl}) \quad (2.35)$$

Expanding the exponential term as McLaurin series,

$$F = K' I_0 \epsilon C l \left[1 - \frac{\epsilon C l}{2!} + \frac{(\epsilon C l)^2}{3!} - \dots \right] \quad (2.36)$$

For $\epsilon C l < 0.05$, the subsequent terms in above equation can be neglected compared to 1 and hence

$$F = K' I_0 \epsilon C l \quad (2.37)$$

Thus for low concentrations, (absorbance < 0.05) the fluorescence intensity varies linearly with concentration. For large C, such that $A > 0.05$, the higher order terms become important and the linearity is lost.

The first step in the fluorescence spectroscopy is to record the excitation spectrum by fixing the emission wavelength. Subsequently the emission spectrum is recorded by fixing the excitation wavelength (λ_{ex}) corresponding to the maximum absorption in the excitation spectrum. In TRFS, the emission spectrum is recorded as a function of delay time to generate $I(\lambda, t)$, which can be converted into $I(t)$ for selected λ_{em} values. Alternatively one can generate $I(\lambda)$ spectra by selecting different delay times, whereby the emission spectra due to different species can be obtained.

In fluorescence titration, the fluorescence emission intensity at a particular wavelength (λ) for i th injection ($F^i(\lambda)$) is related to the concentration of fluorescing species.

$$F_i(\lambda) = \sum K'_j(\lambda) C_{ij} \quad (2.38)$$

The procedure for determination of stability constant from fluorescence titration is same as that for potentiometric titration (described in section 2.2.1). In the present work, fluorescence spectroscopy was used to determine stability constant of Eu(III) complexes. Eu(III) is a very good fluorescence probe for studying the complexation reactions of lanthanides and trivalent actinides (as an analogue). A typical fluorescence

spectrum of Eu(III) in aqueous medium is given in figure 2.10. A typical decay profile of fluorescence intensity with time for Eu(III)_{aq} given in figure 2.11

The fluorescence decay spectra were fitted into multi-exponential function to obtain the lifetime of the excited ⁵D₀ state of Eu(III).

$$I(t) = \sum_n I_n^0 \exp(-t / \tau_n) \quad (2.39)$$

where I_n^0 is the initial intensity of the nth species having lifetime τ_n . The contribution of each species in the fluorescence (f_n) of can be obtained from,

$$f_n = \frac{I_n^0}{\sum I_n^0} \quad (2.40)$$

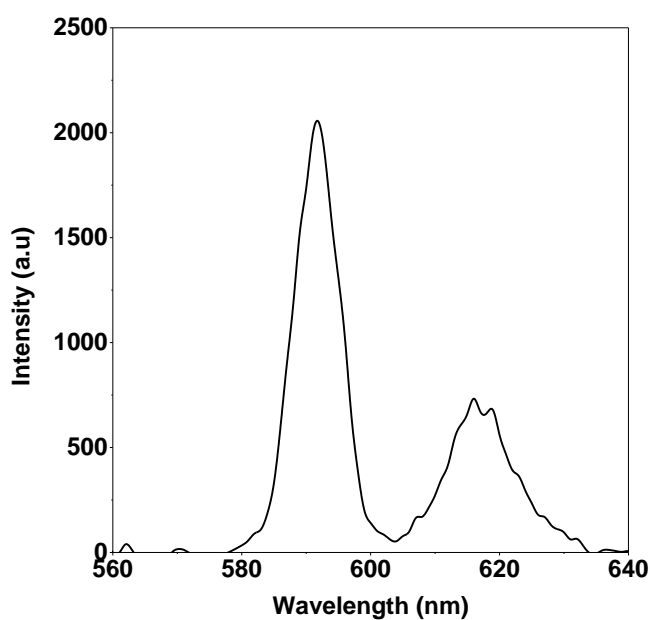


Fig. 2.10: Fluorescence emission spectrum of Eu(III) in aqueous medium

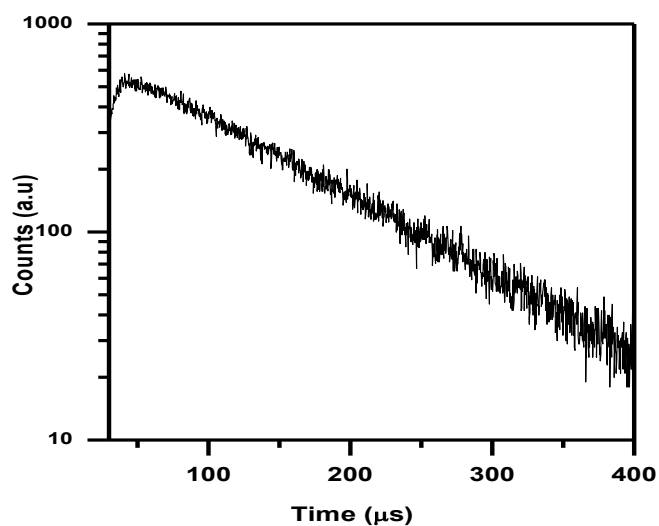


Fig. 2.11: Fluorescence decay of Eu(III) in aqueous medium

In the case of Eu(III) and Cm(III), the fluorescence decay lifetime data have been extensively used to infer about the number of water molecules in the primary coordination sphere of the metal ion. This is due to the fact that the fluorescence decay of 5D_0 excited state of Eu(III) to 7F_j states is quenched by O-H phonons of the H_2O molecules in a non-radiative de-excitation mode. The number of water molecules in turn gives the information about the number of ligands bound to the metal ion and hence the stoichiometry of the complex.

2.4. Calorimetry

Calorimetry involves measurement of heat evolved or absorbed during chemical reaction or physical process. Calorimetry is a direct method of measuring heat changes in a chemical reaction and hence is the best technique to study the thermodynamics of chemical reactions. However, in the case of actinides, the decay heat due to α decay of high specific activity isotopes complicates the data and hence calorimetric

measurements are carried out with long lived isotopes e.g ^{238}U , ^{232}Th or stable analogues such as Eu(III).

The development in calorimetry started in late 18th century when a Scottish scientist Joseph Black recognized the difference between heat and temperature [60]. Though the first primitive ice calorimeter was made by Lavoisier and Laplace, the credit for first modern calorimeter is given to P. E. Brethlot who invented Bomb calorimeter in 1960. He also invented the terms exothermic and endothermic to describe the reaction where heat is released and consumed respectively. Initially, the calorimeters were based on temperature measurements. However, with the development of sophisticated electronics and measuring devices nearly 100 type of calorimeters have been made till now. Thus the classification of these calorimeters on the basis of some characteristics is extremely difficult and calorimeters are classified in large number of possible ways.

2.4.1 Types of calorimeters

Calorimeters are classified in different manner by various authors. Based on the heat changes between the calorimeter and surrounding, they can be classified as adiabatic, semiadiabatic and isothermal [61].

2.4.1.1 Adiabatic calorimeters

In an ideal adiabatic calorimeter no heat exchange takes place between the calorimetric vessel and the surrounding. Figure 2.12 (a) gives variation in T_C with time for ideal adiabatic calorimeter. In case of ideal adiabatic calorimeter, the heat released in the calorimeter increases the temperature of calorimeter by ΔT and the increased T_C remains constant as there is no heat leakage. The heat leakage between calorimeter and surrounding can be reduced by maintaining the temperature difference between sample and surrounding (T_S) close to zero. In order to maintain $T_C = T_S$, the heat is either

released or absorbed from the reaction vessel so as to carry out the reaction under isothermal condition and at the temperature of surrounding.

2.4.1.2 Isoperibole/ Semiadiabatic calorimeter

In isoperibole calorimeters, the surrounding is held at constant temperature ($T_S = \text{constant}$) and heat exchange between calorimeter and surrounding is corrected. Figure 2.12 (b) gives the variation in T_C with time for isoperibole calorimeter. The heat released in the calorimeter increases the temperature of calorimeter by ΔT and decreases at certain rate due to the leakage of heat from calorimeter to surrounding bath.

In adiabatic calorimeters, the heat (Q) is determined by change in temperature.

$$Q = \epsilon_a \Delta T \quad (2.41)$$

where ϵ_a is calibration constant and depends on the heat capacity of the calorimeter.

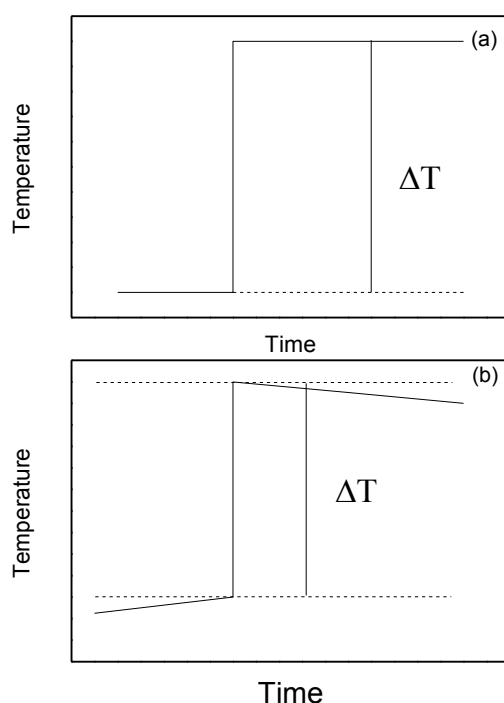


Fig. 2.12: Temperature time curves after a short heat pulse for adiabatic type calorimeter. a) Ideal adiabatic calorimeter b) Semi adiabatic calorimeter

2.4.1.3 Isothermal calorimeter

In isothermal calorimeter the sample and the surrounding are maintained at a constant temperature ($T_C = T_S = \text{constant}$). Isothermal calorimeter can be operated in two modes,

(a) Power compensation mode: The heat absorbed or released during a reaction is compensated by heating or cooling the system, typically using Peltier effect. Thus, measurements in power compensation calorimeter reactions are conducted essentially in isothermal conditions.

(b) Heat conduction mode: In this mode, the heat is allowed to flow from measuring system to surrounding. Heat flow is measured by thermopiles placed between calorimetric vessel and heat sink.

In isothermal titration calorimeter the predetermined volume of titrant is added to reaction vessel and heat on each addition is measured. It is an established and invaluable technique to determine thermodynamic parameters for molecular associations. This technique has been extensively used in the field of biochemistry. The isothermal titration calorimeter has also been used to study actinide complexation with process ligands as well as carboxylates.

2.4.2 Instrumentation

The calorimeter used in the present work (TAM III (Thermometric, Sweden) is an isothermal titration calorimeter (heat conduction type). The specifications of the TAM III calorimeter are given in table 2.1. The design of calorimetric assembly is given in figure 2.13.

Nano-calorimeter TAM-III is twin type calorimeter which contains two vessels, namely a reaction vessel and a reference vessel having capacity of 4 ml each. The reaction vessel is of insertion type in which titration assembly is taken out after each experiment,

cleaned, charged outside and inserted again for next experiment. There are five metallic bolts which are in thermal contact with surrounding. The reaction vessel is inserted into the calorimeter in four steps. At each step the titration assembly is equilibrated for 5 minutes. The differential signals from two vessels are recorded to avoid thermal or electrical disturbances. The heat capacity of the reaction vessel and reference vessel is balanced by keeping the same volume of solutions in both sides in order to minimize the short term noise. The titrant is delivered in the reaction vessel containing, typically, 2.7 ml of titrand, through a stainless steel injection needle (length 1m and internal diameter 1.5×10^{-4} m) connected to the Hamilton syringe containing the titrant. The syringe is driven by Lund Syringe pump. The temperature of the bath is maintained at $25.000^\circ (\pm 0.0001)$ C. Before each experiment the instrument is calibrated electrically and the performance of the instrument is tested by measuring $\log \beta$ and ΔH_C for the reaction between BaCl_2 and 18C6 in water. The heat at each injection is obtained by integrating power vs time graph using TAM assistant program [62].

Table 2.1: Specifications of the TAM III calorimeter

Specifications			
Thermostat		Nanocalorimeter	
Thermal media	Oil	Short term noise	< 20 nW
Temperature Range	15-150° C	Baseline drift	< 50 nW
Accuracy	< 1° C	Accuracy	< 1%
Long term stability	< 50 nW /24 h	Precision	± 100 nW

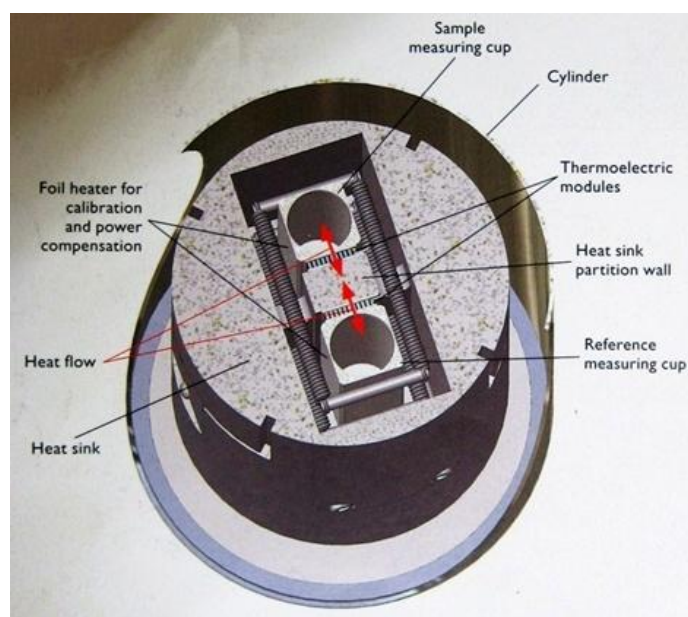
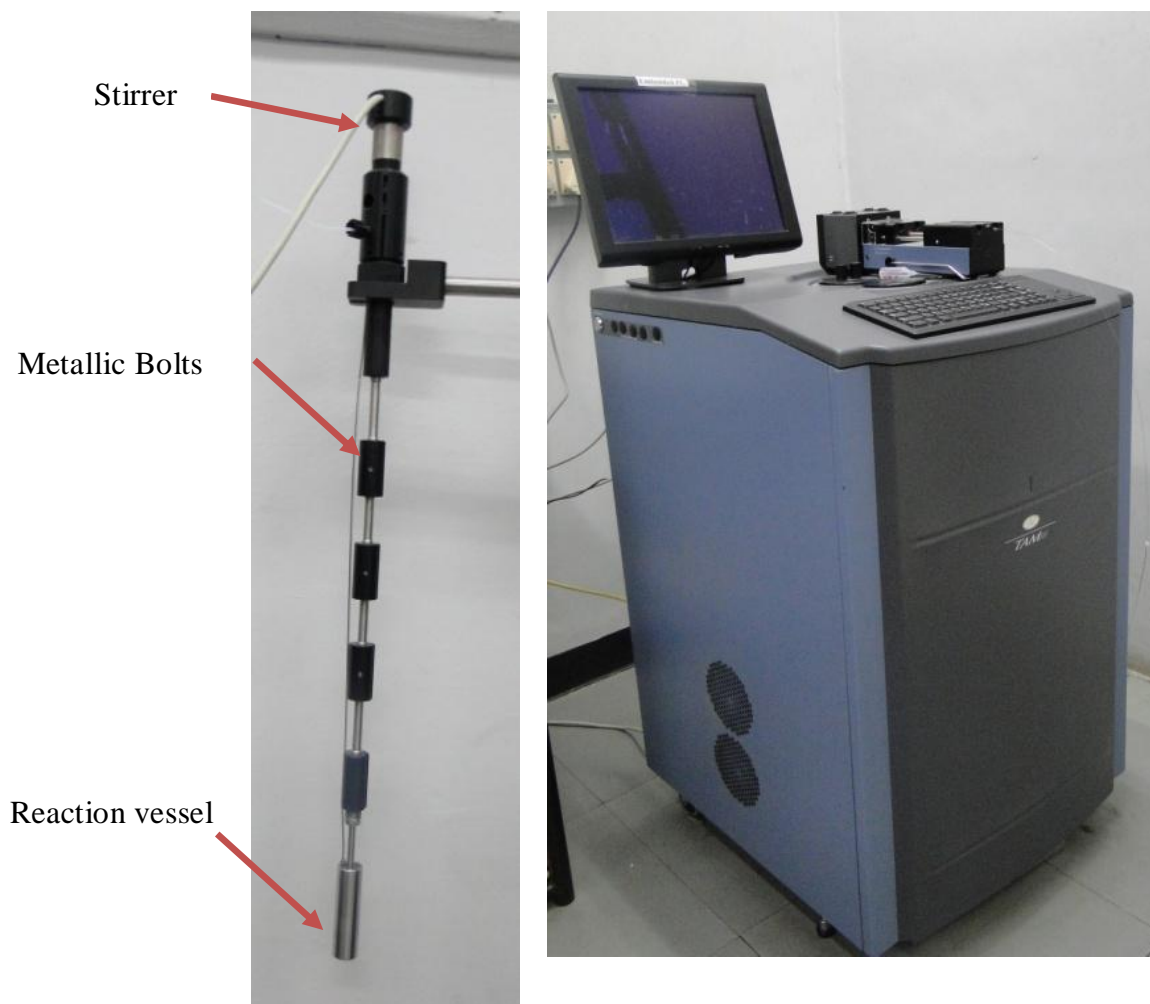


Fig. 2.13: Titration Calorimeter

(a) Picture of titration calorimeter (TAM III, Thermometric Sweden) (b) Titration assembly (c) Cross sectional view of calorimeter

2.4.3 Methodology

The raw calorimetric data consist of thermal power, P, which is related to heat flow (dQ/dt) by the following equation,

$$P = \frac{dQ}{dT} + C \left(\frac{dT}{dt} \right) \quad (2.42)$$

where C is heat capacity of the vessel including its content and half of thermopile and dT/dt is the rate of temperature change of the vessel. The second term corresponds to the heat accumulated temporarily in the reaction vessel owing to its heat capacity. Assuming the complete heat flow through the thermopile, heat flow is related to temperature change by following equation.

$$\frac{dQ}{dT} = G_{tc} n \Delta T \quad (2.43)$$

where G_{tc} is the thermal conductance associated with each thermocouple, n is the number of thermocouples and ΔT is the temperature difference between the calorimetric vessel and heat sink. Thermopile is the device which converts thermal energy to voltage signal. It consists of thermocouples connected in series which work on the principle of Seebeck effect. The voltage (V) generated due to temperature difference (ΔT) is given by,

$$V = ne \Delta T \quad (2.44)$$

where e is the Seebeck coefficient. At constant sink temperature, the equation 2.42 can be written as,

$$P = \frac{dQ}{dT} + C \left(\frac{d\Delta T}{dt} \right) \quad (2.45)$$

Using equation 2.43, one gets,

$$P = G_{tc} n \Delta T + C \left(\frac{d\Delta T}{dt} \right) \quad (2.46)$$

Putting ΔT from equation 2.44, equation 2.46 can be written as

$$P = \frac{G_{tc} V}{e} + \frac{C}{ne} \frac{\partial V}{dt} \quad (2.47)$$

Rearranging equation 2.47, one gets the Tian equation.

$$P = \varepsilon_c \left(V + \tau \frac{dV}{dt} \right) \quad (2.48)$$

where τ is the time constant of the instrument and is given by $\tau = C/(G_{tc}n)$ and ε_c is the calibration constant ($\varepsilon_c = G_{tc}/e$)

Due to thermal inertia of the system, the power vs time graph is often distorted from the actual kinetics of the heat flow and after the each injection, it takes a long time for the power to come back to base value. In order to get the precise kinetic information and reduce the experimental time, power vs time is constructed using “dynamic correction” procedure based on Tian’s equation (2.48). Dynamic correction involves construction of power vs time graph calculated using time constant which is determined from the shape of cooling curve following switching off of electrical heating current. In cases where the sample is solid or not well stirred, extended Tian equation, which includes two time constants is more appropriate [63].

$$P = \varepsilon_c \left(V + (\tau_1 + \tau_2) \frac{dV}{dt} + \tau_1 \tau_2 \frac{d^2V}{dt^2} \right) \quad (2.49)$$

The TAM assistant program used in the present work corrects the power vs time data in a dynamic mode. The heat released, Q , can be obtained by integrating power vs time graph.

$$Q = \int P dt \quad (2.50)$$

Thus integration of equation (2.48) results in

$$Q = \varepsilon_c \int V dt \quad (2.51)$$

Thus the calibration constant of heat conduction calorimeter does not depend on heat capacity of the system. The sensitivity (S) of a heat conduction calorimeter can be defined as

$$S = \frac{V}{\frac{dQ}{dt}} \quad (2.52)$$

Combining equation (2.43, 2.44 and 2.52) one gets,

$$S = \frac{e}{G_{tc}} = \frac{1}{\varepsilon_c} \quad (2.53)$$

Thus, the sensitivity of a heat conduction calorimeter is independent of the number of thermocouples in the thermopile. Figure 2.14 gives a typical power vs time curve for a rapid chemical reaction.

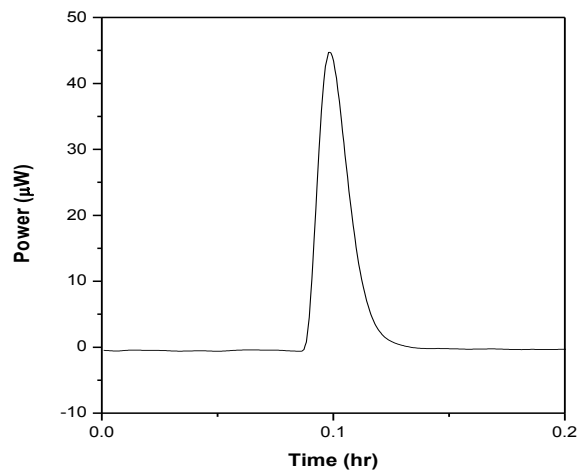


Fig. 2.14: Calorimetric peak for a fast chemical reaction

2.4.4 Calibration of calorimeter

2.4.4.1 Electrical calibration

The signal generated in the calorimeter on release or absorption of heat is in the form of V (voltage across thermopile) vs. time. In order to obtain power vs time using equation 2.48 or 2.49 the calibration constant ϵ_c and time constant (τ)/ time constants (τ_1 and τ_2) need to be determined. Electrical calibration is precise and convenient method for calibration as electrical power can be measured with high accuracy. Electrical calibration can be carried out using insertion heater or permanently installed heaters. Four resistors in series are permanently installed at corners of the reaction and reference vessel of TAM III. A known amount of heat can be supplied to reaction vessel for fixed period of time. The calibration and time constants are determined by fitting power vs time profile in Tian's equation (2.48) /Extended Tian's equation (2.49). These constants are later used for dynamical correction of power vs time graph.

2.4.4.2 Chemical Calibration

In order to test the overall performance of the instrument including testing of its injection system, it is often desirable to carry out the chemical calibration of the calorimetric system. The chemical reaction used for calibration (test reaction) should have well known thermochemical properties. The chemicals used should be readily available in good quality and should not be expensive, hazardous and unstable. Some of the commonly used reactions for calibration of calorimeter are given below [64, 65].

- a) Complexation of calcium by EDTA
- b) Reaction between Ribonuclease A and Adenosine mono phosphate (AMP)
- c) Reaction between 2'-CMP (cystidine 2' monophosphate) and Bovine pancreatic ribonuclease A
- d) Protonation of Tris(hydroxymethyl) amino methane (TRIS)

- e) Dilution of 10% (w) propanol
- f) Dilution of aqueous urea
- g) Acid base titration
- h) Complexation of barium/strontium with 18 Crown 6.

In the present work reactions d, e, g and h were used.

In the case of (1:1) adduct formation reactions, all the thermodynamic parameters (ΔG_C , ΔH_C and ΔS_C) can be determined in single titration. The magnitude of the peaks depends on ΔH_C whereas shape of the curve depends on $\log \beta$. In order to obtain good calorimetric titration profile, the product (P) of stability constant of the complex (β) and the concentration of titrand (C), should be in the range 1-1000 for the chemical reaction. When $P > 1000$, the transition in heat values at equivalence point is too sharp to obtain sufficient points in transition region. In case of reactions with $P < 1$, the titration curve is too broad.

(i) Thermodynamics of Ba^{2+}/Sr^{2+} complexation by 18 Crown 6:

The $\log \beta$ as well as ΔH_C of the complexes depends on the solvent composition due to change in the relative stabilization of metal ion, ligand and complex. Thus, the shape as well as the magnitude of titration profile changes with solvent composition. In order to check the performance of calorimetric system for different ΔH_C and $\log \beta$, the thermodynamic parameters for complexation of Ba^{2+} and Sr^{2+} with 18 crown 6 were determined in different water ethanol compositions with ethanol mol fraction (X_E) varying from 0 to 0.74 [66].

The solution of 18 Crown 6 in binary mixture water – ethanol was titrated with $Sr(NO_3)_2$ and $Ba(NO_3)_2$ solution in the same medium. The concentration of 18 Crown 6 was chosen such that P value is in the range 1 to 100 so as to get good titration profile.

The data analysis was carried out using TAM assistant program. A typical output of calorimeter for the reaction of Sr^{2+} with 18 crown 6 in water is given in figure 2.15.

Typical calorimetric data for complexation of Ba^{2+} by 18 Crown 6 at two water-ethanol compositions ($X_E = 0, 0.42$) are given in figure 2.16. The data were analysed to obtain the thermodynamic parameters ($\log \beta$ and ΔH_C) using the methodology described in next section. The results are given in Table 2.2. The thermodynamic parameters for pure water are in agreement with those reported by Izatt et al [67].

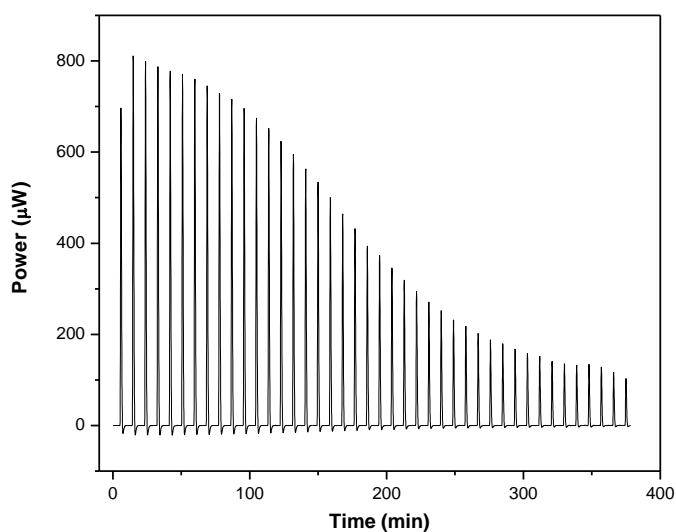


Fig. 2.15: Calorimetric data (Power Vs Time) for titration of 18Crown 6 solution by Sr^{2+} solution in pure water. Cup solution: 2.7ml of 20mM 18Crown 6 in pure water, Titrant: 0.5M $\text{Sr}(\text{NO}_3)_2$ in pure water.

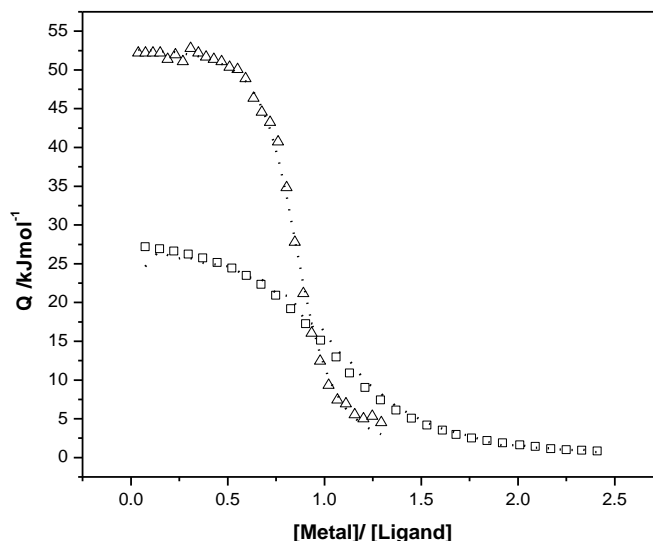


Fig. 2.16: Calorimetric titration curve for Ba²⁺-18Crown 6 complexation

(a) (Symbol: □) Cup Solution: 2.7 ml of 3.8mM 18 Crown 6 in pure water, Titrant: 5μl injection of 0.151 M Ba(NO₃)₂ solution in pure water (b) (Symbol: Δ) Cup Solution: 0.986 mM of 18C6, Titrant: 10 μl injection of 9.966mM Ba(NO₃)₂ solution in water ethanol binary mixture (X_E = 0.42). Dotted line represents the data fitted for *K* and Δ*H*_C.

Table 2.2: Stability constant, enthalpy and entropy of complexation of Sr²⁺-18C6 and Ba²⁺-18C6 in water ethanol binary mixture

<i>X_E</i>	0	0.03	0.12	0.24	0.42	0.74	
Log β	2.74±0.04	3.05±0.09	3.46±0.05	4.00±0.08	4.39±0.30	5.80±0.09	
Sr ²⁺	-Δ <i>H</i> _C (kJ/mol)	14.50±0.96	16.99±0.12	31.00±0.27	31.70±0.3	32.76±0.50	35.57±0.60
	<i>T</i> Δ <i>S</i> _C (kJ/mol)	1.14±0.96	0.42±0.17	-11.25±0.27	-8.87±0.31	-7.70±0.60	-2.46±0.60
log β	3.65±0.09	4.14±0.08	4.56±0.09	5.20±0.09	6.20±0.2	-	
Ba ²⁺	-Δ <i>H</i> _C (kJ/mol)	29.00±0.38	33.10±0.30	43.50±0.35	43.84±0.62	47.9±0.38	-
	<i>T</i> Δ <i>S</i> _C (kJ/mol)	-8.16±0.39	-9.46±0.31	-17.47±0.36	-14.15±0.62	-12.5±0.42	-

2.4.5 Determination of ΔG_C , ΔH_C and ΔS_C

2.4.5.1 Determination of $\log \beta$ and ΔH_C using titration calorimetry

The overall complexation of ligand (L) with metal ion (M^{2+}) is represented by following equation,



The cumulative stability constant of complex ML_n (β_n) is given by,

$$\beta_n = [ML_n]^{2+} / [M^{2+}][L]^n \quad (2.55)$$

Using the following mass – balance equations, the concentrations of free metal ion $[M^{2+}]$ and free ligand $[L]$ can be related to total concentration of metal ion ($C_{M,i}$), and ligand ($C_{L,i}$)

$$C_{M,i} = [M^{2+}]_i + \sum \beta_n [M^{2+}]_i [L]_i^n \quad (2.56)$$

$$C_{L,i} = [L]_i + \sum n \beta_n [M^{2+}]_i [L]_i^n \quad (2.57)$$

The heat Q_i^r measured at each injection is related to the concentration of complexes formed and their enthalpy of formation (ΔH_{Cn}).

$$Q_i^r = -(V_i \sum \beta_n \Delta H_{Cn} [M^{2+}]_i [L]_i^n - V_{i-1} \sum \beta_n \Delta H_{Cn} [M^{2+}]_i [L]_{i-1}^n) \quad (2.58)$$

Nonlinear least square fitting of the Q_i^r data was carried out using equation (2.58), in conjunction with equations 2.56 and 2.57, to obtain the β_n and ΔH_{Cn} values. The first data point (Q_1) is ignored due to the diffusion of the solution from capillary to the reaction vessel even before the first injection.

This methodology can be used reliably for simple complexation reactions only, as the number of unknown parameters increases with simultaneous formation of higher complexes. Also, in the case of reactions where conditions, such as, pH changes during the calorimetric titration, above methodology cannot be used. In such cases, the stability constant needs to be provided using other experimental techniques, such as,

potentionmetry, spectrophotometry etc which can be conducted in parallel or under similar conditions.

2.4.5.2 Determination of ΔG_C , ΔH_C and ΔS_C using potentiometry and calorimetry

In the case of complexation of metal ion with acidic ligands like carboxylates, the complexation process is accompanied by protonation/deprotonation of ligand. Thus, thermodynamic parameters for ligand protonation are required during calorimetric data analysis for complexation. The stability constants and protonation constants are obtained by potentiometric titrations. The methodology for determination of enthalpy of protonation and complexation is given below.

(i) Enthalpy of protonation

The enthalpy of protonation of ligand is obtained by titrating the protonated ligand solution with base or titrating deprotonated ligand anion with acid solution. The net heat obtained in protonation reaction is the sum of the heat due to formation of mono- and di-protonated ligand and also due to heat of neutralization. For instance, the Q_i^r for protonation of dicarboxylate, can be related to ΔH_{P1} and ΔH_{P2} (enthalpy of stepwise protonation) by following relation:

$$\begin{aligned} Q_i^r (Cal) = & \Delta H_{P1} (v_i^{HL} - v_{i-1}^{HL}) \\ & + (\Delta H_{P1} + \Delta H_{P2}) (v_i^{H_2L} - v_{i-1}^{H_2L}) \\ & + (\Delta H_n \cdot \Delta v_{H_2O}) \end{aligned} \quad (2.59)$$

where v_i^X is the number of moles of species 'X' in the cup after ith injection which were calculated using Hyperquad Simulation and Speciation software (HySS 2006).

$$v_i^X = V_i^T [X]_i \quad (2.60)$$

ΔH_n is the enthalpy of neutralization. ΔH_{P1} and ΔH_{P2} is calculated by nonlinear least square fitting of Q_i^r data using equation 2.59. A typical calorimetric titration data for protonation of succinate anion is given in figure 2.17

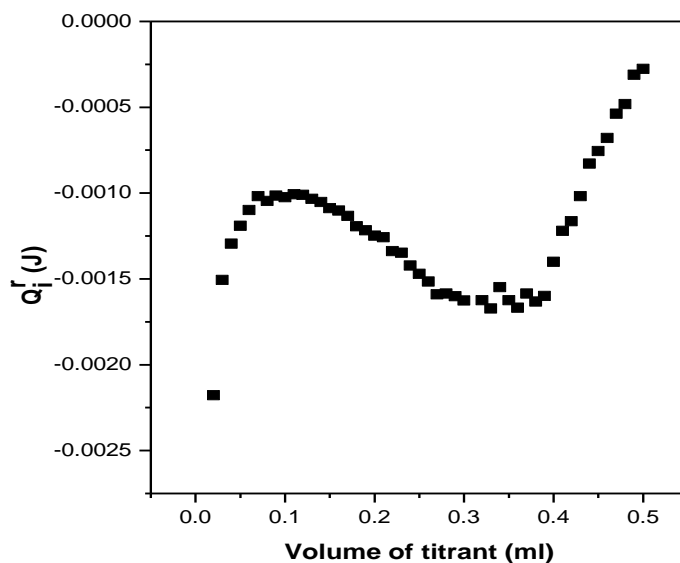


Fig. 2.17: Calorimetric data for protonation of succinate (0.004 M) with 0.0512 M HClO₄

(ii) Determination of enthalpy of complexation

For determination of enthalpy of complexation from calorimetry, the acidic metal ion solution is titrated with buffered ligand solution. The Q_i^r is the resultant of heat involved in formation of different complexes formed as well as protonation/deprotonation reactions. For instance, in the case of metal ion dicarboxylates, where three successive complexes ML_1 , ML_2 and ML_3 are formed, Q_i^r can be related to enthalpy values by following equation,

$$\begin{aligned}
 Q_i^r = & \Delta H_{C1}(v_i^{ML} - v_{i-1}^{ML}) + (\Delta H_{C1} + \Delta H_{C2})(v_i^{ML_2} - v_{i-1}^{ML_2}) \\
 & + (\Delta H_{C1} + \Delta H_{C2} + \Delta H_{C3})(v_i^{ML_3} - v_{i-1}^{ML_3}) + \Delta H_{P1}(v_i^{HL} - v_{i-1}^{HL} - C_{HL}V_i) \quad (2.61) \\
 & + (\Delta H_{P1} + \Delta H_{P2})(v_i^{H_2L} - v_{i-1}^{H_2L} - C_{H_2L}V_i)
 \end{aligned}$$

ΔH_{cj} ($j = 1, 2, 3$) is the stepwise enthalpy of complex formation of 1: j complex. The v_i^X is obtained using software Hyperquad Simulation and Speciation (HySS 2006) using stability and protonation constants obtained from potentiometric titration. The ΔH_{p1} and ΔH_{p2} are obtained from calorimetric titration data obtained in separate experiment (as described above)

The calorimetric data can also be presented in the form of heat per mol of metal ion (h_{vi}) vs n_{avg} . h_{vi} can be calculate using

$$h_{vi} = \frac{\sum_i Q_i^r}{n_M} \quad (2.62)$$

where n_M are the moles of metal ion present in the reaction system.

The experimental techniques described above form the basis of the different studies carried out on actinides and lanthanides complexation by carboxylates and ‘N’ donor ligands described in the subsequent chapters.

CHAPTER 3

Thermodynamics of Complexation of Actinides with Simple Carboxylates: Effect of Ligand Structure and Metal Ion Oxidation State

3.1. Introduction

Complexation of actinides with simple carboxylates is important not only from fundamental point of view but also due to their extensive applications in chemical analysis and decontamination procedures. The migration of actinides is influenced by the presence of organic complexing agents in the natural water system. Carboxylate is the predominant function group present in natural organic ligands. These ligands include some of the simple carboxylates like acetate, oxalate, succinate, etc, as well as complex molecules like humic acid and fulvic acid. Complexation studies with simple carboxylates also help in understanding the binding of actinides with humic and fulvic acid.

The studies on complexation of actinides with carboxylates of varying structure and basicity help in understanding the mechanism of complexation. Though lot of data on stability constants of actinide complexes with carboxylates are available in literature, the complete thermodynamic parameters are scarcely available. These parameters provide deeper insight into the various phenomena involved in complexation process. The interaction of actinides with hard donor ligands is essentially electrostatic in nature and depends on the basicity of ligand ($\log K_p$). The linear free energy relationship between $\log K$ and $\log K_p$ has been observed for carboxylates with single bonding functionality. However, for multifunctional ligands, other factors viz. chelate effect, ring size of chelate, unsaturation, ligand configurational and conformational effects or simultaneous participation of other functional groups etc, also affect metal ligand

binding strength. Consequently, no correlation can universally be applied to actinide complexation by multifunctional ligands.

Kitano et al. [68] studied the complexation of Eu(III) by carboxylates, namely, acetate, glycolate, malonate and malate, at 25⁰C. Extensive studies on complexation of U(VI) by carboxylates are available in the literature. U(VI) complexation by dicarboxylates using calorimetry has been studied by Kirishima et al. [69, 70]. The important conclusions drawn from the above studies are that actinide complexation by carboxylates is driven by entropy, with the enthalpy term being small and endothermic in most cases. Recently our group studied the complexation of Eu(III) by carboxylate anions using time resolved fluorescence spectroscopy (TRFS) [71, 72]. Similar studies had been carried out by Choppin et al. [73] and Wang et al. on aliphatic as well as aromatic dicarboxylates [74, 75]. However, the role of multiple functional groups, chelate ring size, unsaturation and ligand conformation in actinide complexation reactions is not fully understood

The work presented in this chapter describes the effect of (i) functional group (ii) unsaturation and (iii) ring size on complexation of actinides by carboxylates using potentiometry and calorimetry.

(i) In order to study the effect of functional group, thermodynamic parameters for complexation of Eu(III) by different carboxylates namely, acetate, α -hydroxy isobutyrate (α -HIB), succinate and phthalate were determined.

(i) The role of unsaturation and conformation of the ligand was studied in complexation of Eu(III) and U(VI) by maleate and fumarate. Apart from potentiometry $\log K$ and number of coordinated water molecules were also determined by TRFS.

(ii) The role of ring size was studied by determining thermodynamic parameters for complexation of Th(IV) with dicarboxylates of increasing chain length namely,

malonate, succinate, glutarate and adipate having the general formula ${}^{-}\text{OOC}-(\text{CH}_2)_n-\text{COO}^{-}$ (n =1-4).

The thermodynamic parameters of complexation of actinide with carboxylates of different structure were determined using potentiometry, fluorescence spectroscopy and calorimetry. The structure of carboxylate ligands was varied so as to reveal the role of above mentioned factors on complexation process. In some of the cases, thermodynamic results were corroborated by theoretical calculations using GAMESS and TURBOMOL program packages. The structures of the carboxylates studied in the present work are given in figure 3.1

Actinides in various oxidation states are present in solution as M^{3+} , M^{4+} , MO_2^{+} and MO_2^{2+} . The coordination space of M^{3+} and M^{4+} is spherical in nature whereas that in actinyl ions (MO_2^{+} and MO_2^{2+}) is restricted to equatorial plane only. The comparison of thermodynamic parameters of various oxidation states of actinides is expected to reveal the effect of ionic potential and coordination space on complexation reactions. Thermodynamic studies were carried out on complexation of Eu(III), Th(IV) and U(VI) by carboxylates. Due to similar chemical properties of lanthanides and actinides with respect to their binding with hard donor ligands and unavailability of actinides in the concentration range required for potentiometry and calorimetry, Eu(III) was used as a chemical analogue of tivalent actinides. In addition, it can be used as a fluorescent probe for determination of stability constant as well as fluorescence lifetime which in turn provides information about the number of water molecules in the coordination sphere of Eu(III). Th(IV) and U(VI) were used as an analogue of tetravalent (Np(IV) and Pu(IV)) and hexavalent (Np(VI) and Pu(VI)) actinides respectively as Np and Pu are difficult to study owing to their variable valency and high specific activity.

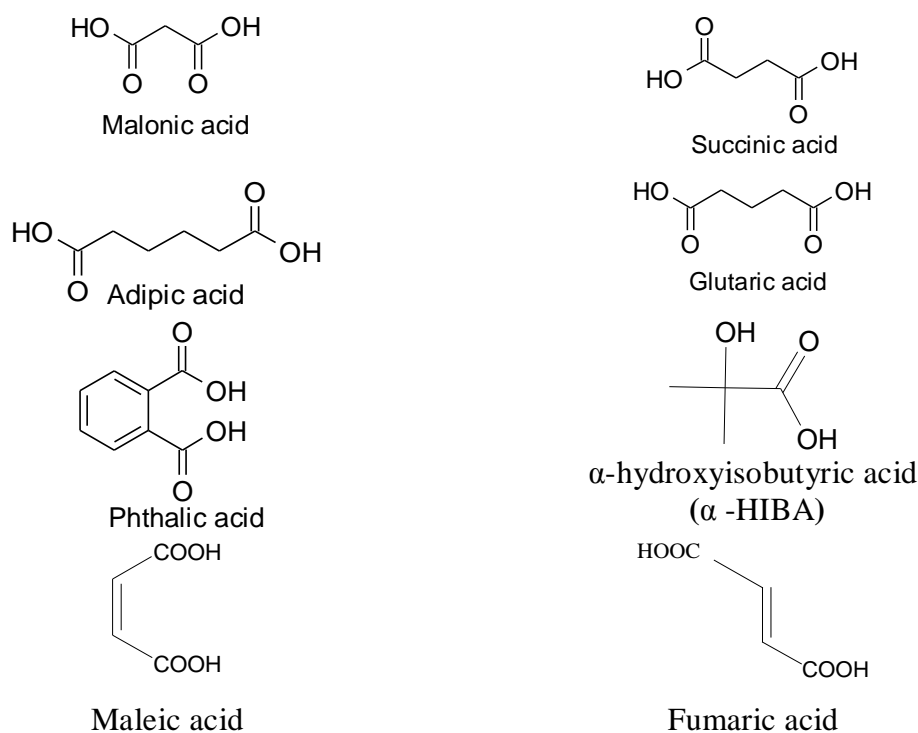


Fig. 3.1: Structure of the carboxylate anions studied for thermodynamic parameters of complexation

3.2. Experimental

The reagents used in the present work were of reagent grade or higher. Solutions were prepared in milli pore water (18.5 M Ω .cm). For determination of protonation constant and ΔH_P , of carboxylates, their sodium salt solutions were titrated with standard HClO₄. The stock solution of Eu(III) and U(VI) were prepared by dissolving Eu₂O₃ and U₃O₈ in HNO₃. Solution was evaporated to dryness. The metal nitrates thus formed were dissolved in HClO₄. The solution was again evaporated to dryness thrice and the residue obtained was dissolved in ~ 0.01 M HClO₄. In the preparation of Th(IV) stock, Th(NO₃)₄·4H₂O was dissolved in water. Th(OH)₄(s) was precipitated by adding NaOH. The precipitate was centrifuged, washed with water and re-dissolved with an excess of perchloric acid. The precipitation and dissolution were repeated three times. The stock solution of Eu(III) and Th(IV) were standardized by complexometric titration with EDTA using Xylenol orange as indicator. The standardization of U(VI) stock

solution was carried out using Davies Gray titration as well as by spectrophotometry using bromo-PADAP as a chromogenic reagent after suitable dilution of the stock solution [76, 77] .

Decarbonated NaOH was used for electrode calibration and for titration of carboxylate solution for determination of their protonation constant. NaOH solution was standardized by potassium hydrogen phthalate as primary standard. For determination of $\log K$, the potentiometric titrations were carried out between acidic metal ion solution with buffered ligand solution. The conditions for potentiometric and calorimetric titrations are given in table 3.1.

The potentiometric titrations were carried out with Metrohm autotitrator 905 having combination glass electrode (cf 2.3.1). The calorimetric titrations were carried out using Isothermal titration calorimeter (TAM III, Thermometric, Sweden). Details of the instruments and data analysis procedures are given in section 2.4.

In the case of Eu(III) maleate and fumarate, TRFS measurements were also carried out to obtain the $\log K$ and stoichiometry of the complexes. The fluorescence emission spectra as well as fluorescence decay lifetime were measured after each addition of ligand solution to the metal ion solution. The details of the instrumentation are given in chapter 2. The fluorescence spectra were analyzed by Hyperquad 2006 to obtain the $\log K$ while fluorescence lifetime was used to obtain the number of water molecules coordinated to the metal ion (as described in section 2.3.3).

Table 3.1a: Experimental conditions for potentiometric titration of metal ions with carboxylates. I = 1.0 M, T= 25°C , Initial volume =20.00 ml

Metal-Ligand	Initial condition of sample Solution in the titration vessel		Titrant solution	
	Metal ion concentration (mM)	Perchloric acid concentration (M)	Total ligand (C _L) (M)	Total Proton (C _H) (M)
Eu(III)-Acetate	7.78	0.012	1.024	0.490
Eu(III)-Succinate	7.78	0.012	0.498	0.576
Eu(III)-Phthalate	7.78	0.012	0.217	0.046
Eu(III)- α -HIB	7.78	0.012	0.999	0.447
Eu(III)-Fumarate	1.00	0.007	0.500	0.186
	3.00	0.012	0.500	0.186
	4.95	0.016	0.500	0.186
Eu(III)-Maleate	3.00	0.011	0.500	- 0.009
	5.00	0.016	0.500	- 0.009
U(VI)- Fumarate	3.00	0.022	0.499	0.150
	5.00	0.023	0.499	0.150
U(VI)-Maleate	0.99	0.022	0.500	0.077
	3.04	0.022	0.500	0.077
	4.99	0.022	0.500	0.070
Th(IV)-Malonate	3.63	0.0165	0.383	0.388
Th(IV)-Succinate	3.63	0.0165	0.401	0.407
Th(IV)-Glutarate	3.63	0.0165	0.198 M	0.000
Th(IV)-Adipate	3.63	0.0165	0.198 M	0.000

Table 3.1b: Experimental conditions for calorimetric titration of metal ions with carboxylates. I = 1.0 M, T= 25°C , Initial volume =2.70 ml

Metal-Ligand	Initial condition of sample Solution in the titration vessel		Titrant solution	
	Metal ion concentration (mM)	Perchloric acid concentration (M)	Total ligand (C _L) (M)	Total Proton (C _H) (M)
Eu(III)-Acetate	7.78	0.012	1.024	0.490
Eu(III)-Succinate	7.78	0.012	0.498	0.576
Eu(III)-Phthalate	7.78	0.012	0.217	0.046
Eu(III)- α -HIB	7.78	0.012	0.500	0.290
Eu(III)-Fumarate	3.00	0.012	0.500	0.186
	4.95	0.016	0.500	0.186
Eu(III)-maleate	3.00	0.011	0.500	- 0.009
	5.00	0.016	0.500	- 0.009
U(VI)- fumarate	3.00	0.022	0.499	0.150
U(VI)-maleate	0.99	0.022	0.500	0.077
	3.04	0.022	0.500	0.077
Th(IV)-Malonate	3.63	0.0165	0.383	0.388
Th(IV)-Succinate	3.63	0.0165	0.401	0.407
Th(IV)-Glutarate	3.63	0.0165	0.198	0.000
Th(IV)-Adipate	3.63	0.0165	0.198	0.000

3.3. Theoretical calculations

The geometry of the unsaturated dicarboxylates and their protonated forms were optimized by density functional methods using the hybrid exchange correlation functional (B3LYP) with the help of GAMESS electronic structure program [78]. Due to the unavailability of small core basis sets for Eu(III) and U(VI) in the GAMESS, calculations for changes in charge distribution upon complexation of Eu(III) and U(VI) by maleate and fumarate were carried out using TURBOMOLE program package [79]. In the case of heavy atoms 28- and 60- electron core pseudo potentials (ECP) along

with corresponding (14s13p10d8f1g)/(10s9p5d4f1g) basis sets were selected for Eu(III) and U(VI), respectively [80, 81]. All other lighter atoms were treated at the all electron (AE) level and the standard def-SV(P) basis sets as implemented in the TURBOMOLE program were used. Geometries of the free fumarate and maleate ligands and their complexes with Eu^{3+} and UO_2^{2+} ions were fully optimized without any symmetry constraint at the density functional level of theory using Becke's exchange functional [82] in conjunction with Perdew's correlation functional [83] (BP86) with generalized gradient approximation (GGA). The charge distribution was calculated by natural population analysis (NPA) in TURBOMOLE.

3.4. Results and discussion

3.4.1 Protonation of ligands

(i) Potentiometry and Calorimetry

The protonation constants ($\log K_P$) for different carboxylates, obtained from data analysis for potentiometric titration, are summarized in table 3.2. The data on enthalpy of protonation (ΔH_P) were taken from literature [69, 84], except for α -HIB and unsaturated carboxylates (Maleate and Fumarate) for which the data were not available under the experimental conditions employed in the present work. The same were determined by calorimetry. The calorimetric titration data for protonation of fumarate and maleate are given in figure 3.2.

The ΔH_P for all the carboxylates are given in table 3.2. The free energy of protonation of carboxylates was determined primarily by the entropy term with the contribution of enthalpy being negligible, indicating the predominant role of solvation / de-solvation of ligand in the protonation reaction. The ΔH_{P1} is more endothermic than ΔH_{P2} for most of the di-carboxylates studied by Kirishima et al. [69] (Table 3.2). The higher dehydration energy associated with the first protonation makes it more endothermic. However

reverse trend was obtained for maleate and phthalate, which could be due to intramolecular hydrogen bonding in mono protonated maleate and phthalate.

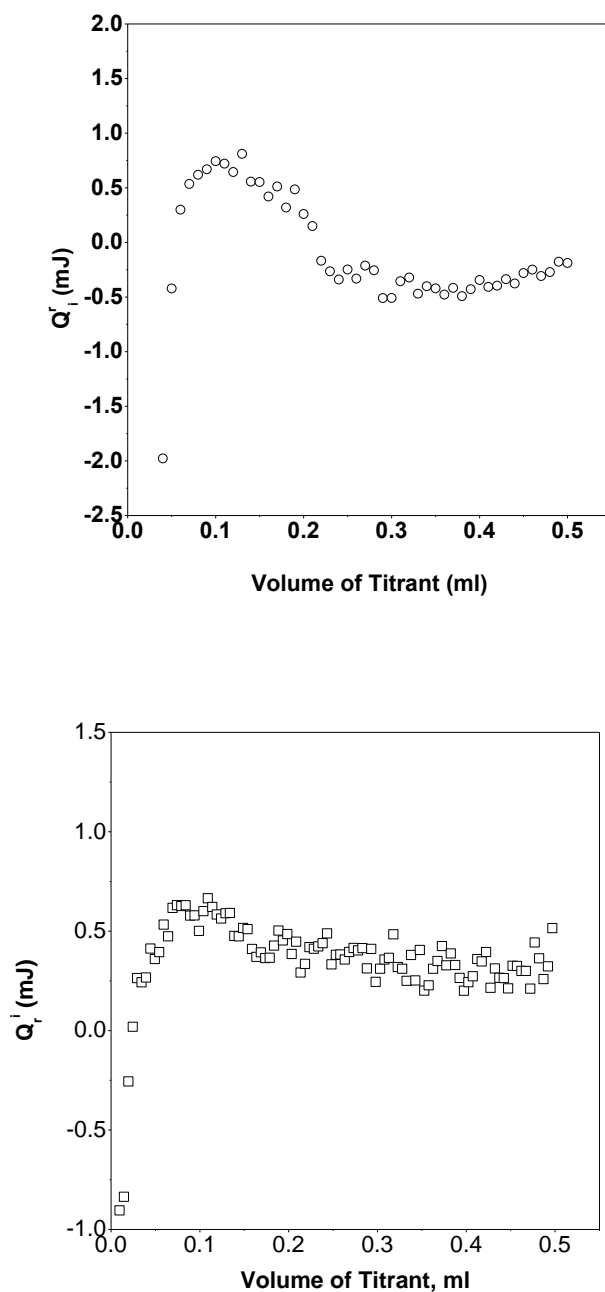


Fig. 3.2 (a): Calorimetric titration of fumarate solution ($C_L = 6.6 \times 10^{-3}$ M, $[\text{OH}^-] = 1 \times 10^{-4}$ M) with 0.098 M HClO₄ (b) Calorimetric titration of maleate solution ($C_L = 4.0 \times 10^{-3}$ M, $[\text{OH}^-] = 1.1 \times 10^{-4}$ M) with 0.098 M

Table 3.2: Thermodynamic data for protonation of carboxylates, at $I = 1.0$ M and 25^0 C

	Reaction	Log K_P	ΔH_P (kJ/mol)	ΔG_P (kJ/mol)	$T\Delta S_P$ (kJ/mol)
Acetate	$L^{2-} + H^+ \rightarrow LH^-$	4.65 ± 0.03 (4.62) ^a	-1.68 ^a	-26.55	24.9
Phthalate	$L^{2-} + H^+ \rightarrow LH^-$	4.66 ± 0.01 (4.61) ^b	0.61 ^b	-26.60	26.0
	$LH^- + H^+ \rightarrow LH_2$	2.66 ± 0.01 (2.64) ^b	1.91 ^b	-15.18	17.09
α -HIB	$L^{2-} + H^+ \rightarrow LH^-$	3.73 ± 0.01	-2.12	-21.29	19.2
Fumarate	$L^{2-} + H^+ \rightarrow LH^-$	3.98 ± 0.01 (4.11) ^c	1.04 ± 0.10	-22.71	23.75
	$LH^- + H^+ \rightarrow LH_2$	2.91 ± 0.01 (2.89) ^c	-1.10 ± 0.12	-16.60	15.50
Maleate	$L^{2-} + H^+ \rightarrow LH^-$	5.66 ± 0.01 (6.16) ^c	0.28 ± 0.06	-32.30	32.58
	$LH^- + H^+ \rightarrow LH_2$	1.70 ± 0.01 (1.95) ^c	1.40 ± 0.20	-9.70	11.10
Malonate	$L^{2-} + H^+ \rightarrow LH^-$	5.15 ± 0.02 (5.09) ^b	1.81 ^b	-29.40	31.2
	$LH^- + H^+ \rightarrow LH_2$	2.53 ± 0.02 (2.59) ^b	-1.6 ^b	-14.43	12.84
Succinate	$L^{2-} + H^+ \rightarrow LH^-$	5.12 ± 0.01 (5.12) ^b	-2.0 ^d	-29.23	27.2
	$LH^- + H^+ \rightarrow LH_2$	3.99 ± 0.01 (4.04) ^b	-4.47 ^d	-23.05	18.58
Glutarate	$L^{2-} + H^+ \rightarrow LH^-$	4.90 ± 0.03 (4.91) ^b	0.51 ^b	-27.97	28.5
	$LH^- + H^+ \rightarrow LH_2$	4.01 ± 0.03 (4.17) ^b	-1.28 ^b	-22.88	21.60
Adipate	$L^{2-} + H^+ \rightarrow LH^-$	4.97 ± 0.01 (4.92) ^b	0.91 ^b	-28.37	29.3
	$LH^- + H^+ \rightarrow LH_2$	4.09 ± 0.02 (4.29) ^b	-0.27 ^b	-23.34	23.07

^a [68] ^b [69] ^c [85] ^d [84]

Table 3.3: Theoretically calculated free energies of protonation of unsaturated dicarboxylates

Ligand	$\Delta E_1(E(LH)-E(L^{2-}))$ (kJ/mol)	$\Delta E_2(E(LH_2)-E(LH))$ (kJ/mol)	$\Delta E_1 - \Delta E_2$ (kJ/mol)
Maleate	-1857.21	-1336.53	-520.682
Fumarate	-1736.97	-1404.89	-332.072

(ii) Theoretical calculations

Due to the cis configuration of carboxylate group in maleate, the electron charge density is higher in fumarate which makes its $\log K_{P1}$ greater than that for fumarate. However, the trend was reversed for $\log K_{P2}$. The greater stabilization of monoprotonated maleate due to intra molecular hydrogen bonding decreases its affinity for proton, which results in lower $\log K_{P2}$ for maleate compared to fumarate.

The free energies of dicarboxylates and its mono and di protonated forms, ($E(L^{2-})$), $E(LH)$ and $E(LH_2)$ respectively, calculated by ab initio molecular orbital theory are given in table 3.3. The free energy of first protonation $\Delta E_1 (E(LH)-E(L^{2-}))$ is more negative for maleate than that for fumarate while in the case of second protonation $\Delta E_2 (E(LH_2)-E(LH))$, the trend is reversed. The higher charge density of maleate molecule results in higher $E(L^{2-})$ for maleate compared to that for fumarate. However, stabilization of mono-protonated maleate by intramolecular hydrogen bonding leads to lower $E(LH)$ in maleate compared to that in fumarate. Thus, the more negative $\Delta E_1 - \Delta E_2$ for maleate is a result of intramolecular hydrogen bonding.

3.4.2 Effect of functional group: Thermodynamics of Eu(III) complexation by carboxylates

In order to understand the effect of functional group on thermodynamic parameters of Eu(III) complexation, potentiometric and calorimetric titrations were carried out with a monocarboxylate (acetate), hydroxycarboxylate (α hydroxy isobutyrate (α -HIB)), aliphatic dicarboxylate (succinate) and aromatic dicarboxylate

(phthalate). A typical potentiometric data for Eu(III)- α -HIB along with fitted data and speciation obtained using Hyperquad 2008 are given figure 3.3. The stability constants for Eu(III) carboxylates obtained in the present work are in good agreement with the literature data as shown in table 3.4.

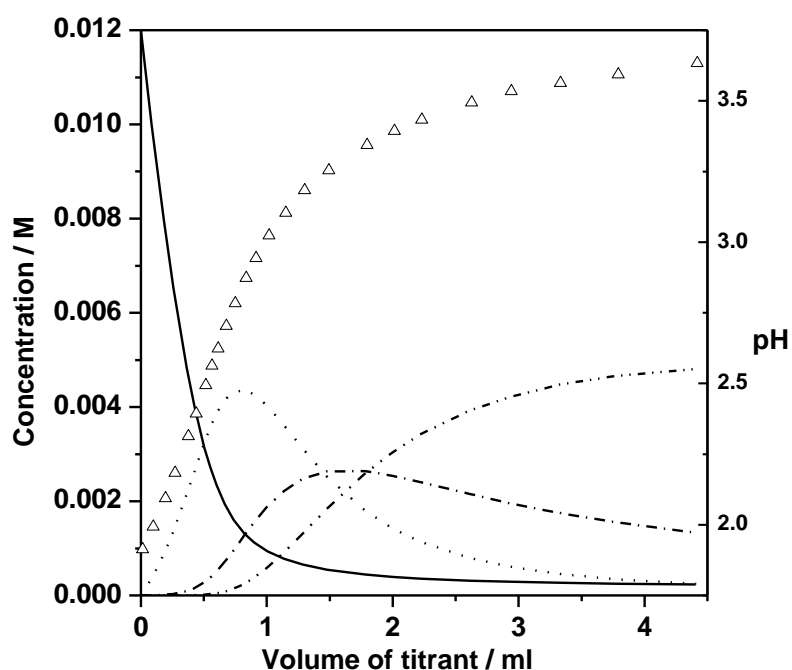


Fig. 3.3: Potentiometric titration data of Eu(III) with α -HIB.

Titration vessel : 20ml of Eu(III) (7.78mM) + HClO₄ (0.012M) Titrant : Total ligand ($C_L = 0.999$ M) + Total Proton ($C_H = 0.447$ M). Symbols : Δ - experimental data (pH), lines : concentration of Eu(III) species (left y axis), — Eu^{3+} , EuL^{2+} , - - - EuL_2^+ , - · - EuL_3

A typical raw calorimetric titration data (power vs time) for Eu(III)-phthalate is shown in figure 3.4. The plots of Q_i^f vs volume of the titrant for complexation of Eu(III) with acetate, succinate, phthalate and α -HIB are given in figure 3.5. The thermodynamic parameters for these systems are given in table 3.4. The literature values of the thermodynamic parameters wherever available are also shown in the table along with the relevant references. In calorimetric curve for acetate and succinate (figure 3.5), the Q_i^f at initial injections are exothermic and as more ligand is added Q_i^f

becomes endothermic. Q_i^f is resultant of protonation and complexation reactions taking place on addition of titrant. During the initial injections the predominant reaction is protonation of the ligand which is exothermic for acetate and succinate. On adding more volume of ligand, the complexation reaction dominates resulting in endothermic Q_i^f . In the case of Eu(III)-phthalate, both protonation and complexation are endothermic which results in endothermic Q_i^f at all the injections. However in case of α -HIB, protonation as well as complexation reactions are exothermic, resulting in negative Q_i^f at all the titration points.

Table 3.4: Thermodynamic data for Eu(III) complexation by carboxylates at 25° C and I = 1.0 M

Ligand	Reaction	Log K	ΔG_c (kJ/mol)	ΔH_c (kJ/mol)	$T\Delta S_c$ (kJ/mol)
Acetate	$\text{Eu}^{3+} + \text{L}^{-} = \text{EuL}^{2+}$	1.97 ± 0.05 (1.97) ^a	-11.2	6.2 ± 0.8 (7.1,8.8) ^a	17.4
	$\text{EuL}^{2+} + \text{L}^{-} = \text{EuL}_2^{+}$	1.48 ± 0.09 (1.41) ^a	-8.4	1.7 ± 0.30 (3.6) ^a	10.1
Succinate	$\text{Eu}^{3+} + \text{L}^{-} = \text{EuL}^{2+}$	3.05 ± 0.046 (2.99) ^c , (2.96) ^b	-17.4	9.5 ± 0.2 (12.4) ^b	26.9
	$\text{EuL}^{2+} + \text{L}^{-} = \text{EuL}_2^{+}$	1.71 ± 0.12 (1.91,0.1M) ^c	-9.80	-	-
Phthalate	$\text{Eu}^{3+} + \text{L}^{-} = \text{EuL}^{2+}$	3.06 ± 0.04 (3.5) ^d	-17.5	10.3 ± 0.20 (U=11.6) ^e	27.8
	$\text{EuL}^{2+} + \text{L}^{-} = \text{EuL}_2^{+}$	1.97 ± 0.05 (1.67) ^d	-11.3	-0.9 ± 0.4 (U= 1.7) ^e	10.4
α -HIB Glycolate ^f	$\text{Eu}^{3+} + \text{L}^{-} = \text{EuL}^{2+}$	2.84 ± 0.04 (2.7) ^g	-16.2	-2.1 ± 0.10 (-4.0) ^f	14.1
	$\text{EuL}^{2+} + \text{L}^{-} = \text{EuL}_2^{+}$	1.87 ± 0.06 (2.24) ^g	-10.7	-5.0 ± 0.05 (-5.3) ^f	5.7
	$\text{EuL}_2^{2+} + \text{L}^{-} = \text{EuL}_3$	1.69 ± 0.07 (1.58) ^g	-9.7	-5.7 ± 0.6 (-6.5) ^f	4.0

^a [68], ^b [69], ^c [74], ^d [75], ^e [69] (Uranyl data), ^f [68] (Glycolate data), ^g [86]

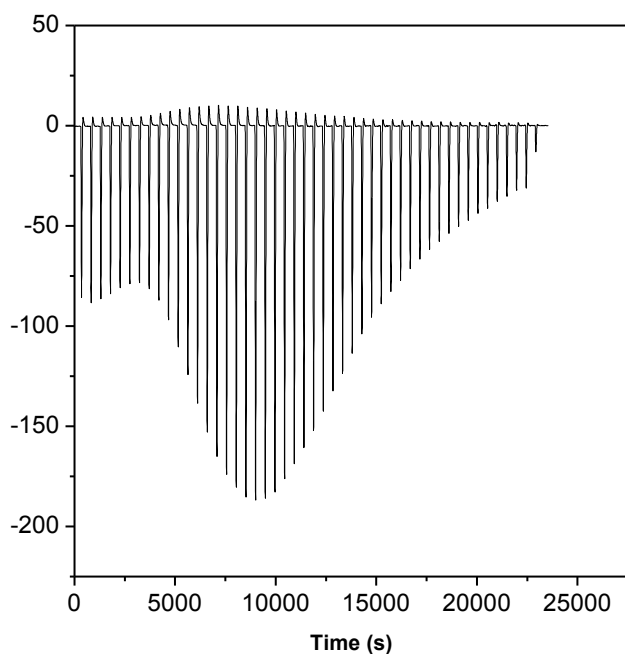


Fig. 3.4: Calorimetric titration data of Eu(III)-phthalate complexation: Titration vessel: 2.7ml of Eu(III) (7.78mM) + HClO₄ (0.012M), Titrant: Total ligand (C_L = 0.217M) + Total proton (C_H = 0.046M)

The four ligands, acetate, α -HIB, succinate and phthalate can be grouped in two classes; the monocarboxylates, (acetate and α -HIB) and dicarboxylates, (succinate and phthalate). Both the monocarboxylates (acetate and α -HIB) are found to form ML, ML₂ and ML₃ complexes with Eu(III). The evidence for the formation of the three complexes was also obtained in TRFS study [71]. The data for Eu(III)-(acetate)₃ has not been reported due to its low concentration.

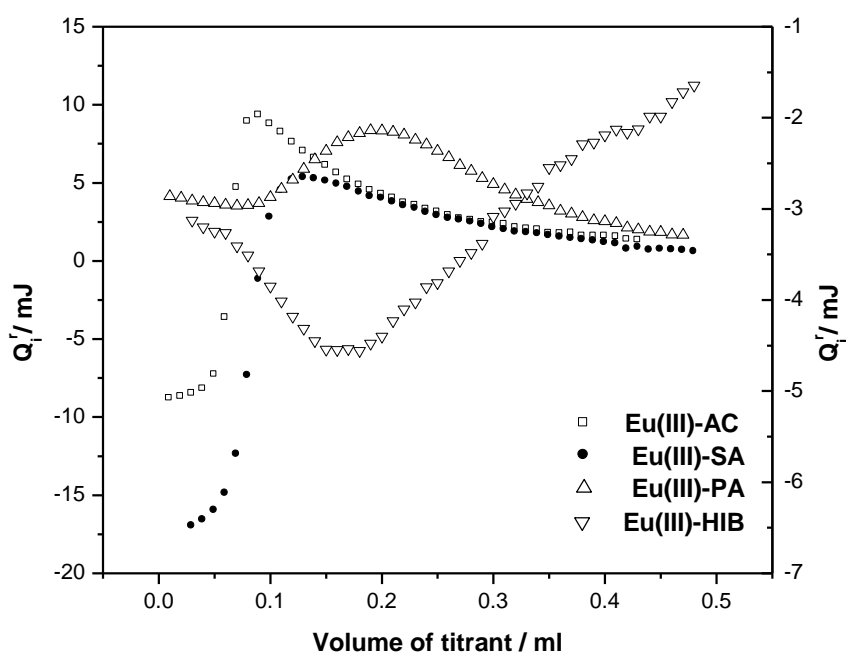


Fig. 3.5: Integrated calorimetric titration data of of Eu(III) solution (2.7ml of 7.78mM Eu(III) in 0.012 M HClO₄) by buffered (left y axis) acetate (AC), succinate (SA), phthalate (PA) and (right y axis) α -HIB (concentrations are given in table 1b)

3.4.2.1. Role of hydroxyl group in Eu(III) complexation by α -HIB

Figure 3.6 shows the plot of $\log K$ vs $\log K_P$ for 1:1 complexes between Eu(III) and carboxylates. Some of the data in the figure have been taken from Choppin et al [86, 87]. The simple monocarboxylates and hydroxy carboxylates fall on two separate straight lines with hydroxy carboxylates having higher $\log K$ than monocarboxylates. The linear correlation between $\log K$ and $\log K_P$ is a manifestation of the electrostatic interaction between metal ion and the ligand anion. α -HIBA being a stronger acid, than acetic acid has weaker conjugate base. However, the $\log K$ of Eu(III)-HIB is much higher than that of Eu(III)-acetate. The higher stability of Eu(III)- α -HIB can be explained only on the basis of participation of hydroxyl group which increases the interaction of ligand with Eu(III).

The linear correlation between $\log K_1$ and $\log K_p$ has also been observed in hydroxy carboxylates but their stability constants as well as slope are higher than monocarboxylates (figure 3.6). The shorter U-O_{eq} bond lengths in UO₂²⁺- α -HIB complexes compared to UO₂²⁺-acetate obtained in extended X ray absorption fine structure spectroscopy measurements further corroborate the chelate formation in the case of hydroxy carboxylate [88, 89].

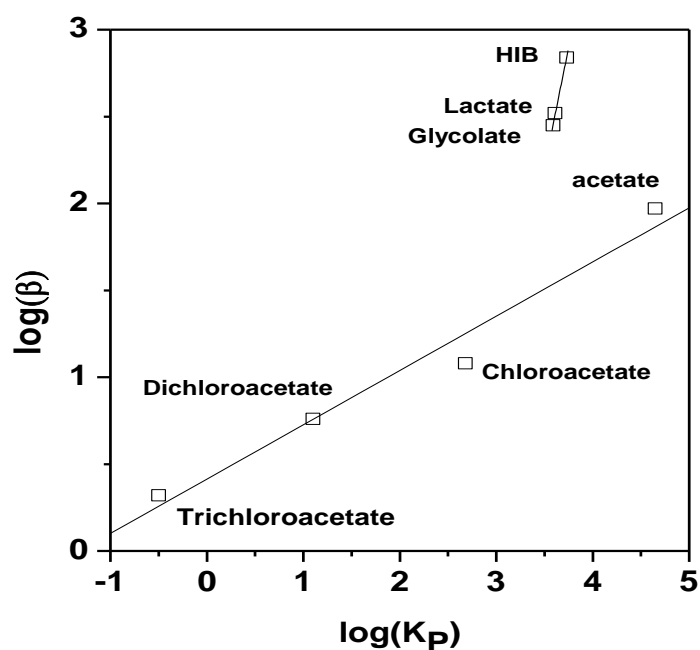


Fig. 3.6: Plot of $\log \beta$ Vs $\log K_p$ for Eu(III) carboxylates

Coordination of metal ion by the carboxylates in the inner sphere can be studied by time resolved fluorescence spectroscopy. The complexation of Eu(III) by α -HIB results in expulsion of water molecules from the primary coordination sphere of Eu(III). The lifetime data of ⁵D₀ excited state of Eu³⁺ have been used to determine the number of coordinated water molecules (nH₂O) [68, 71]. In the case of both acetate and α -HIB, the number of water molecules removed from the coordination sphere of Eu(III) has

been reported to be 1.6 and 2 respectively, which suggests bidentate nature of both the ligands. Acetate binds through both the oxygen atoms of carboxylate group whereas binding of α -HIB take place by carboxylate as well as hydroxyl group. Schematic diagram of proposed binding modes in Eu(III)-acetate and Eu(III)- α -HIB are given in figure 3.7

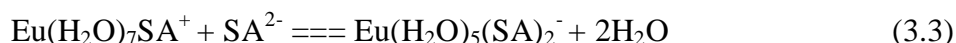
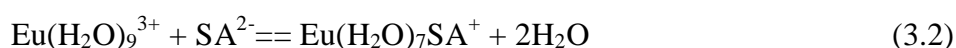


Fig. 3.7: Mode of binding in AC (mode 1) and α -HIBA (mode 2)

The participation of hydroxyl group in binding with metal ion increases its interaction which in turn reflects in ΔH_C of Eu(III)- α -HIB. Thus, unlike simple carboxylates (e.g acetate), exothermic nature of complexation process further corroborates the participation of hydroxyl group.

3.4.2.2 Thermodynamic parameters for Eu(III)-dicarboxylates

In case of dicarboxylates, succinate and phthalate, the potentiometric data analysis revealed formation of ML and ML₂. The complexation reaction can be represented as,



The evidence for the 7 and 5 coordinated water molecules in ML and ML₂ for succinate and phthalate complexes of Eu(III) was obtained from the TRFS measurements [72]. This shows that both succinate and phthalate behave as bidentate

ligands. The $\log K_1$ for Eu(III)-succinate and Eu(III)-phthalate was found to be equal but higher than Eu(III) complexes for acetate and α -HIB. The ΔH_C for complexation of Eu(III)-dicarboxylate were found to be more endothermic compared to monocarboxylate and hydroxycarboxylate. However higher $T\Delta S_C$ values overcompensated the effect of ΔH_C , resulting in higher $\log K_1$ for dicarboxylates. The higher $T\Delta S_C$ in dicarboxylates compared to monocarboxylate supports the chelate formation through two carboxylate groups which leads to expulsion of more water molecules. The more endothermic ΔH_C of complexation is also a consequence of higher dehydration of metal ion as well as ligand.

The ΔH_{C2} is found to be less than ΔH_{C1} in all the cases, which is due to the reduced charge of interacting species in the ML_2 formation. For Eu(III)-phthalate there is significant decrease in ΔH_C from ML to ML_2 (10.3 to 0.3 kJ/mol) whereas the decrease in ΔH_C on successive complexation is less in the case of monocarboxylates (acetate and α -HIB). The large decrease in ΔH_C was also observed in case of UO_2^{2+} -phthalate [73]. This can be explained on the basis of charge neutralization of metal ion during complexation (ML) which is more for dicarboxylates. Thus, the dehydration energy for ML_2 formation is reduced resulting in lower ΔH_C .

3.4.3 Effect of unsaturation in dicarboxylates: Thermodynamics of complexation of Eu(III) and U(VI) by maleate and fumarate

The rigid structure of unsaturated dicarboxylates results in minimal conformational change during complexation reaction. In addition, the π electron cloud of unsaturated ligand has higher tendency to polarize on complexation with metal ion compared to saturated carboxylates. In order to understand the effect of unsaturation in complexation of dicarboxylates, the thermodynamic studies were carried out with maleate and fumarate (figure 3.1) complexes of Eu(III) and U(VI).

Choppin et al determined the thermodynamic parameters (ΔG_C , ΔH_C and ΔS_C) of Eu(III) complexation with maleate and fumarate and attributed the higher stability of fumarate, compared to monocarboxylates, to charge polarization [90]. Thermodynamic study of complexation of lanthanides by various dimethoxybenzoates in aqueous solution, also reveals the enhanced stability of these complexes due to charge polarization [91]. The shift in ^{13}C -NMR which is related to electron density on carbon atom has been used as experimental evidence for charge polarization. Ramamoorthy and Santappa determined the stability constants of U(VI) complexes with maleate and fumarate [85]. The data on enthalpy and entropy of U(VI) complexes with these carboxylates are not available in the literature. Though thermodynamic data for Eu(III) complexation with maleate and fumarate are known, they were determined under the same experimental conditions as for U(VI) for comparison purpose.

The stability constant of Eu(III)-maleate and Eu(III)-fumarate were determined using potentiometry as well as by fluorescence spectroscopy. In addition the fluorescence lifetime data have been used to obtain the information about inner sphere coordination of Eu(III) in complexes. In order to understand the charge distribution in ligands and complexes, ab initio calculation for charge distribution on all the atoms of ligand as well as complex has been carried out by natural population analysis in TURBOMOLE. The stability constants have been compared with that for other carboxylates to investigate the mechanism of the complex formation.

3.4.3.1 Potentiometry

The representative sets of potentiometric data for titration of Eu(III) by buffered fumarate and U(VI) by buffered maleate solution along with the corresponding speciation diagrams are given in figure 3.8 and 3.9 respectively.

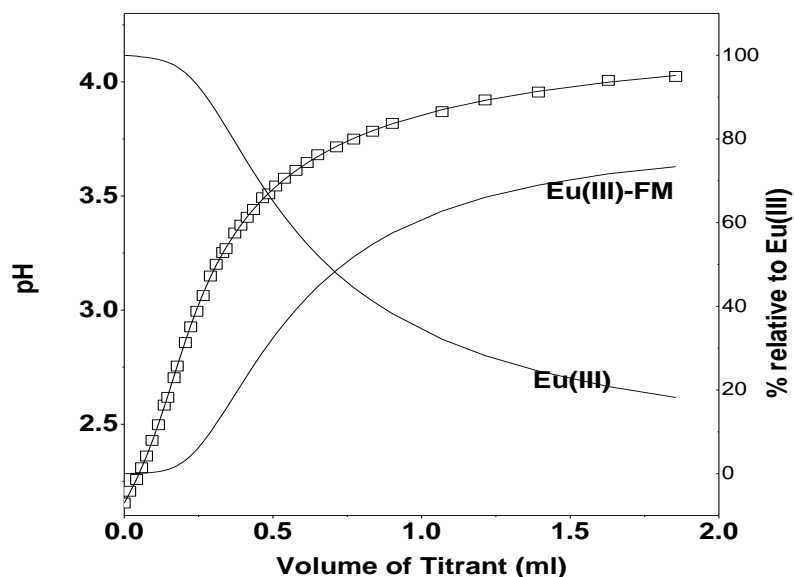


Fig. 3.8: Potentiometric titration of Eu(III) solution ($C_M = 4.95$ mM in 0.007 M HClO_4) with fumarate solution ($C_L = 0.5$ M and $C_H = 0.186$ M)

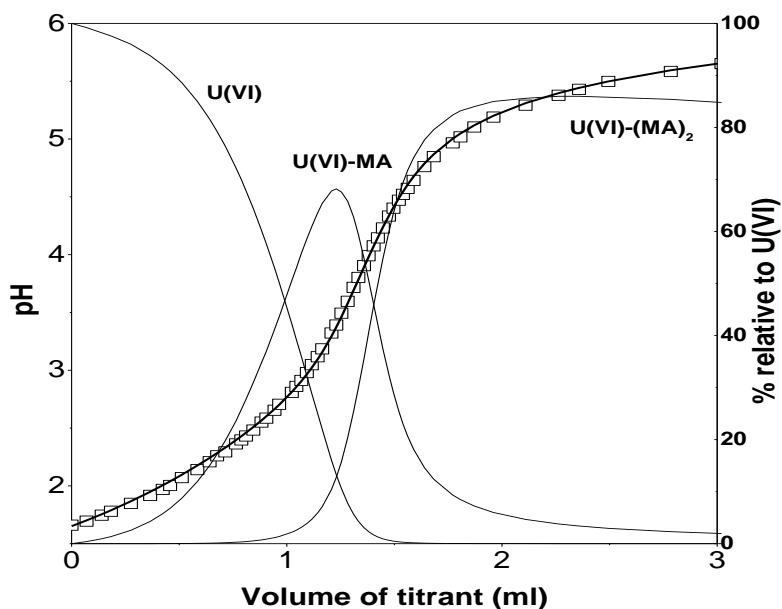


Fig. 3.9: Potentiometric titration of U(VI) solution ($C_M = 5$ mM in 0.022 M HClO_4) with maleate solution ($C_L = 0.5$ M and $C_H = 0.071$ M)

Analysis of potentiometric titration data reveal the formation of only 1:1 complex in the case of Eu(III)-maleate, Eu(III)-fumarate and U(VI)-fumarate while in

the case of U(VI)-maleate apart from 1:1, 1:2 complexes was also observed. The stability constants obtained for Eu(III) and U(VI) complexes of maleate and fumarate are given in table 3.5 along with literature data wherever available. The $\log K$ and ΔH values for Eu(III)-maleate and Eu(III)-fumarate complexes are lower than that reported by Choppin et al. [90]. The difference between the thermodynamic data can be explained on the basis of the different ionic strengths used in the two studies. In the case of U(VI)-dicarboxylates, there is good agreement between the data measured in the present work and that reported in the literature. The higher value of $\log K_1$ reported in [85] could be due to the different ionic strength used in the experiment. There are no literature data on ΔH for U(VI)-maleate and fumarate.

Table 3.5: Thermodynamic data for complexation of Eu(III) and U(VI) with maleate and fumarate at $I = 1.0$ M and 25° C

Ligand	Reaction	$\log K$	ΔH_c (kJ/mol)	ΔG_c (kJ/mol)	$T\Delta S_c$ (kJ/mol)
Maleate	$\text{Eu}^{3+} + \text{L}^{2-} = \text{EuL}^+$	3.15 ± 0.04 (3.83) ^a	10.9 ± 0.3 (14.21) ^a	-17.97	28.8
Fumarate	$\text{Eu}^{3+} + \text{L}^{2-} = \text{EuL}^+$	2.35 ± 0.03 (2.86) ^a	10.1 ± 0.5 (14.37) ^a	-13.41	23.5
Maleate	$\text{UO}_2^{2+} + \text{L}^{2-} = \text{UO}_2\text{L}$	4.63 ± 0.04 (4.46) ^b , (5.15) ^c	20.4 ± 0.4	-26.43	46.8
	$\text{UO}_2\text{L} + \text{L}^{2-} = \text{UO}_2\text{L}_2^{2-}$	2.99 ± 0.02	7.3 ± 0.3	-17.07	24.4
Fumarate	$\text{UO}_2^{2+} + \text{L}^{2-} = \text{UO}_2\text{L}$	2.92 ± 0.03 (3.05) ^c	10.9 ± 0.44	-16.67	27.6

^a [90], ^b [92], ^c [85]

3.4.3.2 Stability constant determination of Eu(III) complexes by TRFS

Complexation of Eu(III) by maleate and fumarate was also studied by TRFS. The fluorescence spectra and lifetime were measured as a function of the volume of titrant. The spectra have been normalized to the intensity of 592 nm peak. Figure 3.12a shows some of the emission spectra of Eu(III)-maleate system recorded during the

fluorescence spectrometric titration of Eu(III) with maleate. The 616 nm peak corresponds to ${}^5D_0 \rightarrow {}^7F_2$ which is hypersensitive due to its electric dipole nature and its intensity with respect to 592 nm peak (${}^5D_0 \rightarrow {}^7F_1$) increases with complexation. The ratio of intensities of 616 to 592 nm peaks, known as the asymmetric ratio (AR) is a measure of the asymmetry of the complex. During the titration, more asymmetric complex, $[\text{Eu}(\text{H}_2\text{O})_{9-x}\text{L}]^+$, is formed from symmetric aquo ion, $[\text{Eu}(\text{H}_2\text{O})_9]^{3+}$. Thus, the AR was found to increase with the volume of the titrant (figure 3.13a), indicating the formation of Eu(III)-maleate complex. Similar data were obtained in the case of Eu(III)-fumarate also (figure 3.13b). The stability constant of Eu(III) complexes with maleate and fumarate were obtained by analysing these spectra using the Hyperquad 2006. The log K values are given in parenthesis in table 3.4 and are in good agreement with those obtained by potentiometry, except that the errors are higher, which is attributed to the scatter in the intensity ratios.

3.4.3.3 Theoretical calculations for Eu(III) and U(VI) with unsaturated dicarboxylate

In order to validate the above hypothesis of charge polarization, the structures of fumarate, maleate and their 1:1 complexes with Eu^{3+} and UO_2^{2+} were optimized and charge density at each atom was calculated as explained in section 3.3. The calculated charge (in units of e) on different atoms in the complex is given in figure 3.11. In case of fumarate, the negative charge on non bonding carboxylate oxygen atoms (O_3/O_4) was found to reduce from (-0.781/-0.784) to (-0.434/-0.360) and (-0.544/-0.499) on complexation with Eu^{3+} and UO_2^{2+} , respectively. The decrease in charge from +3 to +1.759 on Eu^{3+} and from 2.0+ to +0.845 (+1.99 on U and -0.57 on each of the axial 'O' atoms) on UO_2^{2+} upon complexation with fumarate, also points towards polarization of electron charge density from non bonding carboxylate to bonding carboxylate. The

charge distribution of fumarate complex suggests that the complexation of metal ion proceeds through participation of electron charge density from both the carboxylate group thus supporting the experimental observation. In case of Eu(III)-maleate, the charge on Eu^{3+} was reduced from +3 to +1.906 on complexation and in the UO_2^{2+} -maleate complex, the charge on UO_2^{2+} reduced from 2+ to +0.874 on complexation. In spite of lower transfer of charge from the ligand to the metal ion, maleate shows higher stability constant as compared to fumarate and it can be attributed to the formation of stronger 7-membered chelate ring in case of maleate complexes.

3.4.3.4 Linear Free energy relationship

The plots of $\log K_1$ vs $\log K_P$ for complexation of some mono-carboxylates with Eu(III) and U(VI) along with fumarate and maleate complexes are given in figure 3.10a and 3.10b respectively. The data for other carboxylates are taken from literature [93, 94]. As the metal ligand interactions are mainly electrostatic in nature, the $\log K_1$ for mono-carboxylates vary linearly with $\log K_{P1}$. Due to the participation of both the carboxylic group of maleate in bonding, $\log K_1$ was plotted against $\log K_{P1} + \log K_{P2}$. The $\log K_1$ for both maleate and fumarate complexes of Eu(III) and U(VI) are higher than that expected on the basis of linear free energy relationship for monocarboxylates. The higher stability constant of Eu(III)-maleate and U(VI)-maleate can be clearly attributed to chelate formation. However, in case of fumarate complexes, the chelation is not possible because of trans configuration. The $\log K_1$ of Eu(III)-fumarate and U(VI)-fumarate falls in line when plotted against $\log K_{P1} + \log K_{P2}$. This indicates the participation of charge density from both the carboxylate groups of fumarate, which could be due to polarization of electronic charge through conjugated π system [90].

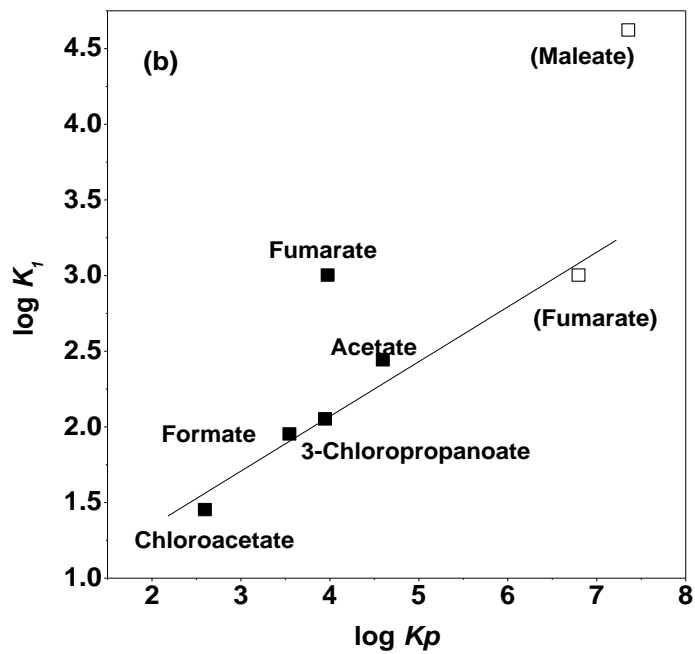
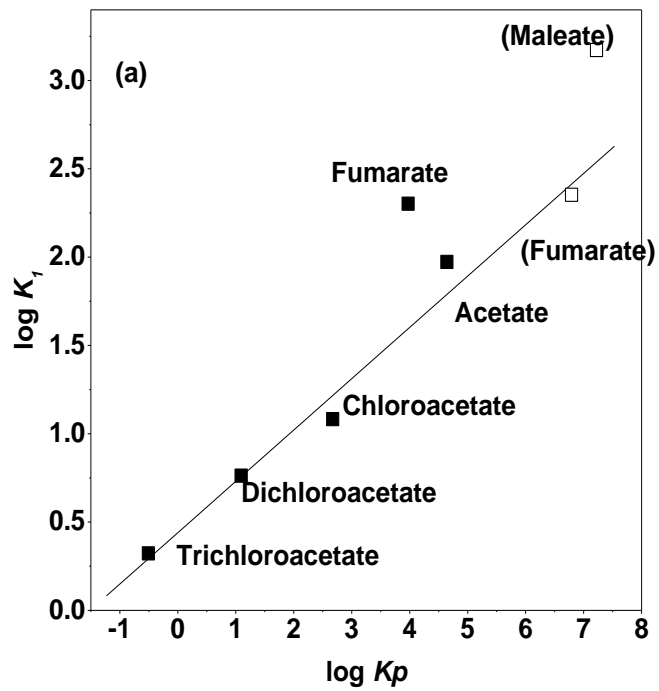


Fig. 3.10: Plot of $\log K_1$ Vs $\log K_p$ for (a) Eu(III) carboxylates (b) U(VI)-carboxylate. Data in parenthesis: plotted vs $(\log K_{P1} + \log K_{P2})$

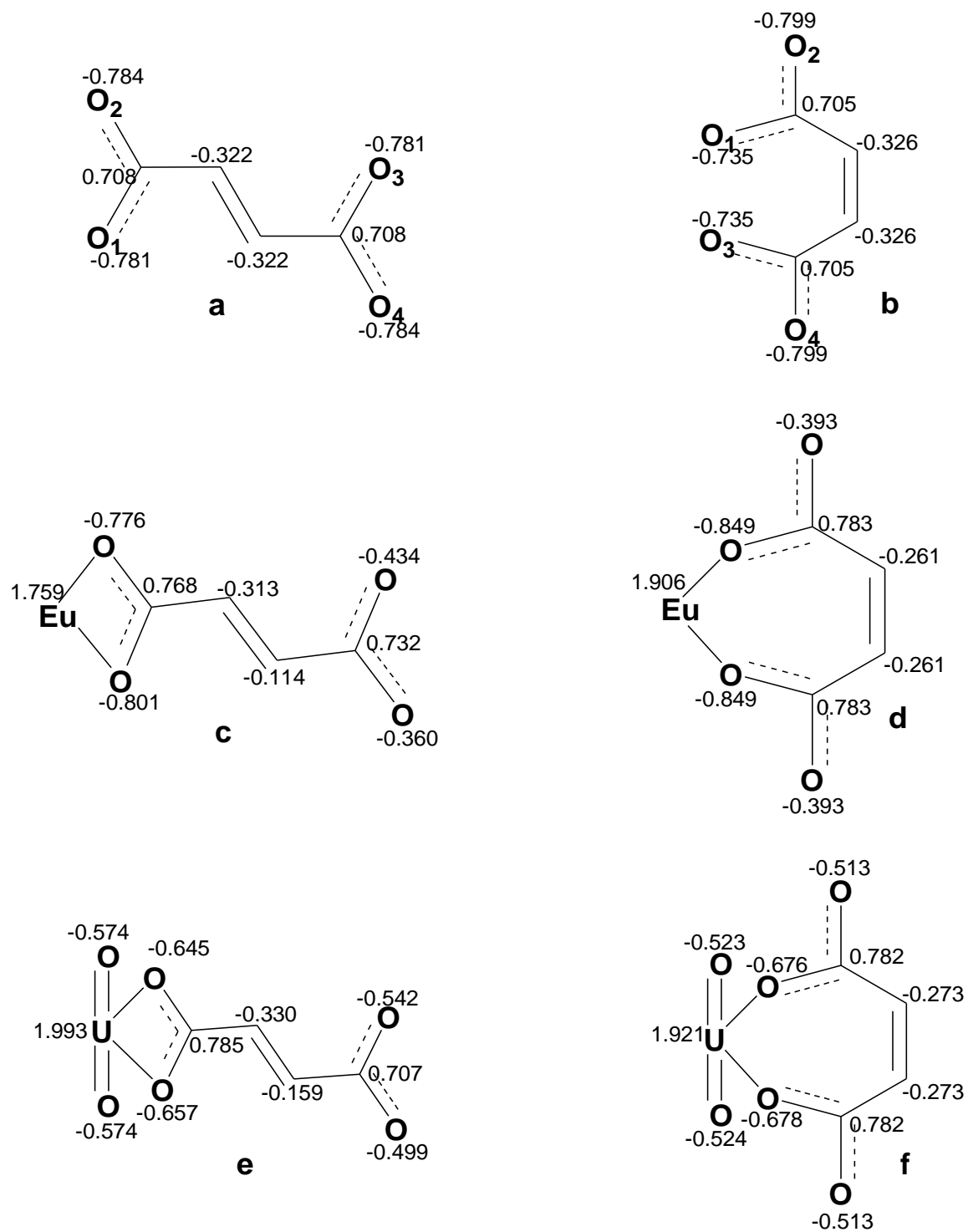


Fig. 3.11: NPA atomic charges of free fumarate (a) and maleate (b) and their 1:1 complex with Eu³⁺ (c and d) and UO₂²⁺ (e and f)

3.4.3.5 Comparison of thermodynamic data for maleate and fumarate

(i) Eu(III)-complexation

Table 3.5 gives the data on thermodynamic parameters for complexation of Eu(III) and U(VI) by maleate and fumarate. The ΔH_C for Eu(III)-fumarate and Eu(III)-maleate are similar and the higher stability in Eu(III)-maleate compared to Eu(III)-fumarate is due to larger $T\Delta S$. The higher dehydration of metal ion and higher metal – ligand interaction in Eu(III)-maleate compared to Eu(III)-fumarate has opposing effect on ΔH_C , which results in nearly equal ΔH_C values (Table 3.5). However higher dehydration of the metal ion and ligand anion increases the ΔS_C for Eu(III)-maleate complexation.

Table 3.6: Results of TRFS measurements on Eu(III)-maleate and Eu(III)-fumarate at I= 0.01 M NaClO₄

Ligand	Reaction	Log K_1	τ (μ s)	Δn
Maleate	$\text{Eu}^{3+} + \text{L}^{2-} = \text{EuL}^+$	3.14 ± 0.06	158 ± 2	2.9
Fumarate	$\text{Eu}^{3+} + \text{L}^{2-} = \text{EuL}^+$	2.15 ± 0.03	128 ± 3	1.3

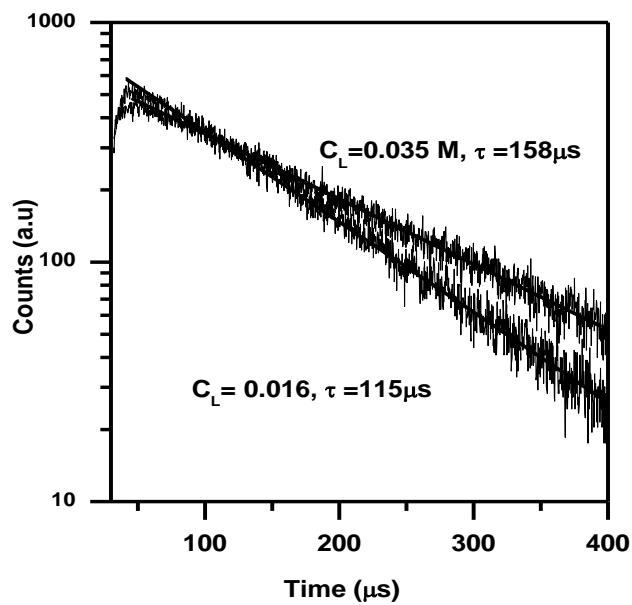
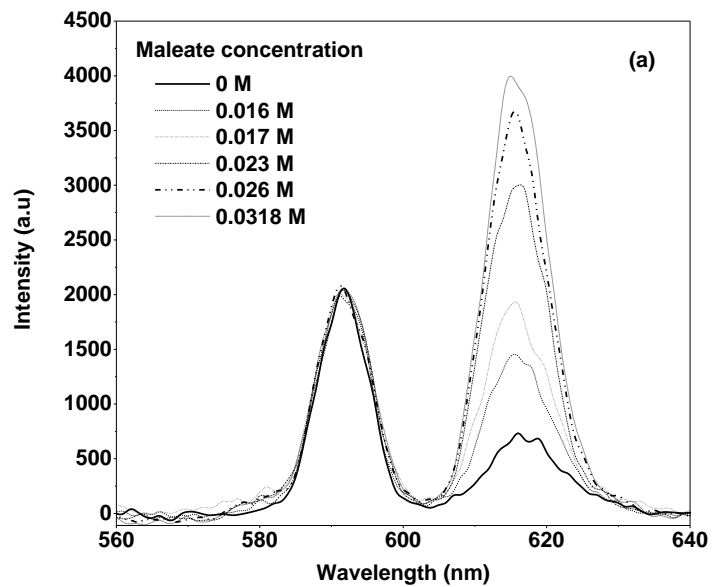


Fig. 3.12: (a) Normalized fluorescence emission spectra of Eu(III) as a function of increasing maleate concentration (b) Decay of fluorescence emission at two different concentrations of ligand (0.016 M and 0.035 M) (Cup solution: 2.7 ml Eu(III) (5 mM in 0.016 M HClO₄), Titrant : Maleate solution (C_L = 0.500 M and C_{OH} = 0.009M))

(ii) Coordination environment in Eu(III) complexes of maleate and fumarate

The figures 3.12b shows the fluorescence decay data for Eu(III)-maleate at two ligand concentrations. The variation of fluorescence decay lifetime with the volume of titrant for Eu(III)-maleate and fumarate systems is shown in figure 3.13a and 3.13b respectively. The single lifetime obtained during the titration indicates the fast exchange of ligand between free and complexed metal ion. The lifetime increases with volume of titrant as more complex is formed and finally levels off at 158 and 128 μs for Eu(III)-maleate and Eu(III)-fumarate respectively. The number of water molecules ($N_{\text{H}_2\text{O}}$) present in inner coordination sphere of Eu(III) was calculated using empirical formula [27]

$$N_{\text{H}_2\text{O}} = (1070/\tau) - 0.62 \quad (3.4)$$

where τ is in micro-second. The $N_{\text{H}_2\text{O}}$ values are 6.1 and 7.7 for Eu(III)-maleate and Eu(III)-fumarate are respectively. The lower $N_{\text{H}_2\text{O}}$ value for Eu(III)-maleate compared to Eu(III)-fumarate suggest the higher dehydration of Eu(III) in Eu(III)-maleate than in Eu(III)-fumarate. The τ value for Eu(III)-fumarate (128 μs) is close to that for Eu(III)-acetate (133 μs) indicating similar type of coordination in the two system (Figure 3.7) [68].

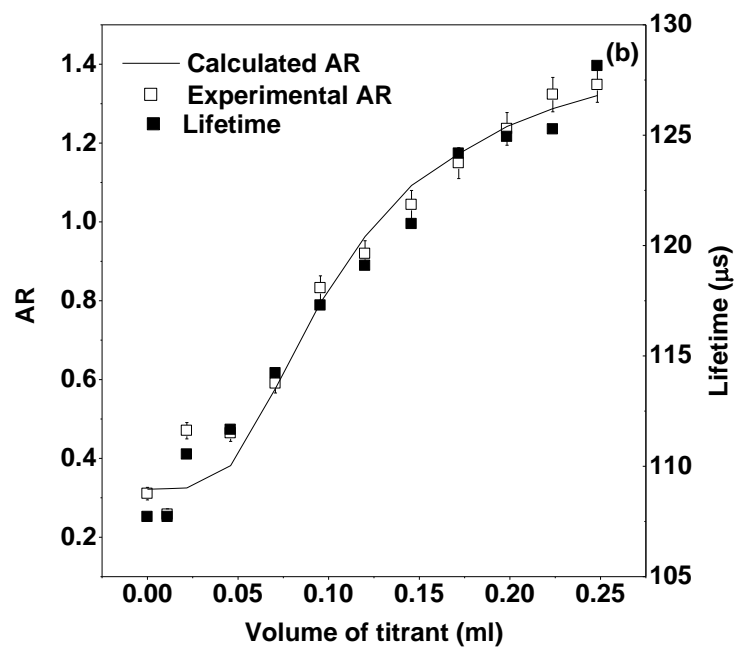
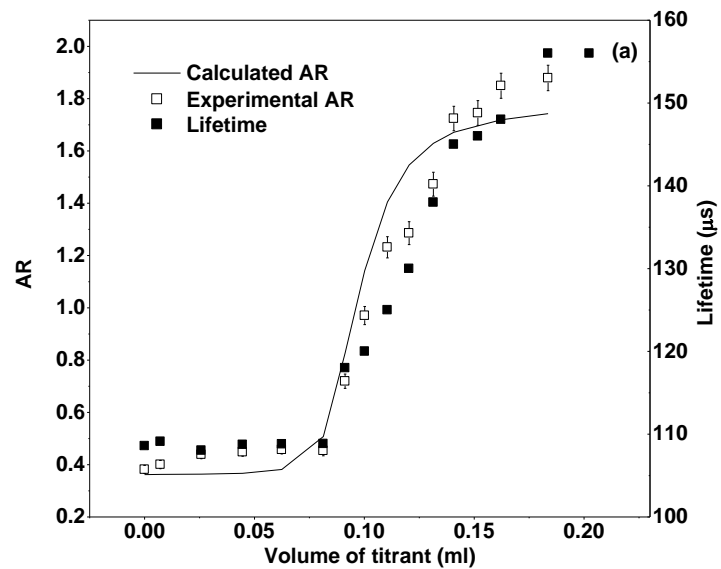


Fig. 3.13: Variation of AR and fluorescence lifetime with volume of titrant

- (a) Titration of 2.7 ml of Eu(III) (5 mM in 0.016 M HClO₄) by maleate solution ($C_L = 0.500$ M and $C_{OH} = 0.009$ M) (b) Titration of 2.7 ml of Eu(III) (3 mM in 0.011 M HClO₄) by fumarate solution ($C_L = 0.500$ M and $C_H = 0.186$ M)

3.4.3.6 Comparison between Eu(III) and U(VI) complexation

Comparison of the $\log K_1$ for Eu(III) and U(VI) complexes with maleate and fumarate (table 3.5) shows that the $\log K_1$ values are higher for U(VI) than that for Eu(III). This can be explained in terms of the higher effective charge (3.33) of UO_2^{2+} than that of Eu^{3+} . The higher endothermic enthalpy of formation of U(VI)-maleate than Eu(III)-maleate suggests greater dehydration of uranyl ion during complexation which is also reflected in the higher entropy term ($T\Delta S_C$). In the case of fumarate the endothermic enthalpy is nearly equal for both the metal ions, while in the case of maleate, U(VI) complexes have higher endothermic enthalpy. The higher dehydration energy in U(VI)-fumarate seems to have been compensated by higher interaction of U(VI) and fumarate.

Tables 3.5 shows that the maleate complexes for both the metal ions are more stable than fumarate complexes, with the difference in the $\log K_1$ of maleate and fumarate being more in the case of U(VI) than that in the case of Eu(III). The ΔH_C value for the 1:1 maleate and fumarate complexes is nearly same in the case of Eu(III) while in the case of U(VI) the same is higher for maleate than fumarate. Thus in the case of Eu(III) the complexation is mainly governed by the entropy factor, while in the case of U(VI) enthalpy factor also plays an important role. This can be explained in terms of the extent of dehydration of metal ion required to accommodate the ligand in the coordination space. In the case of U(VI) the carboxylate ligand is distributed spatially in the equatorial plane of the $[\text{O}=\text{U}=\text{O}]^{2+}$ ion, thereby necessitating the expulsion of more number of rigidly held water molecules than that in the case of Eu(III), wherein the steric strain on the ligand is much less. The higher dehydration of UO_2^{2+} during complexation by maleate ion results in higher entropy and enthalpy of complexation in

U(VI) maleate compared to fumarate. Thus, the effect of chelation and ligand volume (cf maleate complexation) is reflected more in thermodynamic parameters of U(VI) than Eu(III). Similar observation were made by Kirishima et al in case of U(VI) complex with dicarboxylates of different chain length [69]. However, this can be confirmed by measurement of the local structure around the metal ions by techniques such as EXAFS.

3.4.4 Effect of ring size: Thermodynamics of complexation of Th(IV) by dicarboxylates

Ring size of the chelate is one of the important parameters in determining its stability. The dicarboxylates of varying chain length ($\text{OOC}-(\text{CH}_2)_n\text{-COO}^-$) with $n = 1-4$ make an interesting and simple case to understand this phenomenon. $\log K_{p2}$, which is a measure of basicity for dicarboxylate, was found to increase from malonate to succinate and then become constant with the increase in number of the $-\text{CH}_2-$ groups in dicarboxylate ligand. In addition to ring size, ligand basicity also increases from malonate to succinate and then saturates (table 3.2). The thermodynamics of complexation of U(VI) and Eu(III)/Sm(III) (analogue of trivalent actinides) by dicarboxylates has been studied in the literature [69, 73]. However, similar studies with Th(IV) are scarcely available. In the present work, the thermodynamics of complexation of Th(IV) with dicarboxylates of varying chain length was studied using potentiometry and calorimetry.

Tomat et al. [95] determined $\log K$ of Th(IV) complexes with dicarboxylates by potentiometry. However, in recent reports, $\log \beta$ of these dicarboxylates with Th(IV) and U(VI) have shown formation of chelate complexes. Some reports on calorimetric measurements of Th(IV) complexation with oxalate, malonate and succinate are also available in literature [96-99].

3.4.4.1 Potentiometry and Calorimetry

The thermodynamic data on complexation of Th(IV) by malonate, succinate, glutarate and adipate have been measured by potentiometry and calorimetry. The data have been compared with the similar data for U(VI) and trivalent lanthanides to understand the effect of ring size and oxidation state of the metal ion on the thermodynamic parameters. A typical potentiometric data for Th(IV) complexation with malonate along with the speciation obtained from its analysis (Hyperquad 2008) is given in figure 3.14. In order to compare the data with literature data at different ionic strength the $\log K_m$ and $\log K (I = 0)$ were calculated using SIT model (Section 2.2.1). The $\log K_m$ and $\log K$ values are given in table 3.7.

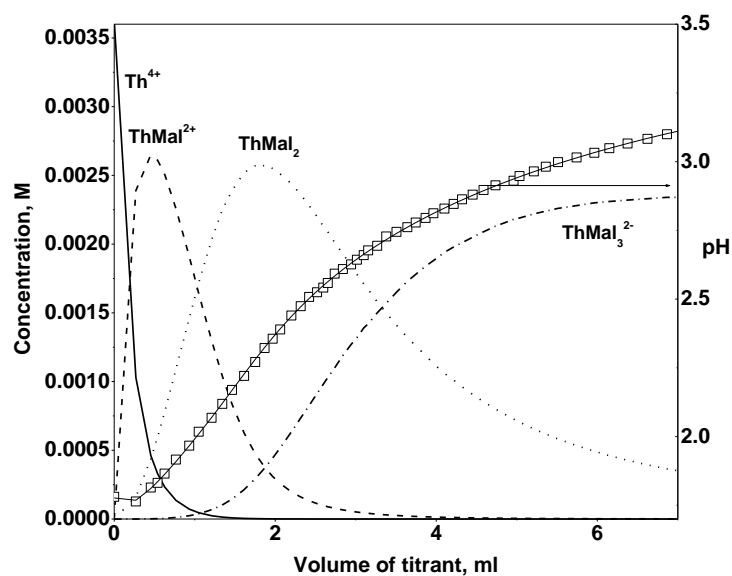


Fig. 3.14: Potentiometric data for Th(IV)-malonate complexation along with speciation diagram (conditions are given in table 3.1)

Figure 3.15 gives the raw calorimetric data for complexation reaction of Th(IV)-malonate. The calorimetric data for complexation in the form of h_{vi} (total heat due to complexation till i th injection per mole of metal ion) vs n_{avg} (number of ligand bound per metal ion) for dicarboxylates (malonate, succinate, glutarate and adipate) along with

the fitted data are given in figure 3.16. The thermodynamic data obtained are also given in table 3.7.

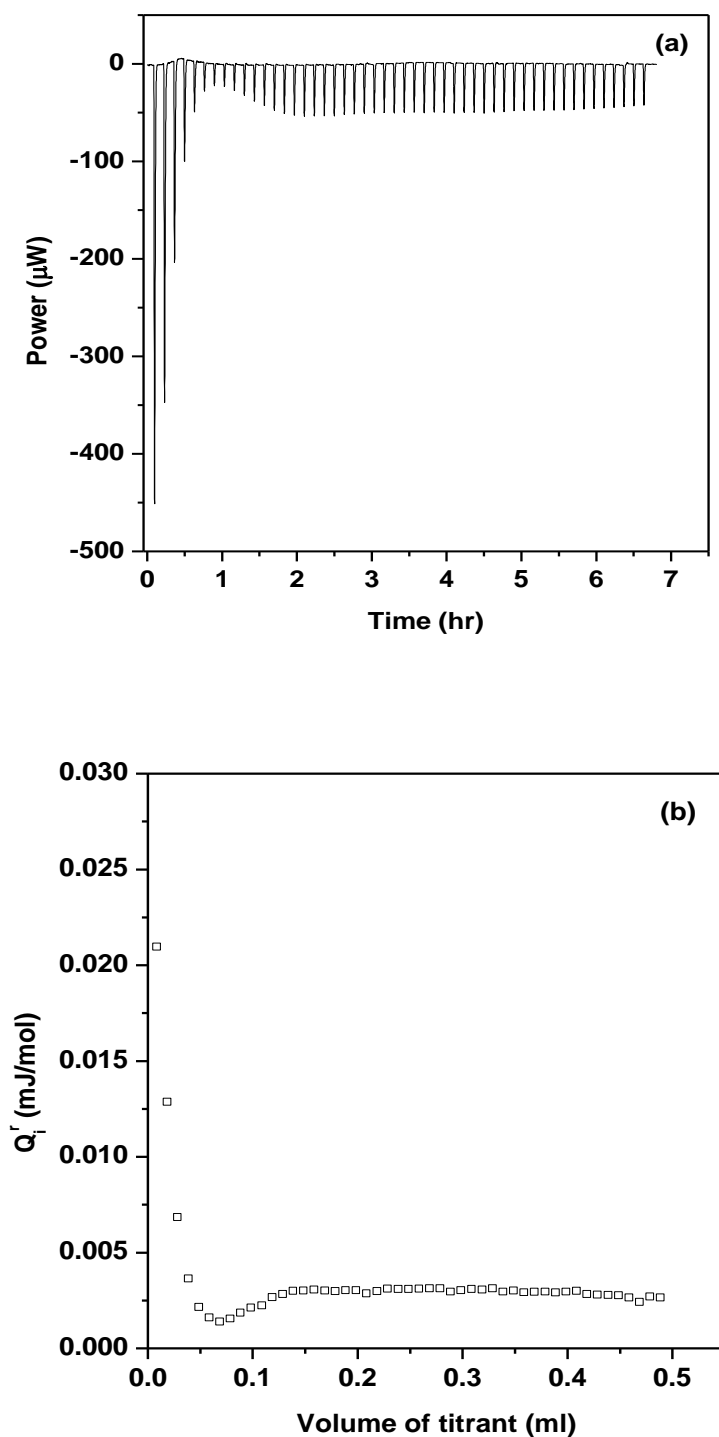


Fig. 3.15:(a) Raw calorimetric data and (b) plot of Q_i^r vs volume of titrant for Th(IV)-malonate . (Injection volume = 10 µl) (conditions are given in table 3.1)

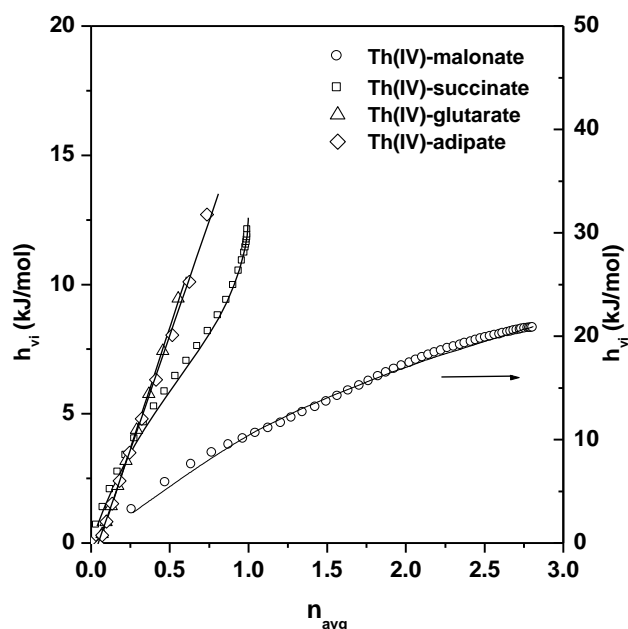


Fig. 3.16: Plot of h_{vi} vs n_{avg} for Th(IV)-dicarboxylate at $I = 1.0$ M at 25° C. Symbols ($\circ, \square, \Delta, \diamond$) : experimental data; lines: fitted data. Th(IV)-malonate (right y axis)

Table 3.7: Thermodynamic quantities of complexation of Th(IV) with dicarboxylates at 25° C, $I = 1.0$ M (NaClO_4) (Conditions are given in table 3.1)

Ligand	Reaction	Log K_{Cj}	Log $K_j(I=0)$	ΔG_{Cj} kJ mol $^{-1}$	ΔH_{Cj} kJ mol $^{-1}$	$T\Delta S_{Cj}$ kJ mol $^{-1}$
Malonate	$\text{Th}^{4+} + \text{L}^{2-} = \text{ThL}^{2+}$	7.25 ± 0.07 (7.47) ^{a,b} (7.42) ^c	9.70 (9.4) ^d	-41.36	11.04 ± 0.30 (11.9) ^a (11.3) ^b	52.4
	$\text{ThL}^{2+} + \text{L}^{2-} = \text{ThL}_2$	5.53 ± 0.10 (5.32) ^a (5.37) ^b , (5.22) ^c	6.99 (6.5) ^d	-31.55	6.1 ± 0.4 (7.2) ^b	37.7
	$\text{ThL}_2 + \text{L}^{2-} = \text{ThL}_3^{2-}$	3.96 ± 0.13 (3.49) ^a (3.7) ^b	3.77 (4.1) ^d	-22.57	4.6 ± 1.4 (4.0) ^b	27.2
Succinate	$\text{Th}^{4+} + \text{L}^{2-} = \text{ThL}^{2+}$	6.4 ± 0.1 (6.23) ^c (6.44) ^a	8.8 (8.4) ^d	-36.5	17.2 ± 0.5 (18.6) ^a	53.7
	$\text{Th}^{4+} + \text{HL}^- = \text{ThLH}^{3+}$	3.60 ± 0.1 (3.6) ^a	4.5	-20.54	12.2 ± 0.9 (8.53) ^a	32.7
Glutarate	$\text{Th}^{4+} + \text{L}^{2-} = \text{ThL}^{2+}$	6.2 ± 0.1	8.6 (8.0) ^d	-35.4	19.3 ± 0.7	54.7
Adipate	$\text{Th}^{4+} + \text{L}^{2-} = \text{ThL}^{2+}$	6.2 ± 0.1	8.6 (8.0) ^d	-35.4	18.3 ± 0.4	53.7
Acetate ^e	$\text{Th}^{4+} + \text{L}^- = \text{ThL}^{2+}$	3.81 ± 0.02	4.66	-21.73	12.2 ± 0.2	33.94

^a [96] ^b [99] ^c [95] ^d [100] ^e [101]

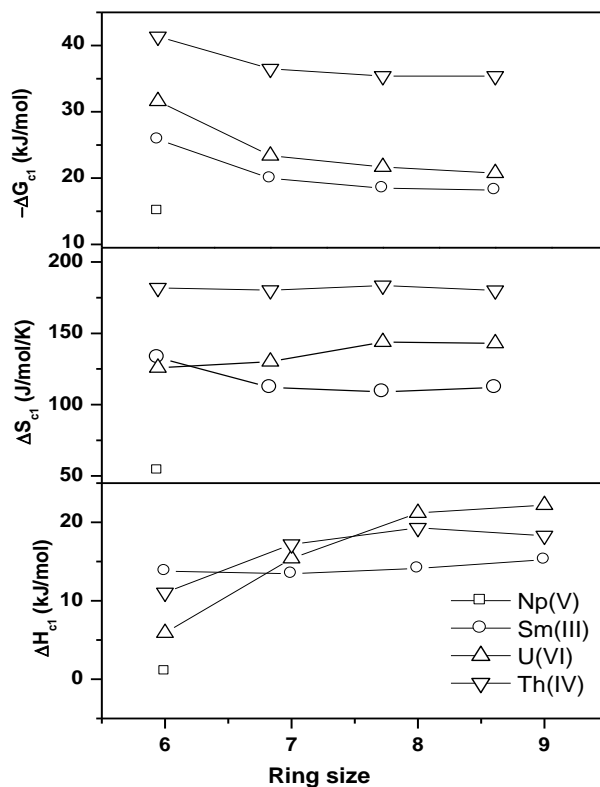


Fig. 3.17: Thermodynamic parameters of Np(V), Sm(III), U(VI), Th(IV) (1:1) complexation with dicarboxylates

The $\log K$ for Th(IV)-succinate are in good agreement with values reported by Di Bernado [96]. Tomat et al. [95] reported only acido complexes for glutarate and ruled out the possibility of formation of bidentate chelate complexes for glutarate and adipate, though, recent reports [69, 100] have shown the formation of cyclic chelate complexes with glutarate and adipate for Th^{4+} , UO_2^{2+} and Eu^{3+} . The results obtained in the present study also support the same. Higher $T\Delta S_C$ values of (1:1) Th(IV)-dicarboxylates compared to acetate clearly suggest that all the dicarboxylate ligands bind as chelate. $\log K_j$ values obtained in present work are found to be higher than that of Sasaki et al [100] wherein the experiments were carried out using radiotracer of

Thorium. Due to the low concentration of Th^{4+} , higher complexes (ML_2 , ML_3) have been reported for succinate, glutarate and adipate [100], which were not observed in the present study owing to precipitation of complexes.

The ΔH_C for Th(IV)-malonate and Th(IV)-succinate obtained in present work are in good agreement with those reported in literature [96, 99]. However ΔH_{Cj} for glutarate and adipate are not available in literature. The similar thermodynamic parameters for protonated complex of Th(IV)-succinate (ThLH^{3+}) and Th(IV)-acetate complex [101] indicate similar binding in the two complexes.

3.4.4.2 Variation of thermodynamic parameters with chain length of dicarboxylate

The thermodynamic quantities (ΔG_C , ΔH_C , $T\Delta S_C$) for complexation of dicarboxylates with Th(IV) are plotted in figure 3.17, along with that for U(VI) and Sm(III) taken from literature [69, 73]. The data for Np(V)-malonate is also shown in the figure [102]. The stability of the Th(IV)-dicarboxylates decreases from malonate to glutarate and then remains constant in adipate. The trend obtained for ΔH_C is similar to that obtained for ΔG_C . However, there is not much change in $T\Delta S_C$ as the chain length increases. This suggests that the variation in $\log K$ among Th(IV)-dicarboxylates is mainly due to change in ΔH_C .

(i) Variation in $T\Delta S_C$

The two factors which affect the $T\Delta S_C$ are (i) water molecules released during the dehydration of metal ion and the ligand anion and (ii) change in the conformational entropy of ligand due to complexation. Owing to the high ionic potential of Th^{4+} , the large increase in entropy during dehydration dominates the conformational entropy, and hence $T\Delta S_C$ can be related to water molecules released during dehydration. Nearly constant $T\Delta S_C$ values for all dicarboxylates (figures 3.17) suggests that the extent of dehydration is similar in all the complexes and increase in carbon chain of the ligand

does not significantly affect the dehydration of metal ion. This observation is at variance with that reported in the literature for complexation of Eu(III)/Sm(III) and U(VI) by same family of ligands (figure 3.17). In case of Eu(III)/ Sm(III), $T\Delta S_C$ decreases from malonate to adipate, which has been attributed to loss in conformational entropy of the ligand [73]. Contribution of conformational changes on $T\Delta S_C$ of Eu(III) complexation is also evident from the fact that Eu(III) complex of 1,4 cyclohexyldicarboxylate, which exists primarily in boat conformation is more stable than adipate due to less conformational entropy loss ($40 \text{ JK}^{-1}\text{mol}^{-1}$). In addition, the fluorescence lifetime data of Eu(III)-dicarboxylates obtained by Wang et al. [74] show decrease in the degree of dehydration of Eu(III) ion with increase in carbon chain length. Thus, both the factors, that is, the Eu(III) dehydration and conformational change in ligand, decrease $T\Delta S_C$ with increase in carbon chain length. However, in case of UO_2^{2+} , the entropy was found to increase with chain length of dicarboxylate contrary to the observation in the case of Eu(III) [69]. The higher effective charge of UO_2^{2+} demands higher dehydration which, in turn, depends upon the volume of the ligand owing to restricted space (equatorial plane) available for coordination. In the case of Th(IV), coordination space is spherical and no such constraint exists for ligand to coordinate the metal ion and therefore, the ligand volume does not appear to have any significant effect on $T\Delta S_C$. Further, the predominance of ΔS_C due to dehydration of Th^{4+} over that due to conformational loss makes $T\Delta S_C$ independent of ligand volume.

(ii) Variation in ΔH_C

ΔH_C for Th(IV)-diarboxylates increases from malonate to glutarate and becomes constant in adipate. Complexation enthalpy is resultant of the energy required for dehydration of the metal ion and the energy released in bond formation between metal ion and the ligand as shown in equation 3.5.

$$\Delta H_C = \Delta H_{Th-L} - m\Delta H_{Th-H_2O} \quad (3.5)$$

where m is the number of dissociated water molecules. Assuming the negligible effect of ligand volume in dehydration process, ΔH_C becomes mainly dependent on metal-ligand bond formation. Among the chelates six member ring is found to be more stable and the stability of the complex decreases with further increase in ring size. On this basis, Th(IV)-malonate, which forms six member ring, should be the most stable and the complex stability should decrease with ring size in higher carboxylates, which is indeed the case for 1:1 complexes of Th(IV) as shown in table 3.7. The increase in enthalpy of the complex with chain length can be explained on the basis of ring size in the complex.

Other factor which affects the metal ligand interaction is the ligand basicity. The $\log K_p$ values of dicarboxylates show that, ligand basicity increases from malonate to succinate and then remains constant. On the basis of their ligand basicity, metal ligand interaction should be minimum in Th(IV)-malonate which is contrary to the observed trend. Thus, the trend in ΔH_C reflects the predominant role of ring size in complex stability. Similar observation was made by Kirishima et al. [69] in the case of U(VI)-dicarboxylates. On the other hand, ΔH_C in Eu(III)/Sm(III)-dicarboxylate has been reported to be constant with increasing carbon chain length [73].

3.4.4.3 Effect of oxidation state on $\log K$

The fractional variation of $\log K_1$ among metal ion-dicarboxylates with respect to metal ion-malonate, viz, $((\log K_1 (\text{M-malonate}) - \log K_1 (\text{M-adipate}))/\log K_1 (\text{M-malonate}))$ along the series of dicarboxylates, follows the order $\text{UO}_2^{2+} (0.34) > \text{Sm}^{3+} (0.29) > \text{Th}^{4+} (0.14)$. The small variation in $\log K_1$ along the series in the case of Th(IV) can be attributed to its high ionic potential which dominates over other factors responsible for complexation. However, despite the higher effective charge on UO_2^{2+}

than Sm^{3+} , the restricted coordination space around UO_2^{2+} makes the effect of ligand volume more prominent, resulting in the highest fractional variation. The ionic potential of different oxidation states of actinide ions changes in the order $\text{MO}_2^+ < \text{M}^{3+} < \text{MO}_2^{2+} < \text{M}^{4+}$, which determines the order of metal ion hydration. During the binding of ligand to metal ion, expulsion of more number of water molecules is required for the metal ion having high effective charge. Therefore $T\Delta S_C$ also increases in the same order. Despite the increase in the interaction between the metal ion and the ligand from MO_2^+ to M^{4+} , large dehydration energy makes the process more endothermic for metal ion having high effective charge.

3.5. Conclusion

In the present work potentiometry, calorimetry and TRFS have been used to determine the thermodynamic parameters for complexation of different oxidation states of actinides by carboxylates of varying structures. The complexation of actinides by carboxylates was found to be mainly entropy driven with ΔH_C being nearly zero or positive.

α -Hydroxy-isobutyrate (α -HIB) complexes of Eu(III) have higher stability than that expected on the basis of linear free energy relationship for mono-carboxylates. The higher stability of hydroxy carboxylate complex indicates the participation of hydroxyl group during complexation reaction. The exothermic enthalpy of complexation further supports this hypothesis. The ΔH_C as well as ΔS_C for succinate and phthalate complexes of Eu(III) are more positive compared to monocarboxylates (acetate and α -HIB) which is due to higher dehydration of Eu(III) and dicarboxylate anion. For the same ring size, the increased basicity of aliphatic dicarboxylate (succinate) is compensated by the rigid structure of the aromatic dicarboxylate (phthalate), thereby resulting in nearly equal values of thermodynamic parameters.

The maleate complexes of U(VI) and Eu(III) are more stable than their fumarate complexes indicating chelate formation in the case of maleate. This is further corroborated by higher $T\Delta S_C$ of maleate complexes. The higher dehydration in Eu(III)-maleate compared to Eu(III)-fumarate has been corroborated by their fluorescence lifetime. The linear free energy relationship revealed charge polarization in the case of fumarate complexation with Eu(III) and U(VI), which have been supported by theoretical calculations. The difference in thermodynamic parameters of maleate and fumarate complexation was reflected more in the case of U(VI) compared to Eu(III) which has been attributed to restricted space available for coordination around UO_2^{2+} .

The effect of ring size on thermodynamic parameters of complexation for Th(IV) revealed the dominant role of ring stability in determining ΔG_C (malonate to adipate). The variation in ΔG_C was mainly due to variation in ΔH_C as ΔS_C , which is a measure of metal dehydration, was independent of ligand volume. Comparison with literature reports suggests that the trend in thermodynamic parameters is dependent on oxidation state of metal ion.

CHAPTER 4

Thermodynamics of Complexation of Actinides at Elevated Temperatures

4.1 Introduction

Intense R&D efforts are on, world wide, to explore the possibility of disposal of high level waste (HLW) in underground georepository wherein the HLW (immobilized in glass matrix) will be buried so as to prevent the migration of radionuclides to the biosphere. The assessment of georepository requires understanding of different types of interactions which the radionuclides will undergo in different geological media. The conditions near the vicinity of repository are expected to be affected by thermal and radiation effects. For instance, the temperature is expected to be higher than ambient temperature due to decay heat from radionuclides. The georepositories are proposed to be at 300-1000 m depth from the surface and the temperature and pressure may vary from (60 to 300)° C and (100 to 10 000) kPa [103]. The exact temperature of georepository depends on other factors like predisposal storage time, spacing between waste packages etc. In order to carry out the performance assessment of georepositories or development of technologies for waste disposal and processing, it is important to study the chemical behaviour of actinides at elevated temperatures. Thermodynamic data at such temperatures are required as input in the geochemical codes used to predict migration behavior of radionuclides in the vicinity of the repository. Actinide complexation by carboxylates also assumes significance as the migration of naturally occurring actinides from mill tailing ponds near the uranium mines is of great concern from the point of view of contamination of the biosphere.

Complexation of actinide ions by organic and inorganic ligands present in ground water is an important phenomenon which affects the migration of radionuclides. Most of the thermodynamic parameters available in literature are at 25⁰C [84, 104]. Though the data at elevated temperatures can be obtained using Van't Hoff equation (equation 2.18), the assumption of constant ΔH_C outside the temperature range 20-40⁰C may not be valid and determination of log K at elevated temperatures using Vant Hoff equation may lead to large uncertainty [105]. Hence, there is a need to determine log K at elevated temperatures. In addition to the support for nuclear waste management, thermodynamic parameters at elevated temperatures provide fundamental understanding of actinide complexation chemistry. Recently, L. Rao's group has reported thermodynamic parameters for complexation of U(VI), Th(IV) and rare earths by the organic and inorganic ligands at elevated temperatures [88, 101, 105, 106]. The general observation of these studies is that the stability constant of metal carboxylates increases with the increasing temperature of the reaction system.

4.1.1 Born equation

The interaction of actinides with carboxylates is mainly electrostatic in nature. Thus, the variation in ΔG_C with temperature can be explained on the basis of change in electrostatic interaction due to change in dielectric constant of the medium. A quantitative explanation of the temperature dependence of ΔG_C for complexation of actinides by different ligands has been achieved using modified Born equation [107].

Born equation gives the change in free energy (ΔG), when a sphere of charge e is brought in a uniform medium of dielectric constant, D ,

$$\Delta G = \left(1 - \frac{1}{D}\right) \frac{e^2}{r} \quad (4.1)$$

This equation has been extensively used to calculate free energy for solvation (ΔG_S) of ions in different media [47].

4.1.2 Extended Born equation

Munze et al modified the Born equation to calculate ΔG_C for complexation reactions [48]. The ΔG_C for a complexation reaction involving species 'i' is given by

$$\Delta G_C = \Delta G_0 + RT \sum \ln c_i + RT \sum \ln f_i \quad (4.2)$$

$$\text{with } \Delta G_0 = \sum_i \mu_{oi} \quad (4.3)$$

where c_i is the concentration of species 'i'. As the interaction of actinide ions with ligands are electrostatic in nature. The μ_{oi} can be identified with the electrical work done during the interaction of ions of charge Z_1 and Z_2 at distance d_{12} . Munze replaced the dielectric constant of water by an empirical temperature dependent expression for dielectric constant [48].

$$D = D_0 \exp(-T/\theta) \quad (4.4)$$

where $\theta = 219$ K and $D_0 = 321$

Accordingly equation 4.2 is transformed into the following equation,

$$\Delta G = \frac{Ne^2 \exp(T/\theta) Z_1 Z_2}{D_0 r d_{12}} - RTv \ln 55.5 + RT \sum \ln f(I) \quad (4.5)$$

where, N is Avogadro number and r is the hydrated radius of the metal ion. In the second term of equation 4.5, the concentrations of species other than water have been neglected. v is the change in number of species during complexation, d_{12} is the distance between cation and anion and $\sum \ln f(I)$ is activity coefficient term. Choppin et al used the modified Born equation for calculation of ΔG_C for actinide/lanthanide complexation reactions by introducing an effective dielectric constant (D_{eff}) [108].

The expression for variation of $\log K$ with temperature (T) can be obtained by differentiating equation 4.5 with respect to T .

$$\frac{d \log K}{dT} = -\frac{Ne^2Z_1Z_2}{D_0rd_{12}} \frac{\partial}{\partial T} \left(\frac{T}{e^\theta} \right) \quad (4.6)$$

which reduces to,

$$\frac{d \log K}{dT} = \frac{Ne^2Z_1Z_2}{rd_{12}} \left(\frac{1}{T} - \frac{1}{\theta} \right) \cdot \frac{1}{DT} \quad (4.7)$$

Based on equation 4.7, complexation of cations by anionic ligands should be favoured at higher temperatures as both the terms (Z_1Z_2) and $(1/T-1/\theta)$ are negative resulting in a positive slope of $\log K$ vs T curve [109].

As discussed in earlier chapters, dehydration of metal ion influences both entropy and enthalpy of complexation. However, the Born equation, which takes into account only metal ligand interaction and does not consider hydration effects, provides good estimation of ΔG_C . This can be explained on the basis of cancellation of hydration effects by enthalpy and entropy compensation. This can be understood by separating, ΔG_C in two parts, free energy of reaction (ΔG_R) and free energy of hydration (ΔG_H).

$$\Delta G_C = \Delta G_R + \Delta G_H = \Delta H_R - T\Delta S_R + \Delta H_H - T\Delta S_H \quad (4.8)$$

where ΔH_H and ΔH_R are the enthalpy of hydration and reaction respectively and ΔS_H and ΔS_R are the corresponding entropy terms. In the case of actinide complexation the expulsion of water molecules from highly hydrated metal ion leads to large increase in enthalpy and entropy. Accordingly,

$$|\Delta H_H| > |\Delta H_R| \text{ and } |\Delta S_H| > |\Delta S_R|.$$

As the net hydration decreases upon complexation, ΔH_H and ΔS_H are positive. The fact, that ΔH_C and $T\Delta S_C$ are positive for actinides complexation, suggests these terms are

dominated by hydration effects. Assuming the hydrated species are in equilibrium with bulk solvent [110].

$$\Delta G_H = 0 \quad (4.9)$$

Consequently,

$$\Delta H_H = T\Delta S_H \quad (4.10)$$

The hydration effects in enthalpy and entropy compensate each other leading to (cf equation 4.8).

$$\Delta G_C = \Delta G_R \quad (4.11)$$

In the present work, the thermodynamic parameters for complexation of U(VI) with succinate ion were determined by potentiometry and calorimetry. The variation in the $\log K$ of U(VI)-succinate with temperature has been explained in terms of the modified Born equation described above. The variation of ΔH_C with temperature has been used to determine the ΔC_P of U(VI) succinate. The variation in thermodynamic parameters of U(VI)-succinate with temperature were compared with the reported data for similar systems (e.g oxalate, malonate and acetate) and have been explained on the basis of molecular structure.

4.2 Experimental

4.2.1. Reagents

Uranium stock solution (0.05 M) was prepared by dissolving U_3O_8 (> 99 %) in dilute perchloric acid (0.1 M). The solution was standardized by Davis Gray method [77] as well as by spectrophotometry using bromo-PADAP as a chromogenic reagent after suitable dilution of the stock solution. Succinate solution (0.5 M) was prepared by dissolving known weight of succinic acid (Aldrich, 99.5 %) in milliQ water (18.2 M Ω cm) and addition of dilute NaOH. Ionic strength of the solutions was maintained at 1.0 M using $NaClO_4$ (Aldrich, 99.99 %). The solutions of NaOH were standardized by

titrating with potassium hydrogen phthalate (Merck, 99.8%) as primary standard. All concentrations in molarity refer to $T = 25\text{ }^{\circ}\text{C}$.

4.2.2. Experimental setup

The potentiometric titrations were carried out using Metrohm autotitrator 905. The details of the instrument are given in chapter 2. A double walled reaction vessel was used with the temperature in the reaction vessel maintained by water circulation from the thermostated water bath. The temperature of the thermostated water bath was kept constant and higher than the temperature of reaction vessel due to the heat losses from the circulation system. The fluctuation in the temperature of the reaction vessel during a titration was in the range of $\pm 0.1\text{ }^{\circ}\text{C}$. The electrode was calibrated at each temperature by titration of standard acid with standard base.

The calorimetric titrations at different temperatures were carried out using TAM III. The oil bath of the calorimeter maintains precise temperature ($\pm 0.0001^{\circ}\text{C}$). The instrument was allowed to stabilize at a set temperature at least for 24 h. The titrations were started only when the drift in base line became $< 0.5\text{ }\mu\text{W/hr}$. The calorimeter thermopiles were calibrated electrically at each temperature.

4.2.3. Potentiometric titrations

For the determination of protonation constant of succinate, potentiometric titration of 20 ml of acidified solution of succinic acid (4.0 mM) was carried out with standard NaOH. For the determination of complexation constants, 20.0 ml of uranyl solution (3.0 – 5.0 mM) was titrated potentiometrically with buffered succinate solution (total ligand concentration = 0.500 M, total proton concentration = 0.486 M). The experiments were carried out at different temperatures in the range of 25-65⁰C at steps of 10⁰C. The stability constants were determined by analyzing the potentiometric

titration data using Hyperquad 2008 [57]. The values of K_w at different temperatures were taken from hyperquad data base [111]

4.2.4. Calorimetric titrations

For determination of enthalpy of protonation (ΔH_p), 2.7 ml of sodium succinate (4.0 mM) was titrated calorimetrically with 0.051 M HClO_4 . In order to determine enthalpy of complexation (ΔH_C), the calorimetric titrations were carried out under the conditions similar to those for potentiometric titrations except for the reaction volume (2.7 ml). The calorimetric titrations were carried out at five different temperatures in the range of 25 to 65°C, in steps of 10°C. The details of the methodology for determination of $\log K$ and ΔH_C from potentiometry and calorimetry respectively are given in chapter 2.

4.3. Results and Discussion

4.3.1. Protonation of succinate

A typical potentiometric plot for protonation of succinate at 25 °C is given in figure 4.1 which also shows the speciation diagram obtained by analyzing the potentiometric data using Hyperquad 2008. The protonation constants of succinate are given in table 4.1 for all the temperatures. The data have been reported in molality (K_{PM}) and molality (K_{Pm}). The $\log K_{P1}$ and $\log K_{P2}$ for protonation were found to be nearly constant at all the temperatures.

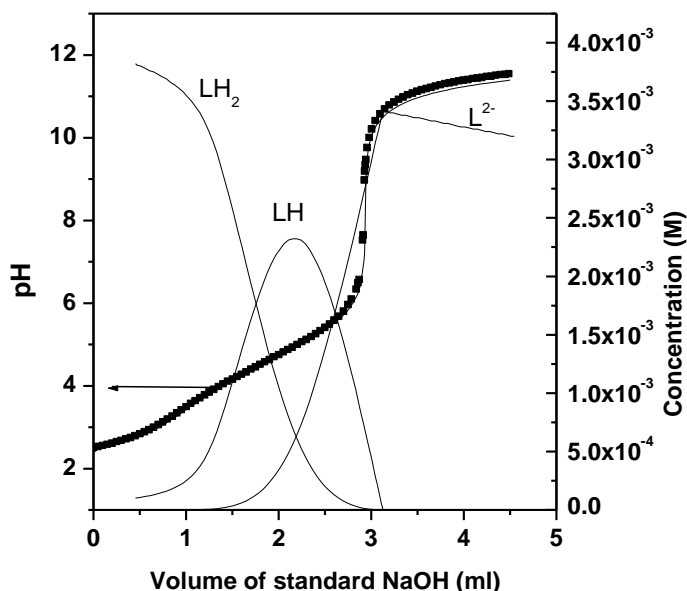


Fig. 4.1: Potentiometry titration of 20 ml of acidified succinic acid (total ligand = 4.0 mM, total proton = 0.011 M) by standard NaOH (0.0766)

Figure 4.2 shows the raw calorimetric data for titration of succinate with perchloric acid at different temperatures. As shown in the figure, Q_i^r becomes more positive with increase in temperature. The ΔH_{P1} and ΔH_{P2} (enthalpy of protonation of succinate) were obtained by the analysis of calorimetric data and using the protonation constants from potentiometric titration and are given table 4.2. The data analysis of calorimetric data revealed negligible contribution of enthalpy and the protonation reactions were found to be driven mainly by ΔS_P . This suggests the dominant role of solvation/desolvation of ligand anion in protonation reactions. The thermodynamic parameters of protonation (ΔG_P , ΔH_P and ΔS_P) obtained at 25⁰ C are in good agreement with those reported by Kirishima et al [69]. The thermodynamic data for protonation of succinate at elevated temperatures have been determined for the first time. The enthalpy of protonation, though small in magnitude, does show an increasing trend towards endothermic values with increasing temperature. However, this is compensated by increase in ΔS_P resulting in near constancy of $\log K_P$ with temperature.

Table 4.1: Protonation constant for succinate at different temperatures (T) and $I = 1.0$ M

Reaction	T ($^{\circ}$ C)	$\log K_{PM}$	$\log K_{Pm}$
$H^+ + L^{2-} = HL^-$	25	5.24 ± 0.03 (5.12) ^a (5.15) ^b	5.22 ± 0.03
	35	5.24 ± 0.03	5.22 ± 0.03
	45	5.23 ± 0.03	5.21 ± 0.03
	55	5.28 ± 0.03	5.26 ± 0.03
	65	5.26 ± 0.03	5.24 ± 0.03
$2H^+ + L^{2-} = H_2L$	25	4.07 ± 0.03 (4.04) ^a (3.95) ^b	4.05 ± 0.03
	35	4.00 ± 0.03	3.98 ± 0.03
	45	3.98 ± 0.03	3.96 ± 0.03
	55	3.99 ± 0.03	3.97 ± 0.03
	65	4.02 ± 0.03	4.00 ± 0.03

^a[69], ^b[84]

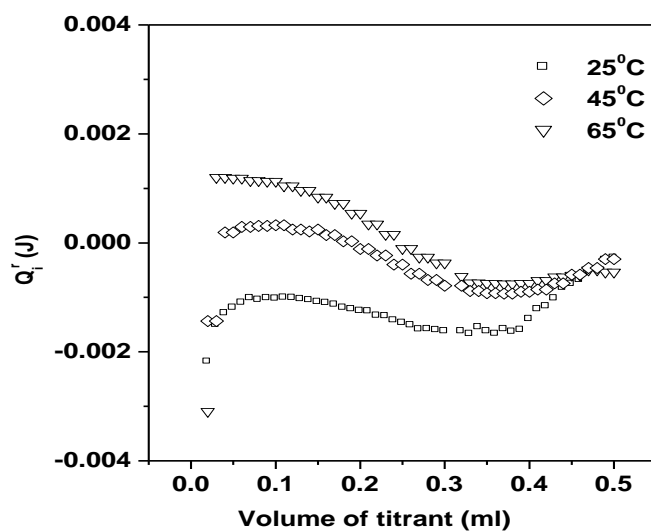


Fig. 4.2: Calorimetric data for protonation of succinate (4.0 mM) with 0.051 M $HClO_4$ at $T = 25^{\circ}C$

Table 4.2: Thermodynamic data for protonation of succinate at different temperatures (T) and $I = 1.0$ M

Reaction	T (°C)	ΔG_P (kJ. mol ⁻¹)	ΔH_P (kJ. mol ⁻¹)	$T\Delta S_P$ (kJ. mol ⁻¹)	ΔS_P (J. K ⁻¹ . mol ⁻¹)
$H^+ + L^{2-} = HL^-$	25	-29.79	-2.0±0.1 (-1.21) ^a (-2.0) ^b	27.8	93.3
	35	-30.80	-0.84±0.2	30.0	97.2
	45	-31.74	-1.3±0.2	30.5	95.7
	55	-33.05	2.4±0.2	35.4	107.9
	65	-33.93	3.7±0.2	37.6	111.2
$2H^+ + L^{2-} = H_2L$	25	-52.9	-6.0±0.2 (-3.46) ^a (6.47) ^b	47.0	157.5
	35	-54.28	-3.8±0.3	50.5	163.8
	45	-55.86	0.74±0.2	56.6	177.9
	55	-57.99	1.7±0.2	59.7	181.9
	65	-59.83	2.7±0.2	62.5	184.9

^a[69], ^b[84]

4.3.2. Complexation of U(VI) by succinate at elevated temperatures

4.3.2.1 Potentiometry

Figure 4.3 shows the raw potentiometric titration data (pH vs volume of ligand) for complexation of uranyl ion with succinate at two temperatures (25 and 65 °C). The fitted data along with calculated speciation diagram, by Hyperquad 2008, are also given in figure 4.3. The analysis of potentiometric data revealed the formation of only 1:1 U(VI)-succinate complex at all the temperatures in the pH range of 1.5 - 4.5. The stability constant data at different temperatures are given in table 4.3 along with the literature data at 25° C. The stability constant at 25° C is in agreement with the reported data. The stability constant was found to increase with increase in temperature. This is in agreement with the literature reports on U(VI) complexation by acetate, oxalate and malonate [88, 112, 113] and this can be explained on the basis of decrease in dielectric constant of water with temperature which in turn increases the electrostatic interaction

between the metal ion and the ligand (cf equation 4.7). With the view to investigate the temperature dependence of stability constants, $\Delta \log K_{1\text{cal}}$ for U(VI)-succinate was calculated at 35, 45, 55 and 65°C with respect to 25°C using modified Born equation 4.7. The d_{12} used in the calculation (2.43 \AA^0) was taken from EXAFS measurements on U(VI)-malonate [113]. The calculated values of $\Delta \log K_{1\text{cal}}$ are given in table 4.4.

Table 4.3: Thermodynamic parameters for complexation of U(VI) with succinate ($\text{UO}_2^{2+} + \text{L}^{2-} = \text{UO}_2\text{L}$) at different temperatures (T) and $I = 1.0 \text{ M}$

T (°C)	$\log K_M$	$\log K_m$
25	4.11 ± 0.04 (4.1) ^a	4.09 ± 0.04
35	4.16 ± 0.03	4.14 ± 0.03
45	4.26 ± 0.03	4.24 ± 0.03
55	4.40 ± 0.03	4.38 ± 0.03
65	4.66 ± 0.04	4.64 ± 0.04

Based on equation 4.7, the ratio of stability constant of 1:1 complex at the highest temperature ($K_{1\text{H}}$) to that at the lowest temperature ($K_{1\text{L}}$), represented as ($K_{1\text{H}}/K_{1\text{L}}$) should vary proportionally with $|Z_1 Z_2|$. L. Rao demonstrated this relationship by comparing $\log K_1$ for Nd(III)-acetate, U(VI)-acetate and Th(IV)-acetate (table 4.5) [105]. Table 4.6 gives the $K_{1\text{H}}/K_{1\text{L}}$ for U(VI)-succinate determined in the present study along with the literature data for other U(VI) carboxylates. The higher value of $K_{1\text{H}}/K_{1\text{L}}$ in U(VI)-succinate than that reported for U(VI)-acetate is consistent with its higher $|Z_1 Z_2|$. However the $K_{1\text{H}}/K_{1\text{L}}$ for uranyl complexation with oxalate and malonate is lower than that for succinate (despite the same $|Z_1 Z_2|$) indicating that apart from electrostatic factor, other factors, such as, variation in ring size, conformational effects, etc., might play important role in determining the temperature dependence of $\log K_1$. For instance, in the case of Eu(III)-lactate, where $Z_1 Z_2$ is negative and $d \log K / dT$ is

expected to be positive on the basis of Born equation, the log K was found to decrease with increase in temperature. [114]

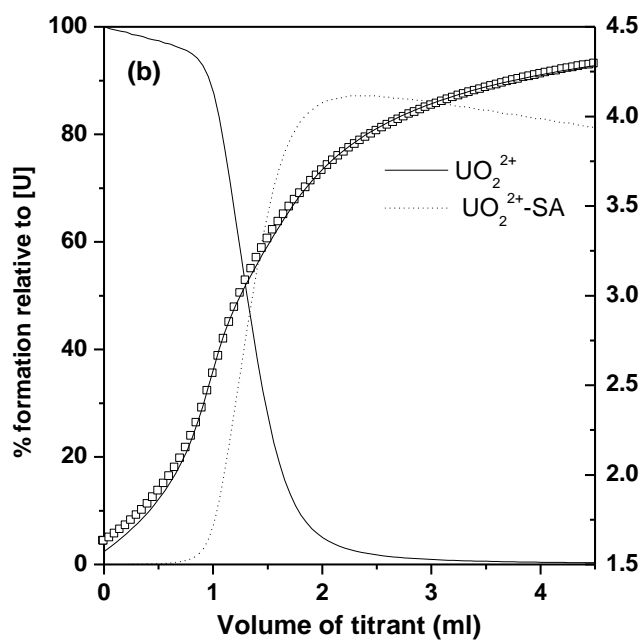
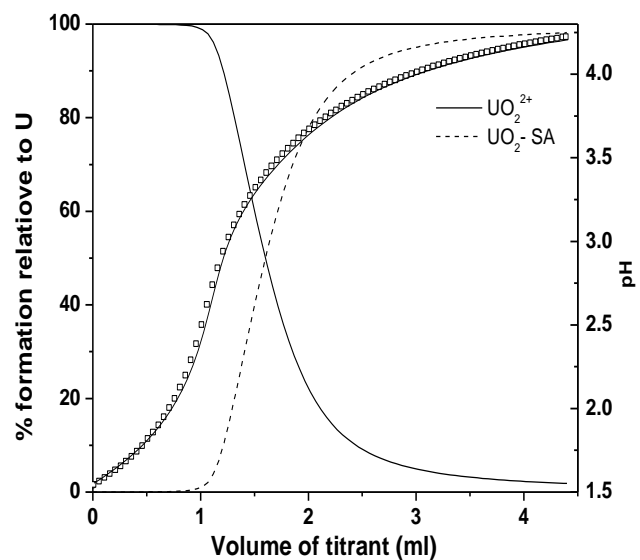


Fig. 4.3: Potentiometric data for titration of U(VI) (5.0 m M in 27.5 mM) with buffered succinate (total succinate = 0.500 M and total proton 0.516 M) at 25⁰C along with the speciation diagram at (a) T=25⁰C and (b) T = 65⁰C.

Table 4.4: Calculated temperature dependence $\log K_1$ for U(VI)-succinate ($\text{UO}_2^{2+} + \text{L}^{2-} = \text{UO}_2\text{L}$)

T(°C)	$\Delta \log K_{1\text{cal}}$ ($\log K_T - \log K_{25}$)
35	0.11
45	0.25
55	0.40
65	0.58

Table 4.5: Effect of temperature on stability constant acetate complexes.

Complex	$ Z_1Z_2 $	$K_{\text{IH}}/K_{\text{IL}}^{\text{a}}$
Nd(III)-acetate	3	2
U(VI)-acetate	3.3	2.5
Th(IV)-acetate	4	2.8

^a K_{70}/K_{25}

Table 4.6: ΔC_p for uranyl complexes with carboxylates.

Metal ion	Ligand	$K_{\text{IH}}/K_{\text{IL}}$	ΔC_p (J mole ⁻¹ K ⁻¹)	Reference
UO_2^{2+}	Acetate	2.5 ^a	110±19	[88]
UO_2^{2+}	Oxalate	0.76 ^a	120±3	[112]
UO_2^{2+}	Malonate	2.8 ^a	96±13	[113]
UO_2^{2+}	Succinate	3.6 ^b	153±4	Present Work

^a K_{70}/K_{25}

^b K_{65}/K_{25}

4.3.2.2 Calorimetry

Table 4.7 gives the raw calorimetric data for titration of acidic uranyl ion solution with buffered succinate solution at different temperatures. The same are plotted in figure 4.4. Q_i^r in the initial injections are exothermic and latter become endothermic. The dominant protonation reactions (which are exothermic) in initial injections result in

exothermic Q_i^r . The same factor is responsible for large difference in Q_i^r for different temperatures at initial injections.

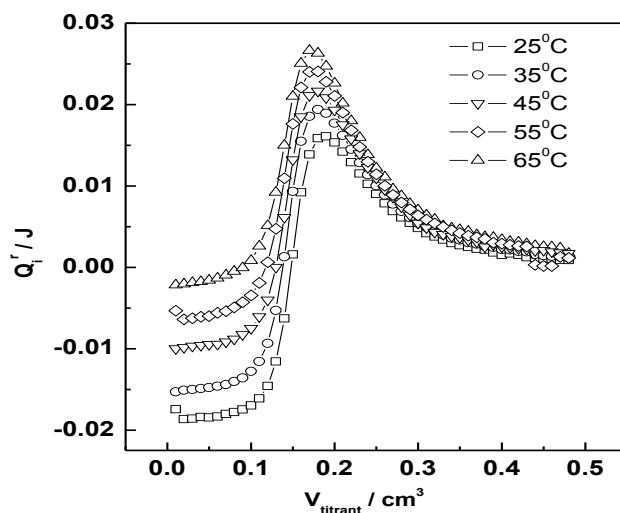


Fig. 4.4: Calorimetric data of titration of U(VI) (5.0 mM in 0.028 M HClO₄) with buffered succinate solution (total ligand concentration = 0.500 M and total proton concentration = 0.516 M) at different temperatures

Table 4.7: Calorimetric data Q_i^r (J) for U(VI)-succinate complexation reaction

Volume of titrant	Temperature (°C)				
	25	35	45	55	65
0.01	-0.01744	-0.01531	-0.00999	-0.00532	-0.00218
0.02	-0.01864	-0.0151	-0.00985	-0.00639	-0.00205
0.03	-0.0186	-0.01502	-0.00966	-0.00625	-0.0019
0.04	-0.0184	-0.0149	-0.00957	-0.00607	-0.00177
0.05	-0.01847	-0.01479	-0.00945	-0.00598	-0.0016
0.06	-0.01834	-0.0146	-0.00943	-0.00559	-0.00132
0.07	-0.01803	-0.01439	-0.00915	-0.00538	-9.67E-04
0.08	-0.01778	-0.01403	-0.00881	-0.00492	-5.13E-04
0.09	-0.01748	-0.0136	-0.00823	-0.00428	-5.68E-05
0.1	-0.01697	-0.01278	-0.00748	-0.00345	8.41E-04
0.11	-0.01611	-0.01157	-0.00606	-0.00192	0.0026
0.12	-0.01459	-0.00934	-0.00399	6.26E-04	0.00512
0.13	-0.01157	-0.00529	3.39E-05	0.00475	0.00921

Volume of titrant	Temperature (°C)				
	25	35	45	55	65
0.14	-0.00628	0.0013	0.00614	0.01094	0.01499
0.15	0.0016	0.00933	0.01323	0.01762	0.021
0.16	0.00922	0.01549	0.01853	0.02211	0.02506
0.17	0.01386	0.01855	0.02112	0.02403	0.02665
0.18	0.01585	0.01938	0.02167	0.02408	0.0263
0.19	0.0161	0.01894	0.02087	0.0228	0.02472
0.2	0.01535	0.01772	0.01932	0.02105	0.02262
0.21	0.01421	0.01622	0.01755	0.01902	0.02018
0.22	0.01291	0.0145	0.0158	0.01684	0.018
0.23	0.01154	0.01287	0.01397	0.0148	0.01594
0.24	0.01025	0.01139	0.01227	0.01296	0.01383
0.25	0.00902	0.01004	0.011	0.01143	0.01219
0.26	0.00787	0.00887	0.00956	0.01001	0.0111
0.27	0.00691	0.00776	0.00862	0.00889	0.00961
0.28	0.00611	0.00686	0.00746	0.00796	0.00879
0.29	0.00547	0.0061	0.00644	0.00715	0.00782
0.3	0.00483	0.0054	0.00545	0.00639	0.00704
0.31	0.00419	0.0049	0.00486	0.00587	0.00642
0.32	0.00377	0.0044	0.00433	0.00539	0.00588
0.33	0.0034	0.00398	0.00407	0.00495	0.00507
0.34	0.00297	0.00358	0.00384	0.00455	0.00482
0.35	0.00272	0.00335	0.00365	0.0042	0.00462
0.36	0.00252	0.00303	0.00338	0.00389	0.00442
0.37	0.00227	0.00285	0.00314	0.00368	0.00399
0.38	0.00217	0.00258	0.00254	0.00349	0.00374
0.39	0.00181	0.00246	0.0028	0.00303	0.00365
0.4	0.00154	0.00219	0.00255	0.00291	0.0034
0.41	0.0017	0.00214	0.00246	0.00278	0.00319
0.42	0.00152	0.00196	0.00234	0.00262	0.0031
0.43	0.00125	0.0019	0.00225	0.00257	0.00289
0.44	0.00113	0.00157	0.00207	3.07E-04	0.00266
0.45	0.00105	0.00144	0.00211	1.55E-04	0.00254
0.46	0.00105	0.00135	0.00192	1.57E-04	0.00251
0.47	9.02E-04	0.00129	0.00181	0.00129	0.00236
0.48	8.87E-04	0.00115	0.00172	0.00115	0.00169

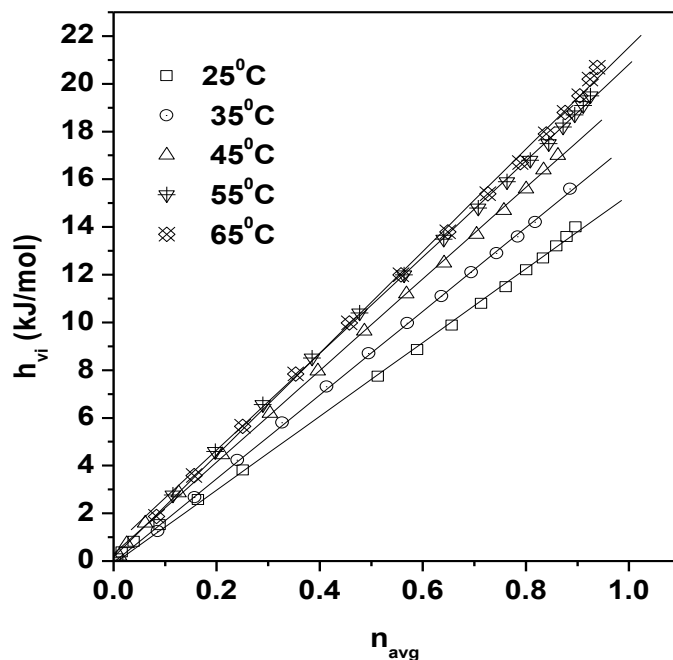


Fig. 4.5: Plot of h_{vi} vs n_{avg} for titration of U(VI) with succinate at different temperatures.

The calorimetric data for U(VI)-succinate in the form of h_{vi} vs n_{avg} is given in figure 4.5. The more positive h_{vi} values at higher temperatures indicate increased endothermicity of complexation at higher temperatures. The enthalpy values (table 4.8) show that complexation of uranyl ion by succinate is endothermic at all temperatures with large favorable entropy contribution. This behaviour is typical of hard acid - base reactions. Figure 4.6 shows the variation of thermodynamic parameters of U(VI)-succinate with temperature. Despite the increased endothermic enthalpy, the complexation is more favoured at higher temperature which is due to larger increase in entropy term ($T\Delta S_C$) (figure 4.6). The increase in $T\Delta S_C$ with temperature is much more than that expected on the basis of 'T' alone. As can be seen from figure 4.6, ΔS_C also increases significantly with temperature resulting in higher stability of complex at elevated temperatures. This can be explained on the basis of increased randomness of

water structure with temperature. Thus, the water molecules released from coordination sphere of metal ion and ligand are more random in bulk water at high temperatures which increases the entropy of complexation [105].

4.3.2.3 Enthalpy-entropy compensation

The increase in ΔH_C with temperature was found to be compensated by increase in $T\Delta S_C$ as shown from the linear relationship (figure 4.7) between the enthalpy and entropy of complexation, which eliminates the contribution of hydration in ΔG_C (cf equation 4.8). Hence, the variation in ΔG_C with temperature can be explained on the basis of metal ligand interaction. Thus, enthalpy – entropy compensation observed in the case of U(VI)-succinate complexation (figure 4.7) explains the successful use of Born equation in explaining the temperature dependence of $\log K$.

Table 4.8: Thermodynamic parameters (ΔG_C , ΔH_C and ΔS_C) for complexation of U(VI)-succinate at different temperatures

Reaction	T (°C)	ΔG_C (kJ. mol ⁻¹)	ΔH_C (kJ. mol ⁻¹)	$T\Delta S_C$ (kJ. mol ⁻¹)	ΔS_C (J. K ⁻¹ . mol ⁻¹)
UO ₂ ²⁺ + L ²⁻ = UO ₂ L	25	-23.35	15.4±0.1 (15.4) ^a	38.8	130.0
	35	-24.43	17.5±0.1	41.9	136.1
	45	-25.83	19.2±0.1	45.0	141.5
	55	27.52	20.2±0.1	47.7	145.4
	65	-30.04	21.4±0.3	51.4	152.0

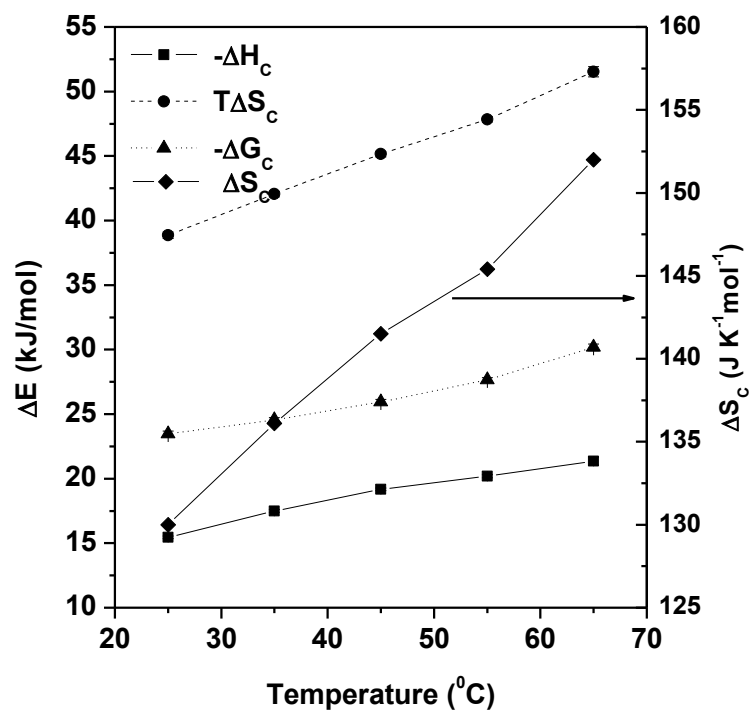


Fig. 4.6: Thermodynamic parameters (ΔG_c , ΔH_c , $T\Delta S_c$ and ΔS_c) for U(VI)-succinate at varying temperatures.

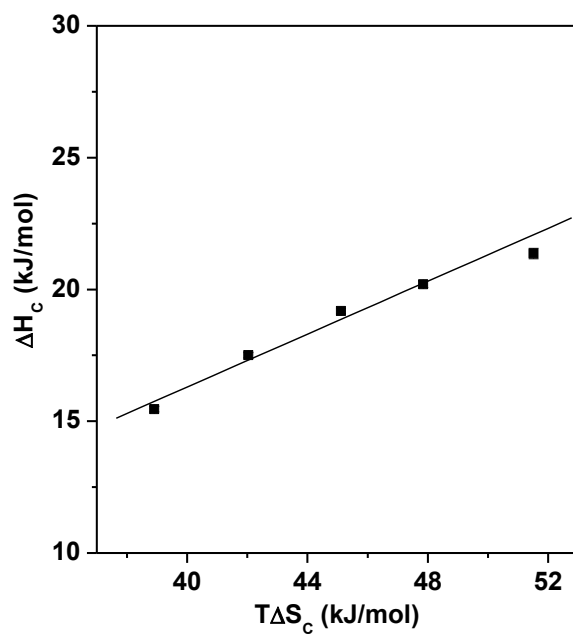


Fig. 4.7 Enthalpy entropy compensation in U(VI)-succinate complexation

4.3.2.4 Heat capacity

The ΔH_C for U(VI)-succinate increases linearly with the temperature (figure 4.6) with the correlation coefficient ($R^2 = 0.98$). This suggests the constancy in molar heat capacity of complexation (ΔC_P) in the temperature range 25-65° C. The ΔC_P value obtained from the slope of plot of ΔH_C vs. temperature is given in table 4.6 along with the literature data for other uranyl carboxylates. Among the U(VI) dicarboxylate complexes, U(VI)-succinate has the higher ΔC_P .

The molar heat capacity of a reaction (ΔC_P) is sensitive to various changes, which the reacting species undergo, as a result of complexation reaction. The factors affecting ΔC_P can be classified in two groups (i) internal factors (ii) external factors (hydration state of species). Internal factors correspond to conformational rearrangement of ligand molecule, modification of internal chelation through hydrogen bonding, strong interaction between oxygenated site and cation. External factors mainly involve reorganization of the solvent shell around the complex formed, partial or complete desolvation of cation and ligand anion [115]. As actinides and dicarboxylates are hard acids and hard bases respectively and their thermodynamics is dominated by hydration effects, the external factors play dominant role in determining the ΔC_P of complexation.

The ΔC_P of reaction depends on the C_P of the metal ion ($C_{P(M)}$), the ligand ($C_{P(L)}$) and the complex ($C_{P(ML)}$) in aqueous solution.

$$\Delta C_P = C_{P(ML)} - C_{P(M)} - C_{P(L)} \quad (4.12)$$

The heat capacity of non polar molecules is known to increase to a large extent with their hydration. In the case of polar compounds the trend is reversed, though to a smaller extent [116, 117]. The large positive ΔC_P for U(VI) carboxylate complexes can thus be attributed to the formation of a relatively non polar molecule from the highly

hydrated cationic and anionic species. High ΔC_P of U(VI)-succinate compared to U(VI)-oxalate and U(VI)-malonate can be attributed to higher alkyl chain which makes the molecule more hydrophobic.

4.4. Conclusions

The stability constant of U(VI)-succinate complex was found to increase with temperature whereas the protonation constants remained nearly constant. The increase in $\log K$ with temperature could be well explained in terms of Born equation for electrostatic interaction between metal ion and ligand anion. The protonation as well as complexation reactions were found to become more endothermic with temperature. However, in the complexation reaction, the increase in enthalpy was overcompensated by the increase in entropy making the reaction more favorable at higher temperatures. The ΔC_P of complexation was constant in the temperature range 25-65°C. The ΔC_P of U(VI)-succinate is higher than that for U(VI)-oxalate and U(VI)-malonate, which has been explained on the basis of their molecular structures.

CHAPTER 5

Thermodynamics of Complexation of Lanthanides with (2,6- bis (5,6- diethyl-1,2,4-triazin-3-yl) Pyridines (Ethyl-BTP)

5.1 Introduction

The spent nuclear fuel is reprocessed to recover the Pu and unburnt U using PUREX process. The raffinate after PUREX process generally contains un-extracted U, Pu and bulk of minor actinides (MAs) such as Am, Np, Cm and host of fission products like Sr, Zr, Mo, Tc, Ru, Pd, Cs, Ba, lanthanides as well as activation products. The most accepted strategy for the management of HLW is to vitrify it in the glass matrix followed by disposal in deep geological repository [13]. Since the half lives of minor actinides concerned range between a few hundreds to millions of years, the surveillance of vitrified waste forms for such a long period is debatable from economical as well as environmental safety considerations. Continuous irradiation of glass matrix by α , β and γ radiations emitted from immobilized radionuclides may alter the glass matrix and thereby facilitate the migration of long lived radionuclides from repository to the environment.

Partitioning and Transmutation (P&T) is being considered as an alternative strategy to alleviate this problem. The P&T process envisages the complete removal of minor actinides from radioactive waste and their subsequent burning in the reactors / accelerators as fuel. This process will lead to generation of extra energy and at the same time would alleviate the need for long term surveillance of geological repositories. The first step in this P&T process is partitioning of minor actinides. As minor actinides constitute predominantly, of trivalent actinides e.g Am, Cm, during partitioning they are

invariably accompanied by lanthanides, which constitute nearly 17% of the total fission products yield. The concentration of lanthanides in the HLW is about few g/l which is much higher than that of MAs (few tens of mg/L). Further, some of the lanthanides have high neutron absorption cross-section thereby affecting the neutron economy of the reactor system if not separated from MAs. There are also reports suggesting the phase separation of lanthanides during the fabrication of special minor actinide (MA) targets for transmutation studies. After partitioning of the MAs, the residual waste can be vitrified and buried in subsurface repositories at a much reduced risk and cost. Hence there is a need for the separation of the lanthanides from long lived actinides.

Separation of Ln(III) from trivalent actinides (An(III)) is a challenging task due to their similar chemical properties. The separation of trivalent actinides from the lanthanides was attempted by exploiting the higher affinity of trivalent actinides for soft (N, S) donor ligands as compared to that of the lanthanides. This is due to the higher spatial distribution of the '5f' orbitals of the actinides compared to the '4f' orbitals of the lanthanides.

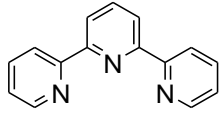
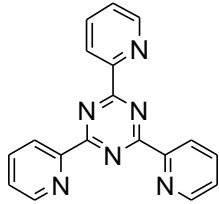
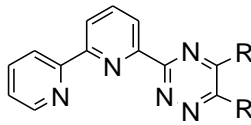
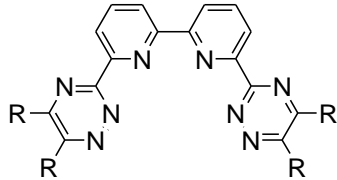
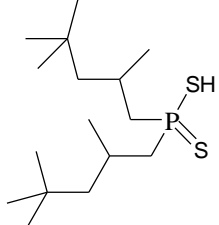
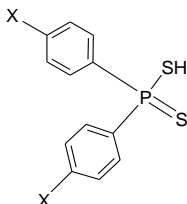
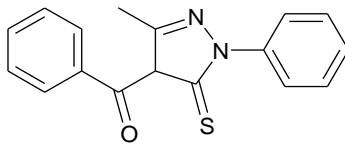
The present chapter describes the work carried out to study the thermodynamics of complexation of lanthanides by N donor ligands, namely, bis triazinyl pyridines (BTPs). These ligands are found to be promising for separation of An(III) from Ln(III) using solvent extraction.

5.1.1 Solvent extraction studies

Various processes which have been developed for Ln(III)/ An(III) separations are based on mainly 'N' and 'S' donor ligands. The structure and name of the process based on various 'N' and 'S' donor ligands are given in Table 5.1. The details of these processes have been summarized in [118-121]. The different extractants are compared on the basis of separation factor (SF), which is a measure of selectivity in solvent

extraction studies. The SF values in the different processes for Ln/An separation are given in figure 5.1.

Table 5.1: Various ‘N’ and ‘S’ donor extractants evaluated for the separation of trivalent actinides and lanthanides

Ligand	Structure
‘N’ donor ligands	
Terpyridine	
2,4,6-Tri(2-pyridyl)1,3,5 triazine	
2-(5,6-Dialkyl-1,2,4-triazinyl)-bipyridine	
6,6’ Bis (5,6 Dialkyl-1,2,4 triazinyl)2,2’bipyridine	
‘S’ donor ligands	
Bis(2,4,4-trimethylpentyl)dithiophosphinic acid (Cyanex-301)	
Bis(<i>p</i>-chlorophenyl)dithiophosphinic acid	
5-Benzoyl-6-methyl-2-phenyl-2-pyrazol-3-thione	

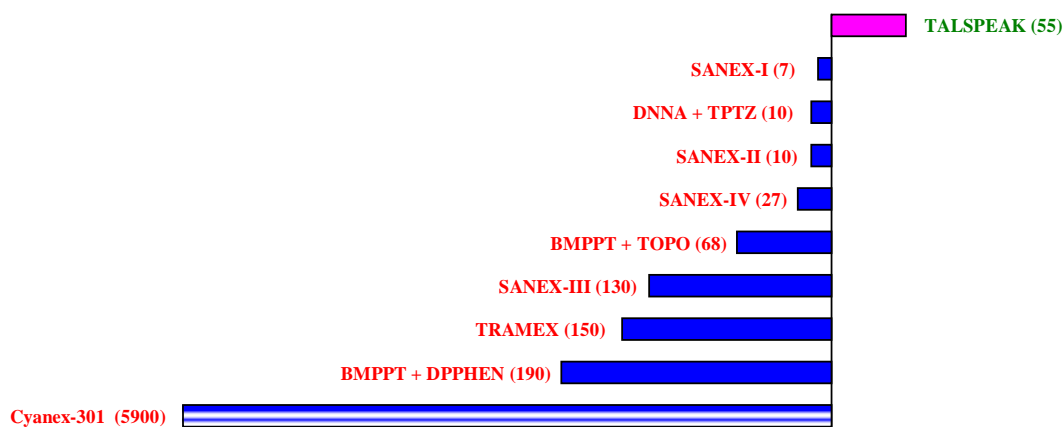


Fig. 5.1: Separation factors for An(III) and Ln(III) using different extractants

5.1.1.1 ‘S’ donor ligands

As shown in figure 5.1, among all the extraction systems used for Ln(III)/An(III) separations, Zhu et. al. has shown the highest separation factor of 5900 for Am(III) over Eu(III) using a ‘S’ donor ligand bis(2,4,4-trimethylpentyl)dithiophosphinic acid (Cyanex-301)[122]. The main limitation of Cyanex-301 is its working pH range, which is >3 . The extraction efficiency can be enhanced by introducing an auxiliary (neutral donor) ligand, viz. tri-n-butyl phosphate (TBP), tri-phenyl phosphate (TPP), diphenyl sulphoxide (DPSO) etc. along with Cyanex-301 [123]. Using synergistic effect with mixture of Cyanex 301 and TBP, Am(III) extraction was possible at lower pH (2.7-2.8). In recent studies, A. Bhattacharyya et al has shown the highest separation factors (~100, 000) with Cyanax 301 in synergistic combination with ‘N’ donor neutral ligands like bipyridyl, ortho phenanthroline etc [17]. In order to further reduce the pH range for Ln(III)/An(III) separation and enhance the radiation and hydrolytic stability, the alkyl group in dithiophosphinate is replaced by chloro phenyl group [124]. However, the S.F obtained was less than those obtained with Cyanax 301.

5.1.1.2 'N' donor ligands

A number of processes have been developed for Ln(III)/An(III) separation using 'N' donor ligands. These processes are named as Selective ActiNide EXtraction (SANEX) processes. A synergistic system of terpyridene and alpha substituted carboxylic acid viz. α -bromodecanoic acid in tert-butyl benzene is used as the organic phase for the selective extraction of the trivalent actinides in the SANEX-I process. Though the extraction could be carried out near pH 2, the reagent used had significant aqueous solubility and resulted in poor S.F (\sim 7). In SANEX – II process, dipyridyl triazine derivative + α -substituted carboxylic acid and a diamide in TPH were found to have good extraction properties even in high nitric acid concentrations (0.2 – 0.3 M). However, the SF remains same as in SANEX – I process. In SANEX-III process another class of ligand based on bis triazinyl pyridine was used. A large number of BTP ligands with different alkyl and aryl substitution in the triazinyl ring were tried for the selective extraction of An(III) over Ln(III). Among the alkyl derivatives, the *n*-propyl derivative of BTP was found to show promising separation behaviour up to the nitric acid concentration as high as 1 M. The separation factor for Am(III) over Eu(III) was found to be \sim 130 at 1 M HNO₃ with a D_{Am} value of 10 [18]. Main advantage of this process is that any auxiliary ligand, like α -substituted carboxylic acids in SANEX-I and SANEX-II, are not required. [125].

5.1.2 Complexation studies with alkyl - BTP

Various alkyl derivatives of BTP have been tried in solvent extraction studies. Methyl and ethyl BTP were not suitable for solvent extraction studies due to their aqueous solubility. Iso-propyl, n-butyl, iso-butyl derivatives of BTP also show similar separation efficiency as the n-propyl derivative, but the extraction kinetics was found to be very slow which is not favourable in the process design. The kinetics of extraction,

Am(III)/Eu(III) selectivity, radiation and hydrolytic stability were found to be dependent on the alkyl (R) substitution on pyridyl or triazinyl ring [14]. Therefore, it is important to understand the effect of alkyl substituent on complexation properties of Ln(III) and An(III) by BTP based extractants.

In literature, most of the complexation studies in homogeneous medium have been reported with n propyl-BTP. Time resolved fluorescence spectroscopy and electron spray ionization mass spectrometry (ESI-MS), have been extensively used to study the complexation of Ln(III) and An(III) with alkyl-BTPs [126-128]. Collete et al [126] studied the complexation of Ln(III) by ESI-MS and it has been observed that methyl BTP forms 1:1 and 1:2 complexes with Eu(III) while iso-propyl BTP exclusively forms 1:3 complex. On the other hand, in the case of n-propyl BTP, there is slight indication of formation of 1:2 complex apart from 1:3. Thus it appears that the stability of complexes of different stoichiometry is dependent on the alkyl chain length of the substituent groups to triazinyl ring.

The structural information about the complexes with BTP derivatives obtained using extended X-ray absorption fine structure (EXAFS) spectroscopy revealed negligible differences in the M-N bond distance between Ln(III) and An(III) complexes [129, 130]. On the other hand, the $\log \beta$ values are nearly three orders of magnitude higher for An(III) complexes than that for Ln(III) complexes [129]. Thus, the selectivity of N donor ligands for An(III) over Ln(III) appears to be mainly due to their higher stability constants. However, little information is available about the thermodynamics of the complex formation of Ln(III) and An(III) with these ligands.

With this in view, in the present work the complexation of lanthanides by ethyl-BTP have been studied using spectrophotometry and isothermal titration calorimetry. The complexation of Ln^{3+} with ethyl-BTP can be expressed as,



The stability constant data obtained with ethyl-BTP were compared with the data for other alkyl substituted BTPs to understand the role of alkyl group in complexation process. The ionic radius/ ionic potential of Ln(III) varies monotonically across the series whereas hydration properties shows sigmoidal behaviour. The variation in stability constant across the Ln(III) series is expected to provide the role of ionic radii in metal ligand interaction as well as in stoichiometry of complex.

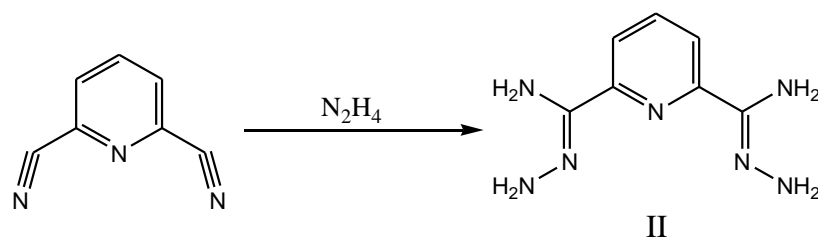
5.2 Experimental

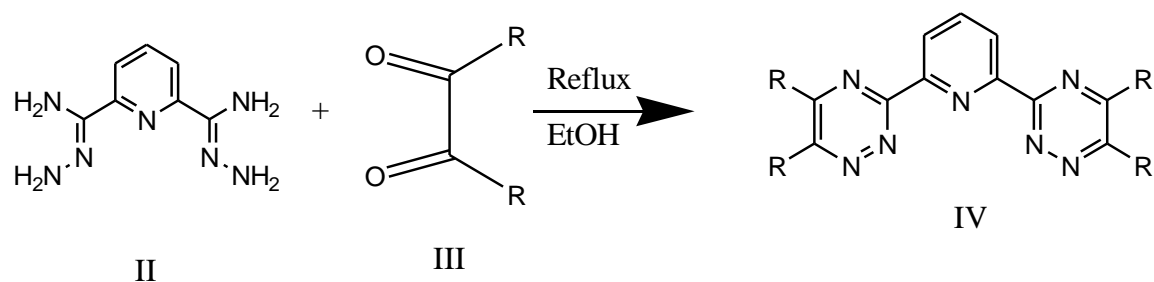
5.2.1 Synthesis of ethyl-BTP (IV)

Ethyl-BTP was synthesized in two steps, as shown in scheme I,

Step 1: Synthesis of 2,6-pyridine carboxamide hydrazone(II): One equivalent of 2,6-pyridine dicyanitrile (I) was allowed to react with two equivalents of hydrazine hydrate in aqueous medium at room temperature for 8 hours. The 2,6-pyridine carboxamide hydrazone thus formed was re-crystallized from water and characterized by NMR, elemental analysis and melting point (230⁰C) [131]

Step 2: Synthesis of ethyl-BTP: 2.6 mmol of 2,6-Pyridine carboxamide hydrazone and 5.2 mmol of hexane-3,4-dione (III) were allowed to react in ethanol medium at refluxing temperature for 2.5 hrs to synthesize ethyl -BTP (IV) (yield = 58%). The solid product was filtered and re-crystallized from ethanol medium. The products were characterized by ¹H-NMR (1.43 (t, 12H, CH₃-CH₂-triazine), 2.93-3.15 (m, 8H, CH₃-CH₂-triazine), 8.08 (t,1H,H₄ pyridine), 8.7(d,2H,H₃,H₅ pyridine)) and elemental analysis (C: 65.84% (65.31%), H: 6.39% (6.63%), N: 27.85% (28.06%)).





Scheme 5.1

5.2.2 Reagents

All reagents used were of reagent grade or higher. HPLC grade methanol was used in preparation of all solutions. The stock solution of ethyl-BTP was prepared in 100% methanol. The Ln(III) solutions were prepared by dissolving metal-oxides in nitric acid which was then evaporated completely. The metal-nitrates thus obtained were dissolved in methanol. The concentration of the metal ions in the stock solutions was determined by EDTA titration using xylenol orange as indicator. The ionic strength of all the solutions was adjusted to 0.01 M by adding appropriate amount of tetra propyl ammonium nitrate (TPAN).

5.2.3 Spectrophotometry

Spectrophotometric titrations were carried out with a (JASCO-V530) spectrophotometer by following the π - π^* absorption bands of ethyl-BTP in the wavelength range 200-420 nm. The spectrophotometric titrations of ethyl-BTP solution with Ln(III), namely, La(III), Nd(III), Eu(III), Tb(III) Ho(III) Tm(III) and Lu(III) were carried out at 25⁰C and constant ionic strength of 0.01 M (TPAN). The solution of ethyl-BTP (1.0×10^{-4} M) in methanol medium was titrated with Ln(III) solution (4.9×10^{-3} – 2.0×10^{-2} M) until the variation in absorption spectra became negligible.

5.2.4 Theoretical calculations

In order to understand the effect of substitution on the stability of the complex, the geometry of the different R-BTP, (R= H, methyl, ethyl, n-propyl and iso propyl)

molecules were optimized at Hartree Fock level using GAMESS electronic structure program [78]. The valence triple zeta 6-311-G(d,p) type basis set were used for the calculations. Final energies of the molecules and Mulliken atomic charges were also calculated after geometry optimization.

5.2.5 Time resolved fluorescence spectroscopy (TRFS)

TRFS studies were carried out using an Edinburgh F-900 unit equipped with M 300 monochromators. A Xenon flash lamp with frequency range of 10–100 Hz was used as the excitation source. In case of Eu(III)-ethyl-BTP, the excitation spectrum, recorded by fixing λ_{em} at 616 nm, showed the maximum absorbance at 248 nm, which was fixed as λ_{ex} for subsequent measurement of emission spectra (560-750 nm) and life time spectra. Lifetime spectra were recorded in the time range of 0.01 – 4 ms, with $\lambda_{em} = 616$ nm and the frequency of Xe lamp fixed at 10 Hz. The fluorescence emission and lifetime spectra of Eu(III) in methanol (1.0×10^{-4} M) ($I = 0.01$ M) were also recorded to compare with the spectra due to Eu(III)-ethyl-BTP complexes. The fluorimetric titration of ethyl-BTP solution by Eu(III) solution were carried out with varying ligand to metal ratio (8.3 – 1). The fluorescence lifetimes were obtained by fitting the fluorescence decay data in following equation.

$$I(t) = \sum_n I_n \exp(-t/\tau_n) \quad (5.2)$$

where I_n is the intensity due to nth component at zero time and τ_n is fluorescence lifetime of nth component.

5.2.6 Microcalorimetry

For the measurement of complexation enthalpy of Eu(III)-ethyl-BTP, 1.0×10^{-3} M ethyl-BTP solution was titrated with a methanolic solution of 6.0×10^{-3} M $\text{Eu}(\text{NO}_3)_3$. In the case of Tb(III)-ethyl BTP, the 3.0×10^{-4} M ethyl-BTP was titrated with 1.22×10^{-3} M Tb(III) solution. The heat Q_i at each injection obtained by the integrating power vs time

signal [62] was corrected for the heat of dilution of titrant $Q_i(\text{dil})$ to obtain the net heat of reaction Q_i^r .

$$Q_i^r = Q_i - Q_i(\text{dil}) \quad (5.3)$$

$Q_i(\text{dil})$ was measured by titrating the blank solution (0.01 M TPAN) with Ln(III) solutions.

5.3 Results and Discussion

5.3.1 Spectrophotometry

Typical absorption spectra recorded during the titration of ethyl-BTP with Eu(III) are given in figure 5.2. Due to the shift in absorption spectra of ethyl-BTP upon complexation with Ln(III), four isobestic points were observed. The detailed procedure of data analysis of spectrophotometric titrations by software Hyperquad 2006 is given in section 2.1.6. The spectrophotometric titration data as plot of absorbance vs volume of the metal ion solution is given in figure 5.3a and b for Eu(III)-ethyl-BTP and La(III)-ethyl-BTP respectively. The speciation diagram is also shown in figure 5.3.

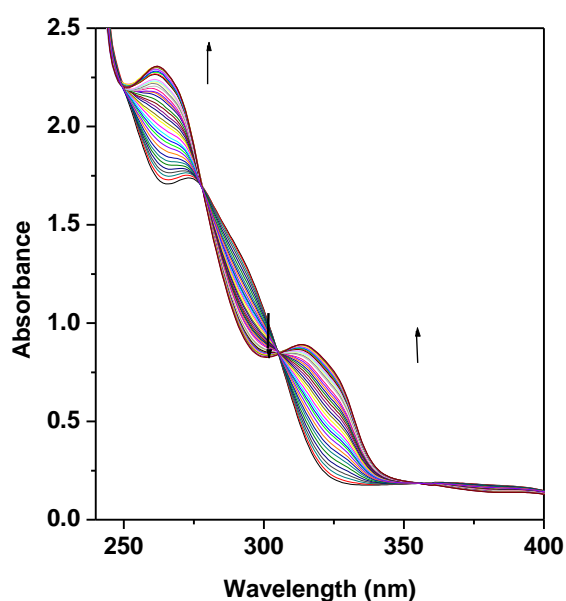


Fig. 5.2: Spectral variation of Ethyl-BTP (1.0×10^{-4} M) on titration with Eu(III) solution (3.8×10^{-4}) in methanol at $I = 0.01$ M (TPAN)

The analysis of spectrophotometric titration data revealed the formation of 1:1 complex for La(III), 1:2 and 1:3 complex for Nd(III) and Eu(III) and only 1:2 complex for Tb(III), Ho(III), Tm(III) and Lu(III). The $\log \beta_{1n}$ for Ln(III)-ethyl BTP complexes in methanol medium ($I = 0.01 \text{ M}$) determined in the present work are given in table 5.2 along with the literature data for n-propyl-BTP complexes wherever available. Similar observations on the stoichiometry of complexes have also been made in the case of n propyl-BTP by Bruder et al [132]. The $\log \beta_{11}$ of La(III)-ethyl-BTP was found to be equal to that reported for La(III)-n propyl-BTP. However, $\log \beta_{12}$ and $\log \beta_{13}$ values obtained for Eu(III)-n-propyl-BTP complexes [132] are higher than that obtained in the present work.

5.3.2 Theoretical Calculations

As the metal ligand interactions are mainly electrostatic in nature, ligand basicity is one of the important factors determining complex stability. In order to understand the effect of alkyl group substitution on ligand basicity, the Mulliken charges were calculated for different R-BTPs ($R = \text{H, methyl, ethyl, n propyl and iso propyl}$). The calculated Mulliken charges on all the N atoms (central nitrogen (N_C) and lateral nitrogen (N_L)) are given in table 5.2. The complexation of metal ion by ligands results in redistribution of electron density in the molecule; therefore the total charge on different rings is an important quantity to compare. The total charge on different rings (central (q_C) and lateral (q_L)) (figure 5.4) are given in table 5.2. The charges in the case of H-BTP are in agreement with those reported by Ionova et al [133]. In all the R-BTPs, q_C was found to be positive which is responsible for the lowest affinity of H-BTP for metal ions among the terdentate nitrogen donor ligands like terpyridine, 2,6-bis(pyridin-2-yl) 4-amino-1,3,5-triazine, 2,6-bis(pyridin-2-yl) pyrimidine, 2,6-bis(benzimidazol-2-yl) pyridine. The q_C in methyl-BTP is less positive compared to that in H-BTP which is

reflected in the increase in $\log \beta_{11}$ for the methyl-BTP. However, q_C remains constant for $R = \text{methyl, ethyl, n-propyl}$ and iso-propyl , indicating negligible change in electrostatic factors with R , which corroborates the constancy of $\log \beta_{11}$ for La(III)-ethyl BTP and $\text{La(III)-n propyl BTP}$ [132] (table1).

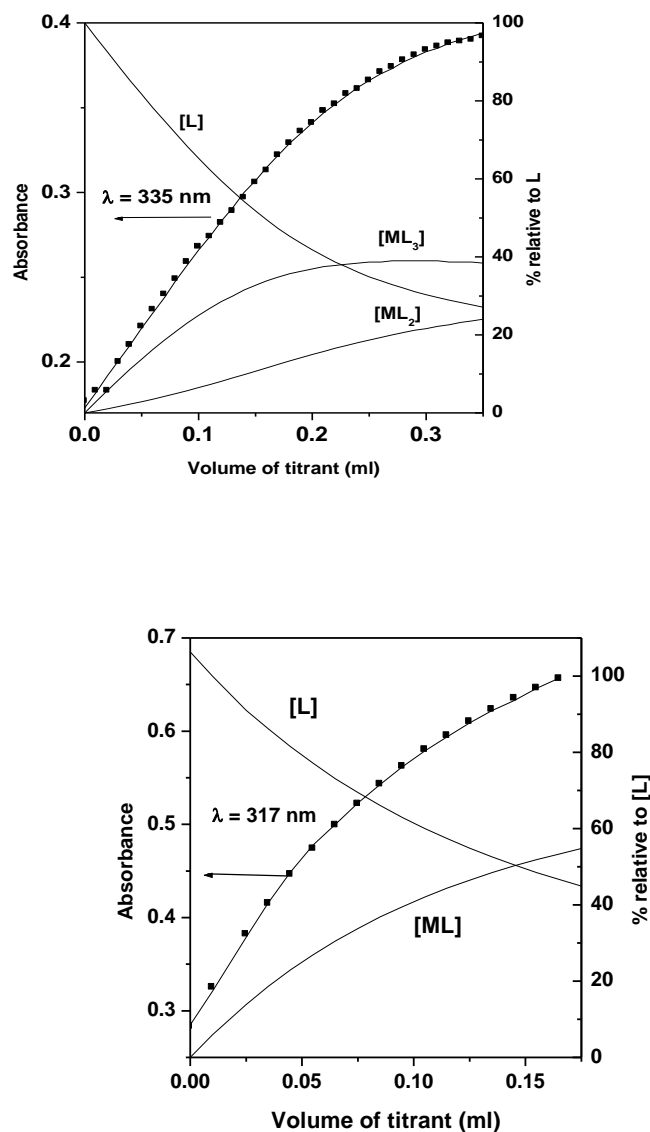


Fig. 5.3: Variation of absorbance for the titration of ethyl-BTP by Ln(III)

(a) Ethyl-BTP solution ($1 \times 10^{-4} \text{ M}$) by Eu(III) solution ($3.8 \times 10^{-4} \text{ M}$) (b) Ethyl-BTP solution ($1 \times 10^{-4} \text{ M}$) by La(III) solution ($4.92 \times 10^{-3} \text{ M}$)

The theoretical calculations thus suggest that the electrostatic interaction between metal ion and ligand remains constant in methyl, ethyl, n propyl and isopropyl derivatives of BTP and any change in stability constant among these derivatives points towards some other phenomena responsible for ligand stability.

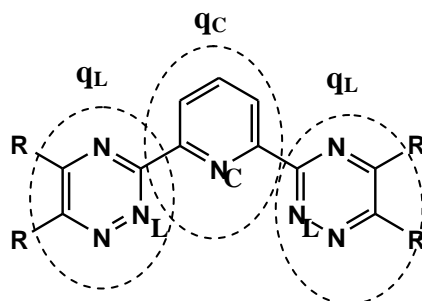


Fig. 5.4: Structure of R-BTP

Table 5.2: Theoretical calculation for charge density distribution in alkyl substituted BTPs.

Ligand	N_C (esu)	N_L (esu)	q_C (esu)	q_L (esu)	$\log \beta_{1n}$ (1: n) (Water-methanol)	Medium
H-BTP	-0.540	-0.303	+0.0729	-0.035	1.6 (1:1)	Water-methanol (1:1 v/v) [133]
Methyl-BTP	-0.542	-0.307	+0.0496	-0.025	2.9 (1:1) 6.3 (1:2)	Water-methanol (1:1 v/v) [126]
Ethyl-BTP	-0.542	-0.304	+0.048	-0.024	8.94 (1:2) 13.61 (1:3)	Methanol [Present work]
n-Propyl-BTP	-0.543	-0.306	+0.046	-0.023	9.5 (1:2) 14.2 (1:3)	Methanol [132]
					6.7 (1:2) 12.0 (1:3)	Water-methanol (1:1 v/v) [126]
Iso propyl-BTP	-0.545	-0.303	+0.0448	-0.0224	14.0 (1:3)	Water-methanol (1:1 v/v) [126]

Table 5.3: Stability constants for complexation of Ln(III) with Ethyl-BTP in methanol medium

Ln(III)	Species		
	1:1	1:2	1:3
La(III)	3.7±0.02 (3.7) ^a		
Nd(III)		8.65± 0.02	13.40± 0.10
Eu(III)		8.94 ± 0.05 (9.5 ± 0.05) ^a (6.3± 0.1) ^b	13.61± 0.10 (14.2± 0.10) ^a (12.0± 0.5) ^b
Tb(III)		9.02 ± 0.02	
Ho(III)		8.58 ± 0.04	
Tm(III)		9.76 ± 0.03	
Lu(III)		10.07 ± 0.05	

^a n propyl-BTP (methanol) [132], ^b n propyl-BTP (water-methanol) [126]

5.3.2.1 Effect of alkyl group on stability constant

Figure 5.5 shows the variation of $\log \beta_{1n}$ for complexes of Eu(III) with the number of carbon atoms (n) in the alkyl group (R) of BTP in methanol as well as water methanol medium including those reported in the literature.

- The $\log \beta_{1n}$ values are almost two orders of magnitude higher in pure methanol medium than that in water-methanol medium. This can be explained on the basis of lesser desolvation energy required for metal ion in pure methanol compared to that in water-methanol medium, wherein the Ln(III) ion is coordinated with water molecules.
- The stability constant was found to increase with increase in alkyl chain length of the substituent (R) group. There are two main factors which change with alkyl group and may affect the stability of these complexes (i) electron density on the BTP molecule (ii) hydrophobic interactions. According to results obtained from theoretical calculations, electrostatic factor remains the same in the case of methyl, ethyl, propyl-BTP and the increase in stability constant can be attributed to

hydrophobic interactions. The predominant role of hydrophobic interaction is also evident from the fact that $\log \beta_{13}$ for Eu(III)-iso-propyl BTP is two order of magnitude higher than that for Eu(III)-n propyl-BTP

- c. In the case of 1:1 complex of La(III)-BTP, the hydrophobic interactions are not important and the stability of the complex is determined mainly by electrostatic interaction. This is evident from similar $\log \beta_{11}$ values for La(III)-ethyl-BTP and La(III)-n propyl-BTP and corroborated by calculated ligand basicity using theoretical calculations.
- d. The slope $\Delta \log \beta_{12} / \Delta n_c$ is more in pure methanol (0.56) than that in water-methanol medium (0.2). This indicates the dominant role of metal ion solvation in determining the stability of the complex in water-methanol medium, which is not so much important in pure methanol. Consequently the substituent effect is more visible in the case of pure methanol medium.

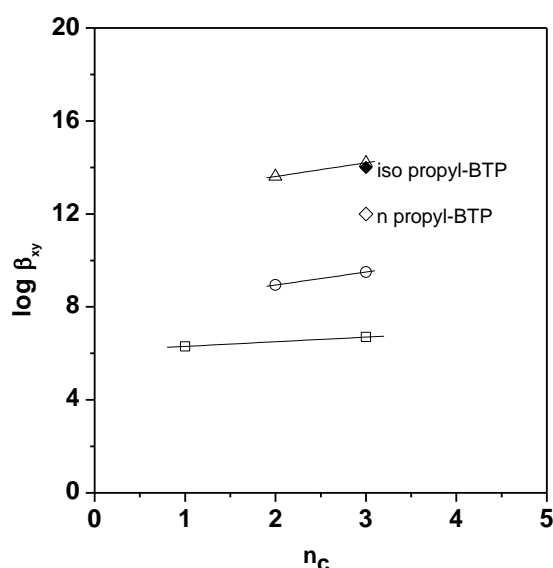


Fig. 5.5: Variation in stability constant with number of carbon atoms (n_c).Symbol: (\square)-water methanol ML_2 (\circ) methanol ML_2 (Δ) methanol ML_3 .

5.3.2.2 Stoichiometry Ln(III)-ethyl-BTP complex

Complexes of different Ln(III) by ethyl-BTP can be placed in three groups depending upon their stoichiometry.

- a. ML only: Ethyl-BTP was found to form only 1:1 complex with La(III) which can be attributed to less metal ligand interaction due to low ionic potential as well as small cavity size of BTP molecules as predicted by theoretical calculations [133].
- b. ML₂ and ML₃: Lighter Ln(III) except La(III) namely, Nd(III) and Eu(III) were found to form 1:2 and 1:3 complexes with ethyl-BTP.
- c. ML₂ only: All the heavier Ln(III) : Tb(III), Ho(III), Tm(III) and Lu(III) formed only 1:2 complex with ethyl-BTP.

The change in the stoichiometry of the complexes across the Ln(III) could be explained on the basis of decrease in coordination number from 9 to 8 near Tb(III) owing to the decrease in ionic radius with atomic number. The coordination geometry of lighter Ln(III) in the first hydration sphere has been obtained primarily from neutron diffraction measurements and shows the formation of nona coordinated complex with a tricapped trigonal prismatic structure. In case of heavier Ln(III), coordination number 8 was observed and the structure obtained was square prismatic [23]. Thus, the formation of ML₃ complex with terdentate BTP ligand is less favourable in heavier Ln(III). Such a change in speciation across the Ln(III) series has also been reported in the literature [134].

5.3.2.3 Variation in log β_{12} across the Ln(III) series

The log β_{12} values for Ln(III) complexes with ethyl-BTP increase from Nd(III) to Tb(III), decrease at Ho(III) and again increase from Tm(III) to Lu(III) (Table 5.2). Figure 5.6 shows the variation of log β_{12} with Z of Ln(III). Though the coordination number is higher in lighter Ln(III) than heavier ones, the hydrated radii of Ln(III) show

reverse trend. The hydration radius is same for lighter Ln(III) (La(III) - Nd(III)) and is smaller than that for heavier Ln(III) (Dy(III) to Lu(III)). Intermediate Ln(III) have hydration radius between lighter and heavier Ln(III). The ‘S’ shaped curve observed for $\log \beta_{12}$ suggests the dominant role of Ln(III) solvation in determining the variation in $\log \beta_{12}$ (table 5.3). Similar trend in $\log \beta_{xy}$ along the Ln(III) series has also been reported in the literature for oxygen as well as nitrogen donor ligands [135, 136]. However, some reports do show monotonic increase in $\log \beta_{13}$ along the Ln(III) series [127].

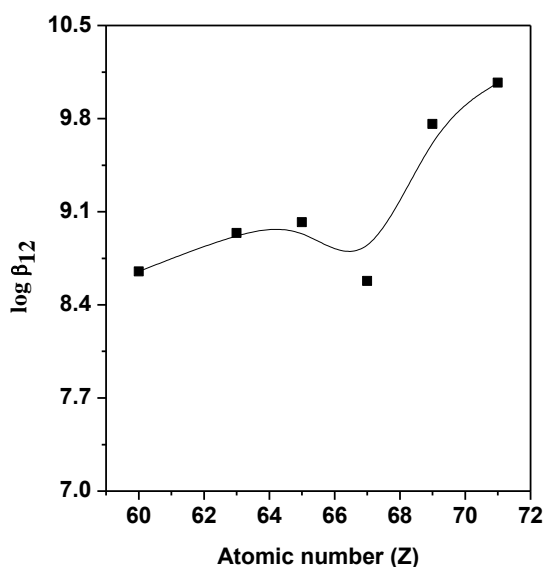


Fig. 5.6: Variation of $\log \beta_{12}$ of Ln(III) complexation with ethyl-BTP at I =0.01 TPAN with Z

5.3.2.4 Cooperative effect

The effective charge on metal ion is reduced on successive complexation with ethyl-BTP. Thus, on the basis of electrostatic interaction only, the trend in stepwise stability constant ($\log K$) is expected to be $\log K_1 > \log K_2 > \log K_3$. In view of non availability of data on $\log \beta_{11}$, it is instructive to compare the magnitude of β_{12} and β_{13}

by suitable scaling. For complexation reactions involving pure electrostatic interactions, $(\log \beta_{13})/3 < (\log \beta_{12})/2$ [137]. In the present case, however, $(\log \beta_3)/3 > (\log \beta_2)/2$ as can be seen from table 5.2 for Nd(III) and Eu(III). Such a trend is indicative of the cooperative phenomenon, wherein the formation of ML_2 facilitates that of ML_3 through hydrophobic interactions [126]. Bruder et al. [132] also observed cooperative effect during the complexation of Eu(III) by hemi-BTP. Thus, the stability constant data further confirm the role of hydrophobic interaction in stabilization of higher complexes.

5.3.3 Time resolved fluorescence spectroscopy (TRFS)

Figure 5.7 shows the fluorescence emission spectra of Eu(III) in methanol along with a typical emission spectrum for Eu(III)-ethyl-BTP (L/M=8.3). The highly intense fluorescence emission of Eu(III)-ethyl-BTP compared to methanol Eu(III) solution, indicates the sensitization of the Eu(III) fluorescence through charge transfer process. Due to forbidden f-f transition, the direct excitation of Eu(III) gives very poor fluorescence yield. However, the excited ethyl-BTP molecule transfers excitation energy to Eu(III) and thereby enhance its fluorescence. The schematic diagram of energy transfer process is given in figure 5.8. Various steps involved in sensitized emission of Eu(III) are as follows:

- a. Absorption of light: The ethyl-BTP molecule, which has high absorption coefficient absorbs, light to populate its excited states
- b. Fast intersystem crossing to populate triplet state of ethyl BTP
- c. Energy transfer from triplet of ethyl-BTP to populate 5D_0 of Eu(III)
- d. Fluorescence Emission from 5D_0 to 7F_j .

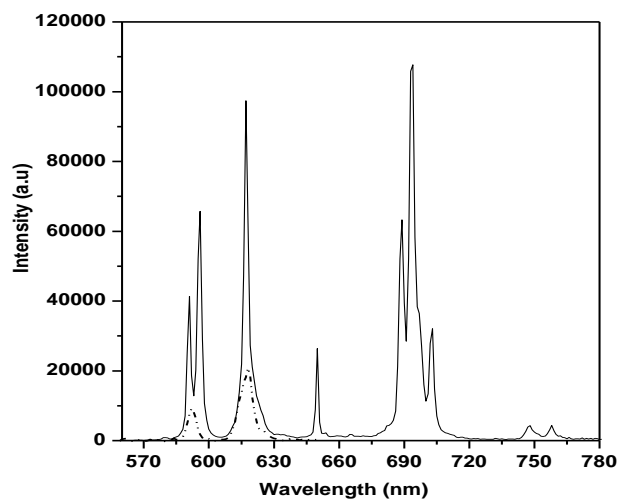


Fig. 5.7: Fluorescence emission spectra of Eu(III) (dashed line) and Eu(III)-ethyl-BTP at L/M = 8.3 (solid line) at I = 0.01 M

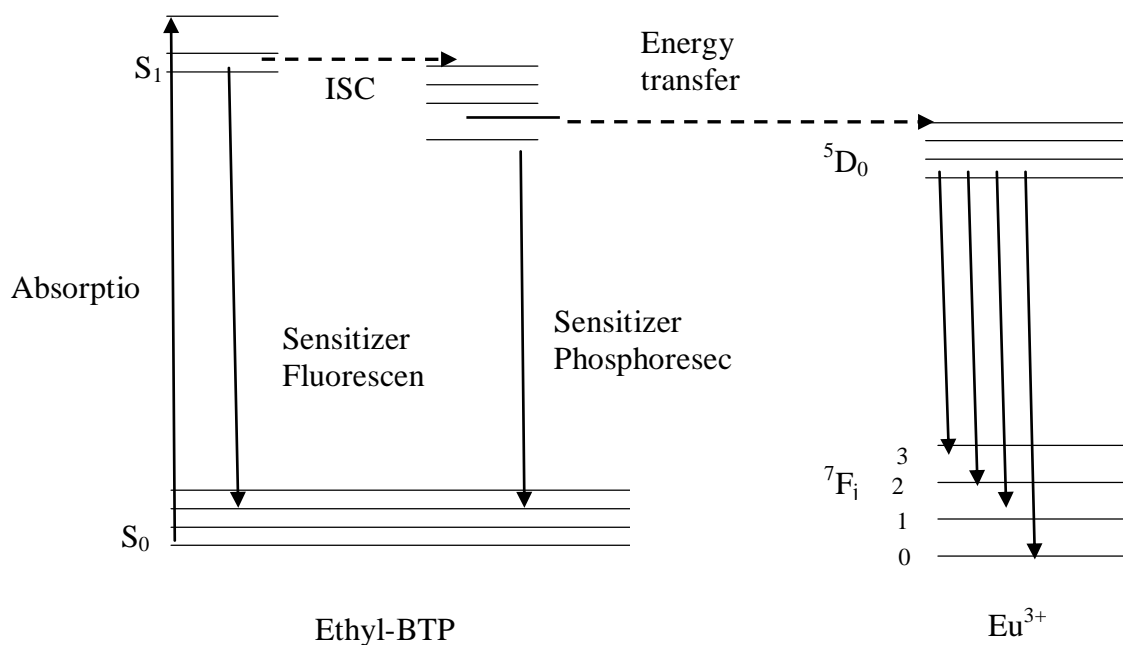


Fig. 5.8: Schematic representation of Eu(III) sensitization process

In methanol medium, Eu(III)-ethyl-BTP, at L/M = 8.3, shows more intense and sharp peaks in fluorescence emission spectrum compared to Eu(III). Further the emission spectra of the complex show splitting of the peaks due to ligand field effect. The asymmetry ratio (AR), defined as the ratio of intensity of 616 nm peak to that of 592 nm peak for Eu(III) in methanol (3.32) is much higher than that in aqueous solution (0.6), indicating the presence of nitrate ions in the inner coordination sphere of Eu(III) giving higher asymmetry to the complex. The AR value for Eu(III)-ethyl-BTP was found to increase from 1.27 to 1.49 on decreasing the ligand to metal ratio (L/M) from 8.3 to 1. The increase in AR with decreasing L/M indicates the formation of a more asymmetric complex with addition of metal ion to ligand. This is consistent with the results of spectrophotometric titrations which showed the formation of ML₃ and ML₂ complexes with the fraction of ML₂ increasing with increasing metal ion concentration.

The luminescence spectra of Eu(III)-ethyl-BTP, showed doublet and triplet at 592 and 690 nm respectively. Similar spectra have also been reported for Eu(III)-(n-propyl-BTP)₃ and Eu(III)(terpyridine)₃. The splitting has been attributed to the distorted D₃ geometry, which agrees with the X ray diffraction data [138]. This suggests that the fluorescence spectrum is dominated by emission due to ML₃ in which the probability of charge transfer from ligand to Eu(III) is higher than that in ML₂.

The fluorescence lifetime of ⁵D₀ state of Eu(III) in methanol medium was found to be 363 μs which is in agreement with the reported value [139]. Further, this is higher than that in aqueous solution (110 μs). The higher lifetime could be due to reduced quenching by -OH phonons in methanol compared to that in water. In addition, unlike in aqueous medium, the nitrate ions can replace methanol molecules from solvation sphere of Eu(III) thereby increasing the lifetime. The decay data of Eu(III) in methanol as well as Eu(III)-ethyl-BTP at L/M= 8.3 are shown in figure 5.9. The fluorescence

decay data show two life time components, whose magnitude remains constant at 2560 ± 150 and $890 \pm 60 \mu\text{s}$ as a function of L/M with the long lifetime component (τ_2) dominating the decay data (table 5.4). Thus the TRFS measurements clearly suggest the formation of two complexes, which is in agreement with the formation of ML_2 and ML_3 in spectrophotometric titrations. The observation of two lifetime components in fluorescence decay data indicates the slow exchange of the ligand between the complex and free ligand unlike in case of carboxylate complexes in aqueous solution [74].

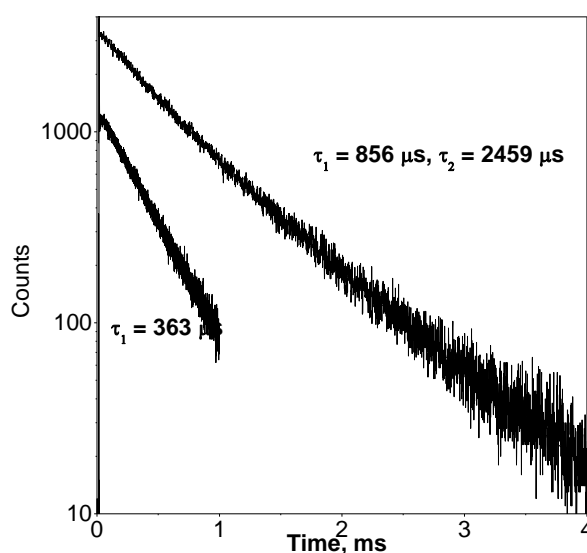


Fig. 5.9: Fluorescence emission intensity vs time for Eu(III)-Ethyl-BTP at ligand to metal ratio 8.3 and Eu(III) in methanol and ionic strength, $I = 0.01 \text{ M}$

Table 5.4: Fluorescence lifetimes (τ_1 and τ_2) at different ligand to metal ratio

[Ligand]/[Metal]	τ_1 (μs)	τ_2 (μs)
8.3	860 ± 30	2469 ± 30
6.3	840 ± 20	2520 ± 40
5	860 ± 20	2560 ± 30
4.2	880 ± 20	2640 ± 30
3.2	940 ± 20	2870 ± 30
2.0	860 ± 40	2400 ± 30
0.7	1020 ± 10	2490 ± 30

Displacement of nitrate and solvent molecules from the inner coordination of Eu(III) by ethyl-BTP will result in decrease in fluorescence decay rate (k_{obs}). Analogous to the empirical relationship prescribed by Kimura and Choppin for Eu(III) [27], linear relationship can be expected for k_{obs} and number of BTP molecules (n_{BTP}) bound to Eu(III).

$$k_{\text{obs}} = A + B n_{\text{BTP}} \quad (5.4)$$

Similar relationship was also observed by Denecke et al. in the TPH/ n-octanol medium [129]. Figure 5.10 shows a plot of k_{obs} vs. n_{BTP} . Based on this plot, it can be concluded that 2560 and 890 μs lifetimes correspond to ML_3 and ML_2 species respectively. The lifetime for ML_3 is close to that for Eu(III) in solid compounds containing no water molecules, and thus indicates the absence of any solvent molecules in the coordination sphere of Eu(III) as well as terdentate nature of ethyl-BTP. The dominance of ML_3 in lifetime data is also reflected in the spectrophotometric data (figure 5.3). The lifetime of ML_3 is in good agreement with that reported in the literature in n-octanol medium (2437 μs) [127].

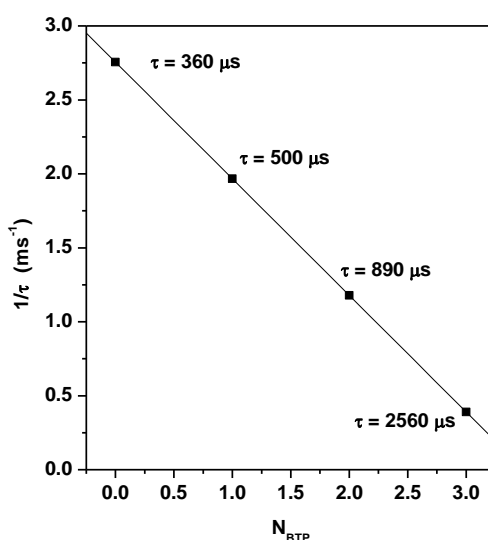


Fig. 5.10: Plot of $1/\tau$ vs. number of BTP molecules (N_{BTP})

5.3.4 Calorimetry

Figure 5.11 gives the raw calorimetric data for titration of ethyl-BTP solution with Eu(III). The Q_i^r represents the sum of the heat of formation of different species involved during titration. For instance, In the case of Eu(III)-ethyl-BTP, where ML_2 and ML_3 was formed, the Q_i^r can be given by

$$Q_i^r = \Delta H_{C3}(v_i^{ML_3} - v_{i-1}^{ML_3}) + \Delta H_{C2}(v_i^{ML_2} - v_{i-1}^{ML_2}) \quad (5.5)$$

where ΔH_{C3} and ΔH_{C2} are the cumulative enthalpy of complexation for ML_3 and ML_2 respectively, v_i^X are the moles of species 'X' at ith injection. The stability constants (β) obtained from spectrophotometric titrations were used to calculate v_i^X for all species while the ΔH_i were obtained by non linear least square fitting of the Q_i^r data (equation 5.5). The thermodynamic data of complexes of Eu(III) and Tb(III) with ethyl-BTP are given in table 5.5. The data show that complexation of Eu(III) and Tb(III) by ethyl-BTP is highly exothermic in nature. ΔH_C is the resultant of the heat released during the complex formation and that required for desolvation of metal ion.

$$\Delta H_C = \Delta H_{\text{bond formation}} - \Delta H_{\text{desolvation}} \quad (5.6)$$

The highly exothermic nature of the complexation reaction suggests strong interaction between ethyl-BTP and Ln(III) ion which can be attributed to the tridentate nature and rigid aromatic structure of ethyl-BTP ligand. The strong metal ligand interaction over-compensates for the desolvation energy.

The ΔH_{C3} for Eu(ethyl-BTP)₃ obtained in the present work is close to that for Eu(n-propyl-BTP)₃ in n-octanol (-70 kJ/mol) but is more negative than (~ -30 kJ/mol) that for Eu(iso-propyl-BTP)₃ in 1:1 (v/v) water – methanol medium [140] which could be explained in terms of the higher desolvation energy required in the water- medium.

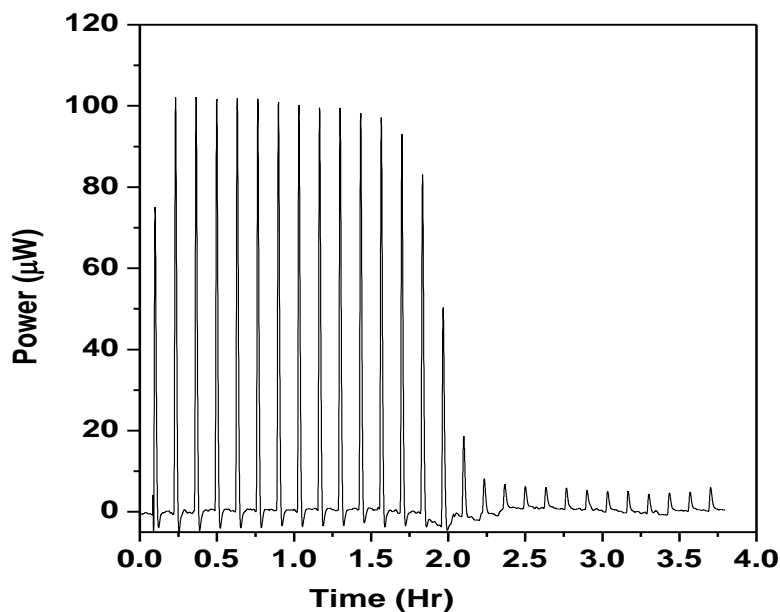


Fig. 5.11: Calorimetric data for titration of Ethyl-BTP with Eu(III) at I = 0.01 TPAN

Table 5.5: Thermodynamic data for complexation of Eu(III) and Tb(III) with ethyl-BTP in methanol medium (I = 0.01 M TPAN)

Metal ion	Species	ΔG_C (kJ/mol)	ΔH_C (kJ/mol)	$T\Delta S_C$ (kJ/mol)
Eu(III)	ML ₂	-51.7	-47 ± 2	4 ± 2
	ML ₃	-77.7	-73 ± 2	5 ± 2
Tb(III)	ML ₂	-51.5	-31 ± 2	20 ± 2

5.4 Conclusion

Early lanthanides (Nd(III) and Eu(III)) form 1:2 and 1:3 complexes with ethyl-BTP in methanol, while latter lanthanides form only 1:2 complex. In the case of La(III) only 1:1 complex is formed with ethyl-BTP. The stoichiometry of the complexes deduced from the analysis of spectrophotometric titrations is corroborated by time resolved fluorescence spectroscopy measurements. The stability constant ($\log \beta_{12}$) for

ethyl-BTP complexes of Ln(III) ions in methanol, follows an ‘S’ shaped curve among the lanthanides, which is a manifestation of increasing ionic potential as well as change in the coordination number of the metal ion. The complexation of Ln(III) by ethyl-BTP is governed largely by enthalpy, with the entropy term constituting a very small factor in the ΔG of complexation. The large exothermic enthalpy for Eu(III)-ethyl-BTP complexes suggests, strong interaction between the metal ion and ligand. The $\log\beta_{12}$ and $\log\beta_{13}$ increase with increasing alkyl chain length of the substituent to the triazinyl ring of BTP.

CHAPTER 6

Summary

The results obtained from the experiments carried out as a part of this thesis are summarized in this chapter.

1. Complexation of Eu(III), a chemical analogue of trivalent actinides, by various carboxylate anions, namely, acetate, alpha hydroxy isobutyrate (α -HIB), succinate and phthalate, have been studied by potentiometry and isothermal titration calorimetry. The potentiometric titration data were used to determine the formation constants of the Eu(III)-carboxylate complexes at 25°C and I=1.0 M.

Isothermal titration calorimetry was used to determine the enthalpy of complexation. The higher stability of Eu(III)- α -HIB compared to that expected on the basis of LFER for monocarboxylates suggests the participation of hydroxyl group which has been further corroborated by thermodynamic data. The enthalpy of formation of all carboxylate complexes was found to be endothermic except for α -HIB and for ML_2 with phthalate. The complexation reaction was found to be controlled by entropy. The higher dehydration of Eu(III) and dicarboxylate anions is reflected in the higher enthalpy and entropy of complexation. The data in conjunction with the time resolved fluorescence spectroscopy measurements performed previously have been used to infer about the structure of the complexes. The thermodynamic data have been explained in terms of hard acid - hard base interaction between Eu(III) and carboxylate anions.

2. The thermodynamic parameters (ΔG_C , ΔH_C and ΔS_C) of complexation of U(VI) and Eu(III) by unsaturated dicarboxylic acids, namely, maleic and fumaric acid, have been determined by potentiometric and microcalorimetric titrations at fixed ionic

strength ($I = 1.0 \text{ M}$) and temperature (25° C). The results show formation of 1:1 complexes by both the ligands with Eu(III). In the case of U(VI), maleate forms both 1:1 and 1:2 complexes, while only 1:1 complex was formed with fumarate. The fluorescence emission spectra of Eu(III) – dicarboxylate solutions at varying ligand to metal ratio were also used to obtain their stability constants. In addition, the fluorescence lifetimes reveal higher dehydration of Eu(III)-maleate compared to Eu(III)-fumarate which corroborates the ΔS_{C} values. The thermodynamic quantities suggest charge polarization effects in the case of U(VI) and Eu(III) complexes of fumarate, which is further corroborated by theoretical calculations. For the same ligand, U(VI) complexes were found to be more stable which was mainly due to higher entropy term. Complexation of Eu(III) and U(VI) by maleate and fumarate is mainly governed by entropy. For the same ligand, U(VI) complexes are more stable compared to Eu(III) complex indicating the complexation is governed by electrostatic interactions. The higher endothermicity in the case of U(VI) complexation suggests the greater degree of dehydration required to accommodate the ligand molecule in the equatorial plane of $[\text{O}=\text{U}=\text{O}]^{2+}$.

3. The thermodynamic quantities (ΔG_{C} , ΔH_{C} & ΔS_{C}) for formation of Th(IV) complexes with dicarboxylate ligands, namely, malonate, succinate, glutarate and adipate were determined using potentiometry and calorimetry to study the effect of chain length. In the case of Th(IV)-malonate, multiple species (ML_i ($i=1-3$)) were revealed from the potentiometric data, while in the case of higher homologues, the data for only 1:1 complex could be obtained owing to precipitation at higher metal concentration. The stability constant of Th(IV) dicarboxylates decrease with increasing carbon chain length from malonate to glutarate indicating the effect of chelate ring size. The complexation of Th(IV) by dicarboxylate is dominated by

entropy, which does not vary significantly with the carbon chain length of the ligand. The variation in $\log K_1$ is mainly due to the enthalpy changes along the series. The increasing enthalpy of Th(IV) dicarboxylate with carbon chain length is explained on the basis of decrease in metal ligand bond strength owing to change in ring size. The stability constants when compared with other actinide oxidation states (III and VI) are in agreement with the trend of $\log K_1$ with effective charge of the metal ion.

4. Complexation of U(VI) by succinate has been studied at various temperatures in the range of 25-65°C by potentiometry and isothermal titration calorimetry at constant ionic strength (1.0 M). The potentiometric titrations revealed the formation of 1:1 uranyl succinate complex in the pH range of 1.5 – 4.5. Stability constant of U(VI) complex with succinate increases with increasing temperature of the reaction system. The enthalpy as well as entropy of complexation increases with temperature but the stability of the complex is predominantly governed by entropy which becomes more favorable at higher temperature. The linear increase of enthalpy of complexation with temperature indicates constancy of the change in heat capacity in the temperature range 25-65⁰ C. The increase in $\log K_1$ with temperature could be well explained in terms of Born equation for electrostatic interaction between metal ion and ligand anion. The data have been compared with those for uranyl complexes with malonate and oxalate to study the effect of ligand size and hydrophobicity on the temperature dependence of thermodynamic quantities.
5. Solvent extraction studies on separation of trivalent actinides from lanthanides using 2,6-bis(5,6-dialkyl-1,2,4-triazin-3-yl) pyridines have shown promising results with respect to separation factor and efficiency in acidic medium. In order to

understand their complexation behavior, the stability constant ($\log \beta$) of trivalent lanthanides (La, Nd, Eu, Tb, Ho, Tm, Lu) with 2,6-bis(5,6-diethyl-1,2,4-triazin-3-yl)pyridine (ethyl-BTP) have been determined in methanol medium (ionic strength 0.01 M) using spectrophotometric titration. The stoichiometry of the complexes are found to vary with ionic size of lanthanide ion. Early lanthanides, Nd(III) and Eu(III) form 1:2 and 1:3 complexes with ethyl-BTP in methanol, while latter lanthanides form only 1:2 complex. In the case of La(III) only 1:1 complex is formed with ethyl-BTP. The stoichiometry of the complexes deduced from the analysis of spectrophotometric titrations of Eu(III)-ethyl-BTP is corroborated by time resolved fluorescence spectroscopic measurements. The stability constant, $\log \beta_{12}$, for ethyl-BTP complexes of Ln(III) ions in methanol, follows an 'S' shaped curve among the lanthanides, which is a manifestation of increasing ionic potential as well as change in the coordination number of the metal ion. Comparison of $\log \beta$ for Ln(III) - ethyl-BTP complexes with other alkyl derivatives showed increase in the stability with increasing length of the alkyl group due to hydrophobic interaction. The complexation of Ln(III) by ethyl-BTP is governed largely by enthalpy. The large exothermic enthalpy for Eu(III)-ethyl-BTP complexes suggests, strong overlap of metal ion and ligand orbitals.

References

1. G.T. Seaborg, *Nucleonics*, 5 (1949) 16.
2. G. T. Seaborg and J. J. Katz, *The Actinide elements*, Ed I, McGraw – Hill book company, Inc (1954) 733.
3. G. T. Seaborg and W. D. Loveland, *The elements beyond Uranium*, Wiley, New York (1990)
4. G. R. Choppin and P. L. Wong, *Chemistry of actinide behaviour in marine system*, *Aquatic Geochemistry*, 4 (1998) 77.
5. Maria Lurdes de Dinis and Antonio Fluza, *Uranium in the environment* (2006) page 609, editors B.J.Morkel and A.H.Berger
6. Lal Singh and Prafulla Soni, *Current Science* 98 (2010) 37.
7. C. Keller, *The chemistry of transuranium elements*. Vol. 3, Verlag Chemie GmbH 294 (1971)
8. *Classification of radioactive wastes, A safety guide*, IAEA safety series 111, G1.1 (1994).
9. D. Banerjee, M. A. Rao and S. K. Samanta, DAE. BRNS Symposium on Emerging Trends in Separation Science and Technology, SESTEC (2006) 264
10. Amar Kumar, L. Varshaney, Prabha Bhalerao, C. P. Kaushik, Kanwar Raj, *Emerging Trends in Separation Science and Technology*, SESTEC 200, 179
11. G. R. Choppin and R. J. Ridberg and J. O. Lilljenzin, *Radiochemistry and Nuclear Chemistry* 2nd edition, Oxford, Butterworth Communication.
12. Composition of HLW calculated, P. V. Achutan (private communication)
13. W. R. Alexander and L. W. McKinley, *Deep geological disposal of radioactive waste*, *Radioactivity in Environment*, Elsevier, Vol.9 (2007).

14. C. Madic, M. J. Hudson, P. Baron, N. Ouvrier, C. Hill, F. Arnaud, A. G. Espartero, J. F. Desreux, G. Modolo, R. Malmbeck, S. Bourg, G. D. Angellis and J. Uhler, EUROPART. European Research Programme for Partitioning of Minor Actinides within High Active Wastes Issuing from the Reprocessing of Spent Nuclear Fuels
15. S. S. Kapoor, *Pramana, J. Physics*, 59 (2002) 941.
16. S. Ansari, P. N. Pathak, P. K. Mohapatra, V. K. Manchanda, Aqueous partitioning of minor actinides by different processes, *Separation and Purification Reviews* (2011) (in press)
17. A. Bhattacharyya, P. K. Mohapatra, V. K. Manchanda, *Solv. Extr. Exch.* 24(1) (2006) 1.
18. Zdenek Kolarik, U. Müllich and F. Gassner, *Solv. Extr. Ion. Exch.*, 17 23 (1999); Z. Kolarik, U. Müllich and F. Gassner, *Ion. Exch. Solvent Extr.*, 17 (1155) 1999.
19. G. Liu and J. V. Beitz, in *The chemistry of the actinide and transactinide elements*, volume 3, chapter 18, edited by L. R. Morss, N. K. Edelstein, and J. Fuger, Springer (2006).
20. *Advanced Inorganic Chemistry* 6th edition, F. A. Cotton, G. Wilkinson, C. A. Murillo and M. Bochmann, John Wiley & Sons, Inc, NY (2004) p1130.
21. M. D. Lind, B. Lee and J. L. Hoard, *J. Am. Chem. Soc.* 87 (1965) 1611.
22. R. J. M. Konings, L. R. Morss, and J. Fuger, in *The chemistry of the actinide and transactinide elements*, volume 4, chapter 19, edited by L. R. Morss, N. K. Edelstein, and J. Fuger, Springer (2006).
23. G. R. Choppin and M.P.Jensen, *The chemistry of the actinide and transactinide elements*, volume 4, chapter 23, edited by L.R.Morss, N.K.Edelstein, and J.Fuger, Springer (2006).
24. B. Fourest, J. Duplessis, F. David, *Radiochim. Acta* 36 (1984) 191.

25. J.C.Sullivan, S.Gordon, D.Cohen, W.A.Mulac and K.H.Schmidt, *J. Phys. Chem.* 80 (1976) 1684.
26. J. Sutton, *Nature*, 169 (1952) 235.
27. T. Kimura and G. R. Choppin, *J. Alloys Compnd.* 213-214 (1994) 313.
28. H. Wimmer, J. I. Kim, R. Klenze, *Radiochim. Acta* 58/59 (1992) 165.
29. T. Fanghanel and J. I. Kim, *Radiochim. Acta* 66/67 (1994) 81.
30. V. Neck, J. I. Kim, *Radiochim. Acta* 89 (2001) 1.
31. R.Guillaumont, T.Fanghanel, J.Fuger, I.Grenthe, V.Neck, D.Palmer and M.H.Rand, Update on the chemical thermodynamics of uranium, neptunium, plutonium, americium, and technetium, Elsevier, Amstrdam (2003).
32. L.R.Morss, K.L.Nash, and D.D.ENSOR, *J.Chem. Soc. Dalton Trans.*, (2000) 285.
33. A.E.Martell, R.M.Smith and R.J.Motekaitis, Critically selected stability constants of metal complexes database version 5.0. NIST standard reference data, Gaithersburg, MD (1998).
34. R.D.Shannon, *Acta Crystallogr.* 32A (1976) 751.
35. G. R. Choppin and L.F.Rao, *Radiochim. Acta* 37 (1984) 143.
36. M.P.Jensen, J.V.Beitz, R.D.Rogers, and K.L.Nash, *J. Alloys Compnd.* 303/304 (2000) 137.
37. M.Eigen and R.G.Wilkins, *Adv. Chem. Ser.* 49 (1965) 55.
38. R.J.Silva and H.Nitsche, *Radiochim. Acta* 87 (1995) 1.
39. F. J. Stevensen, *Humus chemistry: genesis, composition, reactions*, John Wiley & Sons . Inc. (1994)
40. B. Boggs, D. Livermore, M. G. Seitz, *Humic substances in natural waters and their complexation with trace metals and radionuclides: A review*, U. S. Department of Energy, W-31-109-Eng-38.

41. S. N. Kalmykov, A. P. Novikov, A. B. Khasanova, N. S. Scherbina and Yu. A. Sapozhnikov, in: Irina V. Perminova, Kirk Hatfield and Norbert Hertkorn, Use of Humic Substances to Remediate Polluted Environments: From Theory to Practice, NATO Science Series, 2005, Volume 52, Part 2, p 175-184.
42. H. Geckeis, Th. Rabung, T. N. Manh, J. I. Kim and H. P. Beck, Environ. Sci. Technol. 36 (2002) 2946.
43. J. A. Marinsky, Coord. Chem. Rev. 19 (1976) 125.
44. G. S. Manning, Acc. Chem. Res. 12 (1979) 443.
45. I. Grenthe, J. Fuger, R. J. M. Konings, R. J. Lemire, A. B. Muller, C. Nguyen-Trung and H. Wanner, Chemical thermodynamics of uranium, North Holland, Amsterdam (1992).
46. R. Spence, Talanta 15 (1968) 1307.
47. M. Born, Z. Phys. 1 (1920) 45.
48. R. Munze, J. Inorg. Nucl. Chem. 34 (1972) 661.
49. J. N. Brønsted, J. Am. Chem. Soc., 44 (1922) 938; J. N. Brønsted, J. Am. Chem. Soc., 44 (1922) 877; G. Scatchard, Chem. Rev., 19 (1936) 309; E. A. Guggenheim, Oxford: Clarendon Press, 1966
50. K. S. Pitzer, J. Phys. Chem., 77, 268 (1973); K. S. Pitzer, G. Mayorga, J. Phys. Chem., 77 (1973) 2300.
51. W. Nernst, Z. Phys. Chem., 4, 129 (1889); W. Nernst, Z. Phys. Chem., 4 (1889) 373
52. P. Debye and E. Hückell, Physik. Z., 24 (1923) 185.
53. M. S. Sherrill and R. Z. Abegg, Elektrochem. 9 (1903) 549.
54. Bjerrum, P. Hasse and Son, Copenhagen. 1941

55. Bjerrum and Anderson, 1. Kommission Hos Ejnar Munksgaard, Copenhagen, 1945
56. Calvin and Wilson, J. Am. Chem. Soc., 67 (1945) 2003.
57. P. Gans, A. Sabatini, A. Vacca, Talanta 43 (1996) 1739: A. Sabatini, A. Vacca, P. Gans, Talanta, 21,1 (1974) 53.: A. E. Martell and R. J. Motekaitis. The determination and use of stability constants, 1992, 2nd edition, VCH Publishers, New York.
58. P. Gans and B. O'Sullivan, GLEE, a new computer program for glass electrode calibration, Talanta 51 (2000) 33.
59. G. Gran, The Analyst, 77 (1952) 661.
60. Laidler, Keith, J. (1993). The World of Physical Chemistry. Oxford University Press
61. I. Wadso Chem Soc. Rev.(1997) 79: I. Wadso, J. Thermal Analysis and Calorimetry 64 (2001) 75.
62. Data analysis program downloaded from <http://www.box.net/shared/static/ugmd1nqoss.zip> (TAM Assistant CD v1.0.116.37)
63. P. Johansson, I. Wadso, Thermochemica Acta, S. L. Randzio, J. Suukuusk, Biochemical Microcalorimetry, A. E. Beezer, ed, Academic London, 1980
64. I. Wadso and R. N. Goldberg, Pure and Appl. Chem. 73 (2001) 1625.
65. G. Olofsson, D. Berlin, N. Markova, M. Molund, Thermochemica Acta 347 (2000) 31.
66. Neetika Rawat, R.B.Gujar, M.S.Murali, B.S. Tomar and V. K. Manchanda, Thermochem. Acta, 499 (2009) 21.
67. R. M. Izatt, R.E. Terry, B. L. Haymore, L. D. Hansen, N. K. Dalley, A. G. Avondet and J. J. Christensen, J. Am. Chem. Soc. 98 (1976) 7620.

68. H.Kitano, Y.Onishi, A.Kirishima, N.saito and O.Tochiyama, *Radiochim. Acta* 94 (2006) 541.
69. A.Kirishima, Y.Onishi, N.Saito and O.Tochiyama, *Radiochim. Acta* 96 (2008) 581.
70. A.Kirishima, Y.Onishi, N.Sato and O.Tochiyama, *A.J. Chem. Thermodynamics*, 39 (2007) 1432.
71. A.Jain, M. Mohapatra, S. V. Godbole, B. S. Tomar, *Spectrochimica Acta A* 71 (3) (2008) 1007.
72. A.Jain, M. Mohapatra, S. V. Godbole, B. S. Tomar, *Spectrochimica Acta A* 72 (5) (2009) 1122.
73. G. R. Choppin, A.Dadgar and E.N.Rizkalla, *Inorg. Chem.* 25 (1986) 3581.
74. Z.M.Wang, L.J.Van de Burgt and G. R. Choppin, *Inorg. Chim. Acta* 310 (2000) 248.
75. Z.M.Wang, L.J.Van de Burgt and G. R. Choppin, *Inorg. Chim. Acta* 293 (1999) 167.
76. A. H. Khan, V. N. Jha, R. Kumar, S. K. Sahoo, A.K. Shukla, R. M Tripathi, V. D. Puranik, *Management of mill tailings and associated enviromental monitoring in India. Uranium in the environment.* Eds B. J. Merkel, A. H Berger, Springer, Berlin, (2006) 729-737.
77. W. Davies and W. Gray, *Talanta* 11 (1964) 1203.
78. M. W. Schmidt, K. K. Baldrige, J. A. Boatz, S. T. Elbert, M. S. Gordon, J. H. Jensen, K. Koseki, N. Matsunaga, K. A. Nguyen, S. Su, T. L. Windus, M. Dupuis, J. A. Montgomery, Jr. *J. Comput. Chem.* 14 (1993) 1347.
79. R. Ahlrichs, M. Bär, M. Häser, H. Horn, C. Kölmel, *Chem. Phys. Lett.* 162 (1988 : 1989) 165.

80. M. Dolg, H. Stoll, H. Preuss, *J. Chem. Phys.* 90 (1989) 1730, X. Cao, M. Dolg, *J. Chem. Phys.* 115 (2001) 7348, W. Kuchle, M. Dolg, H. Stoll, H. Preuss, *J. Chem. Phys.* 100 (1994) 7535.
81. X. Cao, M. Dolg, H. Stoll, *J. Chem. Phys.* 118 (2003) 487, X. Cao, M. Dolg, *J. Molec. Struct. (Theochem)* 673 (2004) 203.
82. A. D. Becke, *Phys. Rev. A* 38 (1988) 3098.
83. Perdew, J. P. *Phys. Rev. B* 33 (1986) 8822.
84. A. E. Martell, R. M. Smith, R. J. Motekaitis: NIST Critically Selected Stability Constants of Metal Complexes. Version 7, Texas A&M University, College Station, TX (2003).
85. S. Ramamoorthy and M. Santappa *Bull. Chem. Soc. Japan*, 42 (1969) 411.
86. G. R. Choppin and J. A. Chopoorian, *J. Inorganic. Nucl. Chem.* 22 (1961) 97.
87. G. R. Choppin in N. M. Edelstein (ed). *Lanthanide and Actinide Chemistry and Spectroscopy*, ACS, Washington DC, 1980 p173
88. J. Jiang, L. Rao, P. D. Bernardo, P. L. Zanonato, A. Bismondo, *J. Chem. Soc. Dalton Transactions* (2002) 1832.
89. H. Moll, G. Geipel, T. Reich, G. Bernhard, T. Fanghanel, I. Grenthe, *Radiochimica Acta* 91 (2003) 11.
90. G. R. Choppin, A. Dadgar and R. Stampfli, *J. Inorg. Nucl. Chem.* 34 (1972) 875.
91. S. S. Yun, S. H. Bae, S. W. Hong, S. K. Kang, I. H. Kim, J. T. Park, *Thermochim. Acta* 246 (1994) 39.
92. K. S. Rajan and J. Martell, *Inorg. Nucl. Chem.* 29 (1967) 523.
93. J. Huskens, H. Van Bekkum, J. A. Peters, G. R. Choppin, *Inorg. Chim. Acta* 245 (1996) 51.

94. L.Rao, A.Y.Garnov, D. Rai, Y. Xia and R. C. Moore, *Radiochim. Acta* 92 (2004) 575.
95. G. Tomat, L. Magon, R. Portanova, A. Cassol, *Z. Anorg. Allg. Chem.* 393 (1972) 184.
96. P. Di Bernado, A. Cassol, *J. Chem. Soc., Dalton Trans.* (1983) 733.
97. A. Bismondo, S. Sitran, L. Rizzo, *Thermochim. Acta* 124 (1988) 311.
98. J. M. Beiriger, and P. M. Grant, *J. Radioanal. Nucl. Chem., Letters* 154 (2) (1994) 89.
99. T. G Srinivasan, P. Zanonato, P. Di Bernado, A. Bismondo, L. Rao, *J. Alloys Compd.* 408 (2006) 1252.
100. T. Sasaki, Y. Takaoka, T. Kobayashi, T. Fujii, I. Takagi, H. Moriyama, *Radiochim. Acta* 96 (2008) 799.
101. L. Rao, , Z. Zhang, , P. L. Zanonato, , P. Di Bernardo, A. Bismondo, , S. B. Clark, *J. Chem. Soc., Dalton Trans.* (2004) 2867.
102. M. P. Jensen and K. L. Nash, *Radiochim. Acta* 89 (2001) 557.
103. D. T. Reed, S. B. Clark and L. Rao, *Actinide speciation in high ionic strength media*, Kluwer Academic/ Plenum Publishers.
104. F. Crea, C. Foti, S. Sammartano, *Talanta* 75(3) (2008) 775.
105. L. Rao, P. L. Zanonato and P. D. Bernardo, *J. Nuclear and Radiochemical Sciences* 6 (1) (2005) 31.
106. L. Rao, *Chem. Soc. Rev.*, 36 (6) (2007) 881.
107. P. W. Atkins, *Physical Chemistry*, 5th edition, ELBS. Oxford Univ. Press.
108. G. R. Choppin and L. Rao, *Radiochim Acta* 37 (1984) 143.
109. P. L. Zanonato, P. D. Bernardo, A. Bismondo, L. Rao and G. R. Choppin, *Journal of Solution Chemistry* 30 (2001) 1.

110. D. J. G. Ives and P. D. Marsden, *J. Chem. Soc.* (1965) 649.
111. H. S. Harned and B.B. Owen, *The Physical Chemistry of Electrolytic Solutions*, third ed., Reinhold Publishing Corp., New York, 1958.
112. P. Bernardo, P. L. Zanonato, G. Tian, M. Tolazzi and L. Rao, *Dalton Transactions* (2009) 4450.
113. L. Rao, J. Jiang, P. L. Zanonato, P. Di Bernardo, A. Bismondo and A. Y. Garnov, *Radiochim. Acta* 90 (2002) 581.
114. G. Tian, L. R. Martin, L. Rao, *Inorg. Chem.*, 49 (22) (2010) 10598.
115. J. Woznica, C. Lhermet, N. M. Desrosiers, J. Pierre, *J. Chem. Soc. Faraday Trans. 1*, 85 (1709) 7.
116. B. Madan and K. Sharp, *J. Phy Chem.* 100 (1996) 7713.
117. B. Madan and K. Sharp, *J. Phy. Chem. B* 101 (1997) 11237.
118. K.L. Nash, *Solvent Extraction and Ion Exchange*, 11(4) (1993) 729
119. A. Bhattacharyya, Ph. D (Science) Thesis, University of Mumbai, August 2009.
120. Z. Kolarick, *Chem. Rev.*, 108 (2008) 4208.
121. K. L. Nash, *Solv. Extr. Ion Exch.*, 11 (1997) 729.
122. Y. Zhu, J. Chen, and R. Jiao, *Solv. Extr. Ion Exch.*, 14 (1996) 61.
123. C. Hill, C. Madic, P. Baron, M. Ozawa, Y. Tanaka; *J. Alloys and Compounds*, 159 (1998) 271.
124. G. Modolo and R. Odoj, *Solv. Extr. Ion Exch.*, 17(1) (1999) 33.
125. A. Geist, C. Hill, G. Modolo, M. R. Foreman, M. Weigl, K. Gompper, M. J. Hudson and C. Madic, *Solv. Extr. Ion Exch.*, 24 (2006) 463.
126. S. Colette, B. Amekraz, C. Madic, L. Berthon, G. Cote, C. Moulin, *Inorg. Chem.* 41 (2002) 7031.

127. S. Colette, B. Amekraz, C. Madic, L. Berthon, G. Cote, C. Moulin, *Inorg. Chem.* 42 (2003) 2215.
128. S. Colette, B. Amekraz, C. Madic, *Inorg. Chem.* 43 (2004) 6745.
129. M. A. Denecke, P. J. Panak, F. Burdet, M. Weigl, A. Geist, R. Klenze, M. Mazzanti, K. Gompper, *C. R. Chimie* 10 (2007) 872.
130. M. A. Denecke, A. Rossberg, P. J. Panak, *Inorg. Chem.* 44 (2005) 8418.
131. A. Bhattacharyya, T. Gadly, S. K. Ghosh, P. K. Mohapatra, V. K. Manchanda, *Hydrometallurgy* 99 (2009) 18.
132. V. H. Bruder, J. Haddaoui, S. Bouhroum, and F. Arnaud-Neu, *Inorganic chemistry* 49 (2010) 1363.
133. G. Ionova, C. Rabbe, R. Guillaumont, S. Ionov, C. Madic, J. C. Krupa, and D. Guillaneux, *New J. Chem.* 26 (2002) 234.
134. M. G. B. Drew, D. Guillaneux, M. J. Hudson, P. B. Iveson, C. Madic, *Inorg. Chem. Commun.* 4 (2001) 462.
135. M. Miguiritchian, D. Denis, G. Dominique, M. Philippe, C. Madic, M. P. Jensen, K. L. Nash, *Inorg. Chem.* 44 (2005) 1404.
136. G. R. Choppin, *Pure and Appl. Chem* (1971) 21.
137. N. Rawat, R. S. Sharma, B. S. Tomar, V. K. Manchanda, *Thermochimica Acta* 501 (2010) 13.
138. D. Durham, G. Frost, F. A. Hart, *J. Inorg. Nucl. Chem.* 31 (1969) 833.
139. Y. Haas, G. Stein, *Phy. Chem.* 75 (1971) 3668.
140. S. Trumm, P. J. Panak, A. Geist, T. Fanghänel, *European J. Inorg. Chem.* 19 (2010) 3022.

